

# **Wear characterisation in milling of Ti6Al4V – A wear map approach**

by  
Gert Adriaan Oosthuizen

*Dissertation presented for the degree of Doctor of Engineering at the  
University of Stellenbosch*



Promotor: Dr. Andre Francois van der Merwe  
Co-promotor: Prof. Guven Akdogan

Faculty of Engineering  
Department of Industrial Engineering

December 2010

## *Declaration*

By submitting this dissertation electronically, I declare that the entirety of the work contained therein is my own, original work, and that I have not previously in its entirety or in part submitted it for obtaining any qualification.

December 2010

Copyright © 2010 University of Stellenbosch

All rights reserved

## Acknowledgements

I would like to express my gratitude to the following people, who contributed in different ways to this investigation:

My promoter, *Dr A van der Merwe*: for the inspiration behind this investigation and for the financial support from the Industrial Engineering Department at the Stellenbosch University,

My co-promoter, *Prof G Akdogan*: for his encouragement, advice and endurance throughout the course of this work,

*Prof D Dimitrov*: for being the research group leader, his motivation and for his support that enabled the collaborative research study at the Fraunhofer Institute in Germany,

*Prof R Neugenbauer*: for the valuable criticism and for organizing the collaborative research study with the Fraunhofer Institute in Germany,

*Dr S Ozbayraktar*: for organizing the collaborative work with Element Six (Pty) Ltd and guidance throughout the project,

*Dr J Barry*: for the interest in my work, advice and valuable criticism,

*Mr N Treurnicht*: for creating an inspiring working atmosphere and the inputs in our publications,

To all the *staff* and *students* of the Industrial Engineering Department at the Stellenbosch University, the *staff* and *students* at the Fraunhofer Institute in Germany and the *staff* of Element Six (Pty) Ltd in Springs: I extend my heartfelt thanks for maintaining the environments conducive to fruitful research,

*My wife*: for the support, motivation and patience during the less victorious moments through the course of this work,

*My mother and father*: for paying an interest in my chosen field of research and making an effort to understand it,

*My sister*: for her never ending love and support,

*My Heavenly Father*: for granting me the ability and grace to pursue my dreams!

## Opsomming

Inligting rondom freeswerk van Ti6Al4V is beperk en volgens meeste studies is dit nie moontlik om 'n wesentliche toename in die materiaal verwyderingstempo ( $Q_w$ ) te behaal nie. Snybeitel verweringskaarte kan 'n diagnostiese hulpmiddel wees tydens analisering van snybeitels. Snyspoed ( $v_c$ ), maksimum onvervormende spaanderdikte ( $h_{eMax}$ ) en radiale snitdiepte persentasie ( $a_e/\varnothing$  %) is die sleutel veranderlikes om die freeswerk van Ti6Al4V beter te kan verstaan. Die doel van die navorsingstudie was om snybeitel verweringskaarte vir die freeswerk van Ti6Al4V te bou. Die werk vorm 'n fondasie om die eise van freeswerk op die snybeitel beter te verstaan. Sodoende kan die hoof verweringsmeganismes analiseer word. Regstellende aksies wat deur snybeitel vervaardigers ontwikkel is, was ondersoek en integreer met die huidige kennis rondom die falingstipe en verweringsmeganismes.

Aanvanklik was eksperimentele data van agtergrond studies, literatuur en industrie oor die verwerkingstempos en -meganismes rondom die freeswerk van Ti6Al4V versamel. Hiermee is verweringskaarte gebou. Wiskundige modelle wat die verwerking kan beskryf was ook ondersoek. Daarna was werkstuk falingskaarte integreer met die ontwikkeling van die snybeitel verweringskaarte om sodoende die grense in geheel te verstaan. Eksperimentele werk was gedoen om die snybeitel verweringskaarte se uitleg te toets. Sodoende kon die snybeitel verweringskaarte gebruik word om die gedrag van die snybeitel te bespreek en regstellende aksies te ondersoek.

Snyspoed ( $v_c$ ) stem ooreen met die grootte van die termiese lading en  $h_{eMax}$  verteenwoordig die grootte meganiese lading. Die  $a_e/\varnothing$  % omskryf die tydperk van blootstelling aan die termiese lading op die snyrand. Die ondersoek het bewys dat die volgende faktore belangrik is wanneer snybeitel prestasie met die snybeitel verweringskaart evalueer word:

1. Die sleutel tot die ontwerp van snybeitel verweringskaarte is om die mees ekonomies beplande vervangingstyd (SRT) vir spesifieke komponente te identifiseer. Sodoende is dit moontlik om die frees toestande te optimaliseer, waaronder die snybeitels geleidelik sal verweer onder die eise en vir 'n langer tydperk as die ekonomiese SRT sal kan sny.
2. Toename in  $v_c$  sal snybeitelleeftyd (TL) laat afneem. Snybeitels met 'n lae dwarsbreuksterkte, kan 'n minimum  $v_c$  hê waaronder meganiese oorlading plaasvind. Terselfdertyd, kan 'n maksimum TL ('n "sweet spot") bestaan as daar 'n fase verandering in die werkstuk materiaal plaasvind.
3. Toename in  $h_{eMax}$  sal TL laat afneem, maar moet laer as 'n maksimum- en hoer as 'n minimum kritiese waarde wees, om sodoende meganiese oorlading en werksverharding onderskeidelik te vermy.

4. Toename in  $a_e/\phi$  % sal TL laat afneem. Die beste balans tussen TL en  $a_e/\phi$  % is gevind met  $a_e/\phi$  % tussen 30-40% vir growwe freeswerk. In afrondingsfreeswerk is die radiale snit beperk tot 1 mm van die oorblywende werkstuk.

Die ondersoek het bewys dat die volgende faktore belangrik is wanneer werkstukfaling in ag geneem word met snybeitel verweringskaarte:

1. Toename in  $v_c$  sal die werkstukweerstand geleidelik verminder en  $Q_w$  laat toeneem. Ongelukkig is  $v_c$  beperk tot 'n maksimum kritiese waarde om werkstukfaling te voorkom weens 'material burn'. Die snyspoed moet ook hoër as 'n kritiese waarde wees om werkstukklitsing en swak afronding weens spaander probleme te vermy.
2. Toename in  $h_{eMax}$  sal die werkstuk weerstand geleidelik vermeerder en  $Q_w$  laat toeneem. Die  $h_{eMax}$  is beperk tot 'n maksimum kritiese waarde om swak werkstuk afronding, weens die buiging van die werkstuk, te vermy. Terselfdertyd moet  $h_{eMax}$  hoër as 'n kritiese waarde wees om werkstukverharding en -klitsing te voorkom.

Die saamgestelde snybeitel verweringskaarte was bekragtig met eksperimentele werk. Die navorsingswerk het veiligheidsareas identifiseer om Ti6Al4V produktief te frees, sonder om die werkstukoppervlak krities te beïnvloed.

## Synopsis

Information on the milling of Ti6Al4V is limited; with most studies concluding that it is not possible to obtain a significant increase in the material removal rate ( $Q_w$ ). Tool wear maps can be a diagnostic instrument for failure analysis. Cutting speed ( $v_c$ ), maximum un-deformed chip thickness ( $h_{eMax}$ ) and the radial immersion percentage ( $a_e/\phi$  %) are the key variables in understanding the milling of titanium alloys. The objective of this research study was to construct tool wear maps for the milling of Ti6Al4V. This will form the foundation of understanding the cutting demands on the tool, in order to analyse the main wear mechanisms. Remedial actions, which are developed by tool suppliers, can be considered and integrated via this understanding of the failure modes and related mechanisms.

Firstly, experimental data from background studies, literature and industry on wear rates and wear mechanisms pertaining to the milling conditions was gathered to construct the tool wear map. Mathematical models describing the wear behaviour for these conditions were also investigated. Secondly, work piece failure maps have been superimposed onto the tool wear maps constructed to understand the global failure boundaries. Experimentation was carried out to validate the constructed maps. The tool wear map could then be used to discuss the observed effects and consider remedial actions.

Cutting speed corresponds to the magnitude of the thermal load and  $h_{eMax}$  represents the mechanical load. The  $a_e/\phi$  % defines the duration of the exposure to the thermal load at the edge of the cutting tool. This investigation has shown the following issues to be of importance when considering tool performance via the tool wear map approach:

1. The key to designing tool wear maps is to identify the most economic Scheduled Replacement Time (SRT) for the specific components. Knowing the correct SRT makes it possible to optimize the milling conditions so that the cutting tool wears gradually under the cutting conditions, and lasts longer than the economic SRT.
2. Increased  $v_c$  will decrease tool life (TL). However, in low transverse rupture strength tools there may be a minimum  $v_c$  below which mechanical overload may occur. Similarly, a local maximum TL (a *sweet spot*) may exist if there is a phase change in the work piece material.
3. Increased  $h_{eMax}$  will decrease TL. However,  $h_{eMax}$  must be kept below a maximum critical value to avoid mechanical overload, but above a minimum critical value to avoid work hardening.
4. Increased  $a_e/\phi$  % will decrease TL. The best balance of high  $Q_w$  and economic TL is found with  $a_e/\phi$  between 30-40% for rough milling. In finish milling the radial cut is limited to 1 mm finishing stock of the work piece.

This study revealed the following important factors when considering work piece failure in the milling of Ti6Al4V:

1. Increased  $v_c$  will reduce the cutting resistance of the work piece and increase  $Q_w$ . However,  $v_c$  must be kept below a maximum critical value to avoid work piece material burn, but above a minimum critical value to avoid burring and poor surface finish, due to tool build-up and chip jamming.
2. Increased  $h_{eMax}$  will increase the cutting resistance of the work piece and increase  $Q_w$ . The  $h_{eMax}$  must be kept below a maximum critical value to avoid poor surface finish, poor flatness and parallelism (due to work piece bending). Likewise,  $h_{eMax}$  must be kept above a minimum critical value to avoid work hardening and burring.

The constructed tool wear maps are validated with experimental work. This research work identified safe zones to productively mill Ti6Al4V, while producing components with a sufficient surface integrity.

# *Table of Contents*

<b>Declaration</b>	<b>i</b>
<b>Acknowledgements</b>	<b>ii</b>
<b>Opsomming</b>	<b>iii</b>
<b>Synopsis</b>	<b>v</b>
<b>LIST OF FIGURES</b>	<b>x</b>
<b>LIST OF TABLES</b>	<b>xiv</b>
<b>Glossary</b>	<b>xv</b>
<b>Nomenclature and Greek symbols</b>	<b>xix</b>
<b>1. Introduction</b>	<b>1</b>
<b>1.1 The evolving market: Growing demand</b>	<b>2</b>
<b>1.2 Requirements for the demand</b>	<b>5</b>
<b>2. Literature study</b>	<b>10</b>
<b>2.1 Tool wear</b>	<b>10</b>
2.1.1 Flank wear	13
2.1.2 Crater wear	13
2.1.3 Main wear mechanisms	14
2.1.3.1 Abrasion	15
2.1.3.2 Adhesion	15
2.1.3.3 Diffusion	15
2.1.3.4 Chemical reactions	18
2.1.3.5 Thermal cracks	19
2.1.3.6 Plastic deformation	19
<b>2.2 Segmented chips</b>	<b>20</b>
<b>2.3 Cutting temperature</b>	<b>23</b>
<b>2.4 Cutting forces</b>	<b>26</b>
<b>2.5 Surface integrity</b>	<b>29</b>
<b>3. Integration of current understanding of milling Ti6Al4V</b>	<b>32</b>



<b>3.1</b>	<b>Thermal demands</b>	<b>33</b>
3.1.1	Thermal load	34
3.1.2	Exposure time	34
3.1.3	Thermal shock	36
3.1.4	Milling strategy	38
<b>3.2</b>	<b>Mechanical demands</b>	<b>40</b>
3.2.1	Mechanical load	40
3.2.2	Vibration during milling	44
3.2.2.1	Chatter	45
3.2.2.2	Forced vibration	46
<b>3.3</b>	<b>Influence of milling parameters on the cutting demands</b>	<b>47</b>
3.3.1	Effect of cutting speed ( $v_c$ )	47
3.3.2	Effect of radial immersion ( $a_e$ )	50
3.3.3	Effect of maximum un-deformed chip thickness ( $h_{eMax}$ )	51
3.3.4	Effect of axial immersion ( $a_p$ )	52
<b>3.4</b>	<b>Influence of milling parameters on the wear phenomena and wear mechanisms</b>	<b>52</b>
<b>4.</b>	<b>Experimental approach and output</b>	<b>55</b>
<b>4.1</b>	<b>Experimental approach</b>	<b>55</b>
4.1.1	Defining the field of interest	55
4.1.2	Collecting experimental data and information	55
4.1.3	Constructing the tool wear maps	56
4.1.4	Superimposing the data	56
4.1.5	Experimentation	56
<b>4.2</b>	<b>Experimental output</b>	<b>57</b>
<b>5.</b>	<b>Experimental work</b>	<b>58</b>
<b>5.1</b>	<b>Rough milling with carbide tool material</b>	<b>58</b>
5.1.1	The effect of chip dynamics	58
5.1.1.1	Experimental setup and design	59
5.1.1.2	Experimental results	60
5.1.2	Conventional- and transition-speed milling tests	65
5.1.2.1	Experimental setup and design	65
5.1.2.2	Experimental results	66
5.1.3	Static interaction of WC-Co/Ti6Al4V diffusion-couple	72
5.1.3.1	Experimental setup and design	72
5.1.3.2	Experimental results	76
<b>5.2</b>	<b>Finish milling with PCD tool material</b>	<b>78</b>
5.2.1	High-speed milling tests	78
5.2.1.1	Experimental setup and design	78
5.2.1.2	Experimental results	80
5.2.2	Static interaction of PCD/Ti6Al4V diffusion-couple	88
5.2.2.1	Experimental setup and design	89

5.2.2.2	Experimental results	93
<b>6.</b>	<b>Discussion</b>	<b>95</b>
6.1	Rough milling with carbide tool material	95
6.2	Finish milling with PCD tool material	96
<b>7.</b>	<b>Conclusion</b>	<b>97</b>
	<b>References</b>	<b>98</b>
<b>Appendix A:</b>	<b>Factors to consider when calculating the SRT value</b>	<b>I</b>
<b>Appendix B:</b>	<b>Tool failures mode limits and remedial actions</b>	<b>III</b>
<b>Appendix C:</b>	<b>Critical cutting tool material properties</b>	<b>VIII</b>
<b>Appendix D:</b>	<b>Altered Material Zones (AMZ's)</b>	<b>XII</b>
<b>Appendix E:</b>	<b>Benchmark component</b>	<b>XV</b>
<b>Appendix F:</b>	<b>Publications</b>	<b>XX</b>

## LIST OF FIGURES

Figure 1.1: Teal Group’s world aircraft forecast (Adapted from [9]).....	3
Figure 1.2: Change in titanium alloy content (% of structural weight) use in aircraft over time [9].....	4
Figure 1.3 Comparison of the machinability ratings of some popular materials [18] .....	5
Figure 1.4: Comparison between the breakdown of costs for a) fifty Ti6Al4V- and b) Aluminium components (Adapted from [21]) .....	6
Figure 1.5: The effect of various machining improvements in titanium machining over time [9].....	7
Figure 1.6: Comparison of the rough- and finish milling costs to machine fifty Ti6Al4V components (Adapted from [21]).....	8
Figure 1.7: Towards evaluating material removal rates per kW of power required [17].....	9
Figure 2.1: The failure mode diagram for a cutting tool material in machining (Adapted from [35]).....	11
Figure 2.2: Importance of different modes of tool resistance when designing tool material for the milling of Ti6Al4V (Combined from [25,12,41]) .....	12
Figure 2.3: Location and shape of crater wear: a) conventional full wear away from the tool tip in machining steels and b) partial crater wear at cutting tool tip in the machining of Ti6Al4V [49] .....	13
Figure 2.4: The performance of various tool materials in the turning of Ti6Al4V [19].....	14
Figure 2.5: Coordinates in the tool–chip diffusion interface [59].....	16
Figure 2.6: Hardness values along with the interface of the diffusion couple [46] .....	18
Figure 2.7 Typical hot hardness characteristics of some tool materials [12].....	20
Figure 2.8: Schematic illustration of a sequence of events, showing various stages involved in segmented chip formation [80] .....	21
Figure 2.9: Quick-stop photomicrographs of Ti6Al4V chips a) shortly after formation of gross crack at free surface and b) about halfway between cyclic cracks [73].....	22
Figure 2.10: Chip morphology of a) experimental results and b) simulation results [75,76] .....	23
Figure 2.11: Tool face temperatures machining Ti6Al4V relative to cutting speed (Adapted from [19,81,41]).....	24
Figure 2.12: Continuous chip formation: Heat generated and dissipated in continuous chip formation (Adapted from [70]) .....	24
Figure 2.13: Segmented chip formation: Heat generated and dissipated in segmented chip formation (Adapted from [70]) .....	25
Figure 2.14: Schematic illustration of force components in a shoulder milling process .....	27
Figure 2.15: Cutting forces finish milling at elevated cutting speeds ( $v_c=100-400$ m/min) [84].....	28
Figure 2.16: Typical cross section of a machined surface (Adapted from [92]).....	30
Figure 2.17: X-ray diffraction analysis of the Ti6Al4V alloy after heating in air atmosphere for 90 min at (a) 400°C, (b) 600°C, and (c) 800°C [46].....	30
Figure 2.18: Hardness variation after machining Ti6Al4V with PCD tool material with a feed rate of 0.15mm/rev and depth of cut of 0.5 mm under conventional flood coolant [95].....	31
Figure 3.1: Tool failure constraints of tool due to the thermal demands on the cutting tool .....	33
Figure 3.2: Insert surface temperature ( $T_v$ ) as a spatial function of exposure time, and depth beneath tool surface (lines are intended for concept explanation only) [24].....	35
Figure 3.3: Temperature fluctuation in continuous (black line) and 50% exposed intermittent (grey line) machining of Ti6Al4V [98].....	36
Figure 3.4: An illustration of a) climb (down) and b) conventional (up) milling [28] .....	38
Figure 3.5: Rubbing in Conventional (Up) milling [102] .....	39
Figure 3.6: Tool failure constraints due to the mechanical demands on the cutting tool.....	40

Figure 3.7: Schematic illustration of the forces acting in primary and the secondary shear zone; and the heat sources (a, b and c) during shear localization [23].....	41
Figure 3.8: Schematic illustrating the key kinematic quantities used in an equation to calculate the maximum effective feed ( $h_{eMax}$ ) .....	42
Figure 3.9: Chip thickness ( $h_e$ ) as a function of rotation angle ( $\varphi$ ) .....	44
Figure 3.10: Analyzing the effect of self-excited chatter in the milling of Ti6Al4V [22] .....	46
Figure 3.11: Schematic effect of cutting speed on tool life (points and trend lines are intended for concept explanation only) [38,24] .....	47
Figure 3.12: Specific cutting force ( $k_c$ ) at elevated cutting speeds ( $v_c=300-4000$ m/min) for TiAl6V4 [85] .....	48
Figure 3.13: Schematic effect of cutting speed on applied stress (points and trend lines are intended for concept explanation only) [16,30,24] .....	49
Figure 3.14: Schematic effect of radial immersion % on tool life (trend lines are intended for concept explanation only) [98,38,24] .....	50
Figure 3.15: Schematic effect of chip load on tool life (bars are intended for concept explanation only) .....	51
Figure 3.16: Illustration of the reduction in tool life as parameters are increased [28] .....	52
Figure 3.17: Influence of cutting parameters on the generic mapping of catastrophic- and non-catastrophic failures (areas are intended for concept explanation only) .....	53
Figure 3.18: Illustration of the tool material property needs and the mechanisms under different physical demands (Arrows and markers are for concept explanation purposes only) .....	54
Figure 5.1: Experimental setup of the cutting tool over the Ti6Al4V work piece and the directions of the force components .....	60
Figure 5.2: Tool and deformation at initial impact ( $\varphi_{st}$ ) of cut ( $v_c=40$ m/min and $h_{eMax}=0.106$ mm) .....	61
Figure 5.3: Illustrating the time difference in the <i>real</i> maximum effective feed and the maximum theoretical value ( $T_3=h_{eMax}$ ) with $v_c=40$ m/min and $h_{eMax}=0.106$ mm .....	62
Figure 5.4: Deformed Ti6Al4V chip surface length of the segmented chip .....	63
Figure 5.5: Illustration of the chip curling on the rake of the tool (Points 1-6 are shown in Figure 5.3) .....	63
Figure 5.6: Tool rotation angle at final part of segment cut ( $v_c=40$ m/min and $h_{eMax}=0.106$ mm) .....	64
Figure 5.7: The experimental setup with the direction of force components, rotation angle ( $\omega$ ) and feed direction .....	66
Figure 5.8: The constructed wear map for rough milling of Ti6Al4V with carbide tools .....	67
Figure 5.9: Failure modes for carbide tools in rough milling of Ti6Al4V .....	68
Figure 5.10: Cutting forces for carbide tools in rough milling of Ti6Al4V .....	69
Figure 5.11: Normalized Cutting Force (NCF) relative to flank wear ( $V_B$ ) .....	69
Figure 5.12: Comparing the influence of $V_B$ , $v_c$ and $h_{eMax}$ on the increase of the NCF .....	70
Figure 5.13: Top-view of the segmented chip formation .....	71
Figure 5.14: Side view of the segmented chip formation .....	71
Figure 5.15: Schematic diagram of the diffusion couple. ....	72
Figure 5.16: Diffusion coefficients at different temperatures .....	73
Figure 5.17: The equipment for the diffusion experiment: a) The Uni-axial hot press and b) the hot-zone components .....	74
Figure 5.18: The temperature profile for the diffusion experiments (Not to scale, for illustrative purposes only) .....	75
Figure 5.19: SEM micrograph of the diffusion couple after heating in argon for 90 minutes at 1000°C .....	76
Figure 5.20: Distribution of elements along the interface of the diffusion couple after heating at 1000°C in argon for 90 minutes under a load of 10 MPa .....	77
Figure 5.21: Distribution of elements along the interface of the diffusion couple after heating at 800°C in argon for 90 minutes under a load of 10 MPa .....	77

Figure 5.22: Experimental setup with the direction of the forces components, rotation angle and feed direction .....	79
Figure 5.23: Performance of different PCD cutting tool material.....	80
Figure 5.24: The constructed wear map for finish milling of Ti6Al4V with PCD tools .....	81
Figure 5.25: Failure modes for PCD tools in the finish milling of Ti6Al4V .....	82
Figure 5.26: Cutting forces for PCD tools in the finish milling of Ti6Al4V .....	82
Figure 5.27 The a) top and b) side view of the Ti6Al4V chips ( $v_c=100$ m/min, $h_{eMax}=0.019$ mm).....	83
Figure 5.28: Influence of cutting speed ( $v_c$ ) and feed rate ( $f_z$ ).....	83
Figure 5.29: Influence of cutting different parameters .....	84
Figure 5.30: SEM EDAX analysis of the material build-up on the PCD tool material, as supporting evidence the build-up is Ti6Al4V .....	84
Figure 5.31: Analysis of material build-up on the PCD using image mapping with the SEM, showing that the build-up is Ti6Al4V on the PCD tool material .....	85
Figure 5.32: EDM sectioned wear scar of the PCD cutting tool, showing the depth of the wear on the flank and rake of the tool.....	86
Figure 5.33: Etched PCD wear scar on the flank of the PCD cutting tool illustrating the different wear regions .....	87
Figure 5.34: Coordinates in the tool–chip diffusion interface [59].....	89
Figure 5.35: Schematic diagram of the diffusion couple .....	89
Figure 5.36: Diffusion coefficients for Co and C at different temperatures .....	90
Figure 5.37: The equipment for the diffusion experiment: a) The Uni-axial hot press and b) the hot-zone components .....	91
Figure 5.38: The temperature profile for the diffusion experiments (Not to scale, for illustrative purposes only).....	92
Figure 5.39: SEM micrograph of the diffusion couple after heating for 90 minutes at 1000°C (5.5 GPa).....	93
Figure 5.40: Distribution of elements along the interface of the diffusion couple after heating at 1000°C in argon for 90 minutes under a load of 5.5 GPa .....	94

## LIST OF TABLES

Table 2.1: Diffusion coefficient of the elements from the cutting tool into the chip, R=8.315/mol·K [64,38,65] .....	17
Table 3.1: Summary of the physical demands milling Ti6Al4V .....	32
Table 3.2: Range of values for heat transfer coefficient [24,99].....	37
Table 3.3: Thermal shock resistance factors [24] .....	37
Table 3.4: Considering the chip thinning factor for various cutting insert geometries [28] .....	44
Table 3.5: Recommended cutting speeds ranges for non-catastrophic tool failure .....	49
Table 3.6: Recommended $a_e/\phi$ (roughing) and $a_e$ (finish) ranges for non-catastrophic tool failure.....	50
Table 3.7: Recommended maximum un-deformed chip thickness ranges for non- catastrophic tool failure .....	51
Table 3.8: Recommended chip load ranges for non-catastrophic tool failure .....	52
Table 5.1: Experimental equipment .....	59
Table 5.2 Calculated and measured time periods for different force components.....	62
Table 5.3: Mechanical and physical properties of the work piece at room temperature.....	65
Table 5.4: Experimental machines and equipment used in the conventional- and transition speed milling tests .....	65
Table 5.5: Experimental cutting conditions of the conventional- and transition speed milling tests .....	66
Table 5.6: Properties of the WC/Co carbide tool material.....	73
Table 5.7: Mechanical and physical properties of the work piece at room temperature.....	73
Table 5.8: Chemical composition of Ti6Al4V (wt.).....	73
Table 5.9: Experimental machines, equipment and conditions used in the static interaction of WC-Co/Ti6Al4V diffusion couple experiment.....	74
Table 5.10 Mechanical and physical properties of the work piece at room temperature.....	78
Table 5.11: Experimental machines and equipment used in the high-speed milling tests.....	78
Table 5.12: Experimental conditions used for the high-speed milling tests .....	79
Table 5.13: SEM EDAX analysis of the material build-up on the PCD tool material as supporting evidence the build-up is Ti6Al4V .....	85
Table 5.14: Properties of the WC/Co carbide tool material.....	90
Table 5.15 Mechanical and physical properties of the work piece at room temperature.....	90
Table 5.16: Chemical composition of Ti6Al4V [wt.].....	91
Table 5.17: Experimental machines, equipment and conditions used for the static interaction PCD/Ti6Al4V diffusion-couple experiments.....	91

## *Glossary*

Abrasion wear	A wear pattern that occurs due to the chips rubbing across the surface of the tool.
Adhesiveness	A term that describes the stickiness of a material.
Allotropy	The property by which certain elements may exist in more than one crystal structure. An allotrope is a specific crystal structure of the metal.
Alloy system	A complete series of compositions produced by mixing in all proportions any group of two or more components, at least of which is metal.
Alpha	The low temperature allotrope of titanium with a hexagonal, close-packed crystal structure.
Alpha-beta structure	A microstructure containing $\alpha$ and $\beta$ as the principal phases at a specific temperature.
AMZ	Altered Material Zones
Annealing	A generic term denoting a treatment, consisting of heating to, and holding at, a suitable temperature followed by cooling at a suitable rate.
ANSI	An organization founded in 1918 that developed standards for industrial products in the United States.
Beta	The high temperature allotrope of titanium with a body-centered cubic crystal structure that occurs above the $\beta$ transus.
Binder	A substance added to the powder to increase the strength of the compact and cement together powder particles that alone would not sinter into a strong object.
Brinell hardness number (HB)	A number related to the applied load and to the surface area of the permanent impression made by a ball indenter.
Brittleness	The tendency of a material to fracture without first undergoing significant plastic deformation. Contrast with ductility.
Built-up edge	It is a condition where some of the work piece material welds to the cutting edge.
CBN	Cubic Boron Nitride
Cemented carbide	Material that is manufactured by combining tungsten carbide (WC)

	powders and binder cobalt powders (Co).
Ceramics	Cutting materials that offers high mechanical and thermal properties.
Cermets	Sintered alloy that is comprised of titanium carbide (TiC), titanium nitride (TiN) and nickel (Ni) binder.
CIS	Standards developed by Japan Cemented Carbide Tool Manufacturers Association.
Coarse grains	Grains larger than normal for the particular wrought metal or alloy or of a size that produces a surface roughening known as alligator skin in wrought metals.
Compact	An object produced by compression of metal powder, generally while confined in a die, with or without the inclusion of non-metallic constituents.
Corrosion	The deterioration of a metal by a chemical or electrochemical reaction with its environment.
Corrosive wear	Wear in which chemical or electrochemical reaction with the environment is significant
Depth of cut	Describe the thickness of the work piece material that is to be removed by the cutting edge when machining.
Ductility	The ability of a material to deform plastically before fracturing. Measured by elongation or reduction of area in a tension test
EDM	Electric Discharge Machining
Fatigue	The phenomenon leading to fracture under repeated or fluctuating stresses having a maximum value less than the tensile strength of the material. Fatigue fractures are progressive, beginning as minute cracks that grow under the action of fluctuating stress.
Fracture toughness	Term that is used as a measure of resistance of a material to failure from fracture from a pre-existing crack.
Hardness	A measure of the resistance of a material to surface indentation or abrasion; may be thought of as a function of the stress required to produce some specified type of surface deformation. There is no absolute scale for hardness.
HPM	High Performance Machining – more associated with roughing operations



HSK	New standard Tooling Interface, which was developed in Germany and describes tooling shanks DIN69893 (DIN 69893) and spindle receivers DIN69063 (DIN 69063).
HSM	High-Speed Machining – more associated with finish operations
Impurities	Undesirable elements or compounds in the material.
Inclusion	A particle of foreign material in a metallic matrix. The particle is usually a compound (oxide, sulphide).
ISO	International Organization for Standardization
Machinability	The relative ease of machining a metal.
Material burn	Term used to describe brittle part due to too high thermal loading. Both oxygen and nitrogen stabilize the $\alpha$ -phase and create a so called $\alpha$ -case which leads to surface integrity problems.
Megatrends	Long-term processes of transformation with a broad scope and a dramatic impact. They are considered to be powerful factors which shape future markets.
Melting point	The temperature at which a pure metal, compound, or eutectic changes from solid to liquid. The temperature at which the liquid and solid are in equilibrium.
Microstructure	Refers to the phases and grain structure present in a metallic component.
NCF	Normalized Cutting Force indicator
Oxidation	A reaction in which there is an increase in valence resulting from a loss of electrons. Contrast with reduction.
Passes	Term given to the number of times the cut needs to be carried out.
PCBN	Polycrystalline Cubic Boron Nitride
PCD	Polycrystalline diamond
Residual stress	Stress remaining in a structure or member as a result of thermal or mechanical treatment or both. Stress arises in fusion welding primarily the weld metal contracts on cooling from the solidus to room temperature.
Rockwell hardness number (HR)	A number derived from the net increase in depth of impression as the load of the indenter is increased and decreased from a fixed load. The numbers are always quoted with a scale symbol.

RT	Room temperature (25°C)
Rupture stress	The stress at failure. Also known as breaking or fracture stress.
SEM	Scanning Electron Microscope
Shoulder milling	A machining process (milling) in which 90° walls can be achieved.
Sintering	A process of heating a material and bonding its powder particles or compressed powder particles.
Spindle	A rotation axis of a machine, on which a cutting tool is mounted.
SRT	Scheduled Replacement Time (e.g. 30 minutes)
Surface Hardening	A generic term covering several processes applicable to a suitable ferrous alloy that produces, by quench hardening only, a surface layer that is harder or more wear resistant than the core.
Vickers Hardness number	An indentation hardness test employing a 136° diamond pyramid indenter (Vickers) and variable loads, enabling the use of one hardness scale for all ranges of hardness.
WC	Tungsten Carbide
XRD	X-Ray Diffraction

## Nomenclature and Greek symbols

$\mu$	Friction coefficient
$a_e$	Radial depth of cut [mm]
$a_p$	Axial depth of cut [mm]
$C$	Heat capacity [J/kg·K]
$E$	Young's modulus or Elastic modulus [GPa]
$F_c, F_{cN}, F_a$	Cutting-, cutting perpendicular-, and axial force components [N]
$F_f, F_s$	Force components caused by friction and chip serration respectively [N]
$F_x, F_y, F_z$	Force components in x-,y- and z directions [N]
$f_z$	Feed per tooth [mm/tooth]
$h$	Heat transfer coefficient [W/m <sup>2</sup> K]
$h_e$	Effective un-deformed chip thickness [mm]
$h_{eMax}$	Maximum un-deformed chip thickness [mm]
$iC$	Inscribed circle of the cutting tool [mm]
$k_c$	Cutting coefficient or Specific cutting force [N/mm <sup>2</sup> ] or [MPa]
$K_{IC}$	Fracture toughness, resistance to crack propagation [MPa.m <sup>1/2</sup> ]
$\kappa_r$	Cutting tool entering angle, due to insert shape [°]
$L_c$	Chip surface length [mm]
$L$	Length of cutter body [mm]
$MF_c$	Product of the mean cutting force when the tool is sharp ( $MF_{c0}$ ) and the effect of $V_B$ on the cutting force [N]
$MF_{c0}$	Mean cutting force when the tool is sharp [N]
$\emptyset$	Tool diameter [mm]
$Q_w$	Material removal rate [cm <sup>3</sup> /min]
$r$	Radius of cutting tool body [mm]
$R$	Thermal shock resistance (valid for $\beta_i \gg 1$ ); temperature drop limit [°C]
$R_f$	Resultant force of the $F_f$ and $N$ [N]

$R_s$	Resultant force of the $F_s$ and $F_n$ [N]
$R_\gamma$	Thermal shock resistance (valid for $\beta_i \ll 1$ ); cooling rate limit [ $^{\circ}\text{C}\cdot\text{m}^2/\text{s}$ ]
$r_m$	Characteristic length or thickness of specimen [m]
$T_0$	Ambient temperature [ $^{\circ}\text{C}$ ] or [K]
$T_c$	Critical tool temperature [ $^{\circ}\text{C}$ ] or [K]
TL	Tool life [m] or [min]
$T_m$	Work piece melting temperature [ $^{\circ}\text{C}$ ] or [K] ( $T_m$ for Ti6Al4V $\approx 1650^{\circ}\text{C}$ )
TRS	Transverse Rupture strength [MPa]
$T_v$	Tool face temperature [ $^{\circ}\text{C}$ ] or [K]
$V_B$	Average flank wear [mm]
$v_c$	Cutting speed [m/min]
$x$	Distance [ $\mu\text{m}$ ], [mm] or [m]
$z$	tooth
$\alpha$	Rake angle [ $^{\circ}$ ]
$\alpha_{CTE}$	Coefficient of thermal expansion [ $^{\circ}\text{C}^{-1}$ ]
$\beta$	Cutting sweep angle [ $^{\circ}$ ]
$\beta_i$	Biot modulus ( $r_m h / \lambda$ )
$\gamma$	Thermal diffusivity [ $\text{m}^2/\text{s}$ ]
$\gamma_a$	Axial angle [ $^{\circ}$ ]
$\delta$	Cutting sweep distance [mm]
$\lambda$	Thermal conductivity [W/m·K]
$\rho$	Density [ $\text{kg}/\text{m}^3$ ]
$\tau$	Exposure time [ms]
$\tau_c$	Critical exposure time [ms]
$\varphi$	Instantaneous angle position of the shoulder mill with respect to the negative y-direction and measured clockwise [ $^{\circ}$ ]
$\varphi_{ex}$	Exit angle of the cutting tool at the end of the cut [ $^{\circ}$ ]

$\varphi_{st}$  Entry angle of the cutting tool at the start of the cut [°]  
 $\omega$  Spindle rotational speed (RPM) [rev/min]

## 1. Introduction

The South African government has successfully included counter trade clauses into recent aircraft acquisition transactions. To support future counter trade opportunities, the Department of Science and Technology (DST) has embarked on a manufacturing capability enhancement programme. Manufacturing processes of light metals with an emphasis on titanium machining for aerospace applications is one of the research initiatives supported by the DST.

The *purpose* of this project was to develop and validate tool wear maps for rough- and finish milling of Ti6Al4V. The tool wear map serves the purpose of clarifying the complex interaction between the machining parameters to process designers. Thereby a knowledge based iterative process improvement is facilitated, simultaneously enhancing machining knowledge needed in South Africa. Prior to this work, tool wear maps have been developed for the turning of steel [1,2]. However, neither maps for the milling of Ti6Al4V were created nor remedial actions to optimize the production process integrated.

The *first objective* was to perform a literature review on the milling of Ti6Al4V with particular reference to the segmented chip formation phenomenon, the cutting temperatures (thermal demands) at the tool edge, the cutting forces (mechanical demands) and work piece surface integrity. This provides a basis towards understanding the demands on carbide- and polycrystalline diamond (PCD) tool materials; to assist in identifying the main wear mechanisms for each at the different conditions.

The *second objective* was to assess the performance of existing tool materials used in industry in order to establish the benchmark for the experiments and to compare the results found in literature. The *third objective* was to establish the preferred working range (Safe Zone) for rough milling using carbide tool materials; and for finish milling using PCD tool materials. The *fourth objective* was to identify the critical wear modes and mechanisms for rough milling using carbide tool materials; and for finish milling using PCD tool materials.

The *approach* was to have an experimental design for both rough- and finish milling conditions to yield conclusive results for interpolation of the effectiveness of the different tool materials. A 3-factor, 3-level design was used in Statistica to analyze the data. The outputs were tool life, wear scar analyses, chip formation and cutting forces. These outputs were compared to diffusion couple experiments in order to understand the wear mechanisms for rough milling using carbide tool materials; and for finish milling using PCD tool materials.

The *goals* of this research are as follows: Identify the boundaries for aerospace applications. Introduce ways to identify the optimum milling condition ranges. Maximize production rate, while reducing the production costs by avoiding un-planned downtime and maintenance.

Chapter 1 outlines the growing demand for Ti6Al4V alloys, the machining challenges and the benefit of machining capability enhancement. Chapter 2 presents a literature review of the current understanding of the factors that influence machining performance. Chapter 3 discuss the different effects of the tool demands on the constructed tool wear map in order to understand tool- and work piece failure better. The maps developed will be used as the framework to discuss a large body of experimental evidence gathered for milling of Ti6Al4V. The results from investigations are presented in Chapters 5 and discussed in Chapter 6. Conclusions and recommendations for future work are presented in Chapter 7.

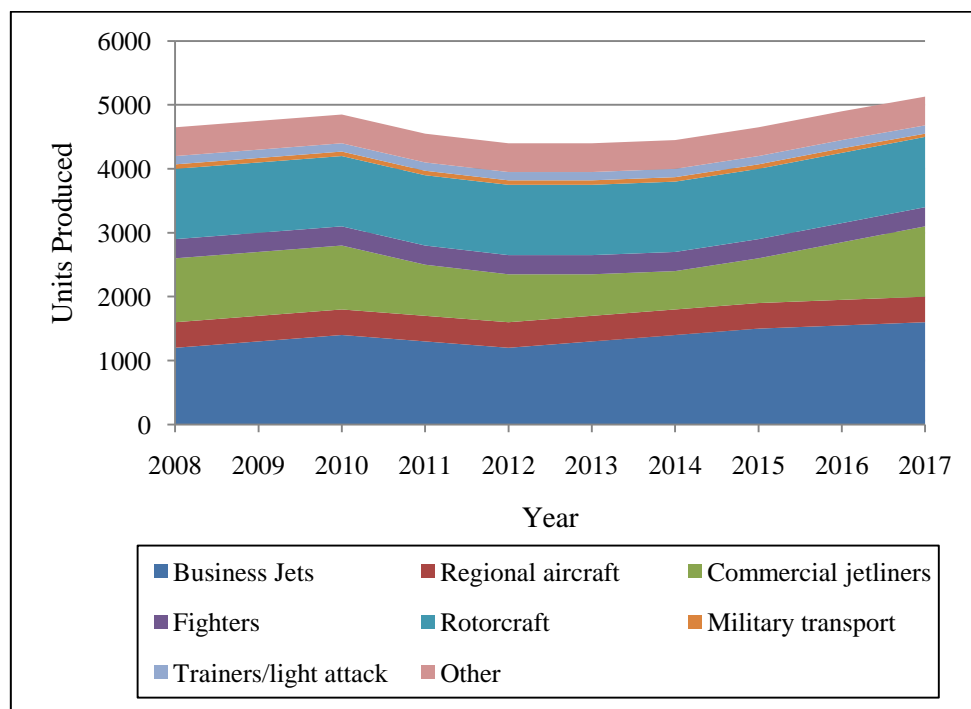
### **1.1 The evolving market: Growing demand**

*Give me six hours to chop down a tree and I will spend the first four sharpening the axe.*  
- Abraham Lincoln, US President (1861-65)

The one word that characterises good business in our time is *speed*. According to the book, *The World is Flat* [3], the twenty-first century will be remembered not for military conflicts or political events, but as the new age of globalization and the *flattening of the world*. The explosion of advanced technologies now means that knowledge, skills and resources have connected all over the planet, levelling the playing field as never before, so that each of us as individuals, businesses, industries or as countries are potentially an equal and a competitor of the other. *Think global, act local*. Today the trend is towards Megatrends. These megatrends are a guide for innovation, which became a relevant strategic issue in many corporate headquarters [4]. In the machining industry, original cutting tools evolve in response to changes in the novel components they make. Accordingly, machine tool builders develop their machining centres to match these trends in product design and engineering processes. These machining companies can gain valuable insights, if information on a megatrend is translated into a company's very own context.

Globalization, energy and resource reversal, climate change and environmental impacts are some of the main megatrends [5] in the manufacturing industry. Climate change and the resulting global environmental concern forced aerospace companies to introduce methods to move to a more environmentally responsible attitude, the so-called greener skies initiative. These megatrends are also directing innovations to the efficient manufacturing of plants to harness energy resources, such as wind- and sea energy turbines. The increase of Chinese, Indians and Brazilians that want to fly is a reflection of the new patterns of mobility [5], which is globally increasing. Outsourcing is enabled by the massive investment in technology of the last decade and now goods, services and skills are sourced easily from almost any part of the globe [6]. The aerospace industry makes use of outsourcing to a large extent in order to keep costs down and stay competitive. This trend caused a shift of technology development towards the suppliers. Technology development to supply the components faster, cheaper and technologically superior is now a challenge shared by the system integrator and

the supplier network. The global civil aviation industry is estimated to contribute 8% of the world's gross domestic product (GDP), or \$3.5 trillion [7]. The Airbus Global Market Forecast anticipates a demand for 24,300 new passenger and freighter aircraft between 2007 and 2026, creating an average delivery rate of some 1,215 aircrafts annually during this twenty year period valued at US\$ 2.8 trillion [8]. The aerospace- and defence industries are currently experiencing substantial growth as illustrated in Figure 1.1. However, it is questionable whether they have sufficient capacity to meet future demands. The following shows the number of aircraft that need to be built over the next several years, based on current orders:



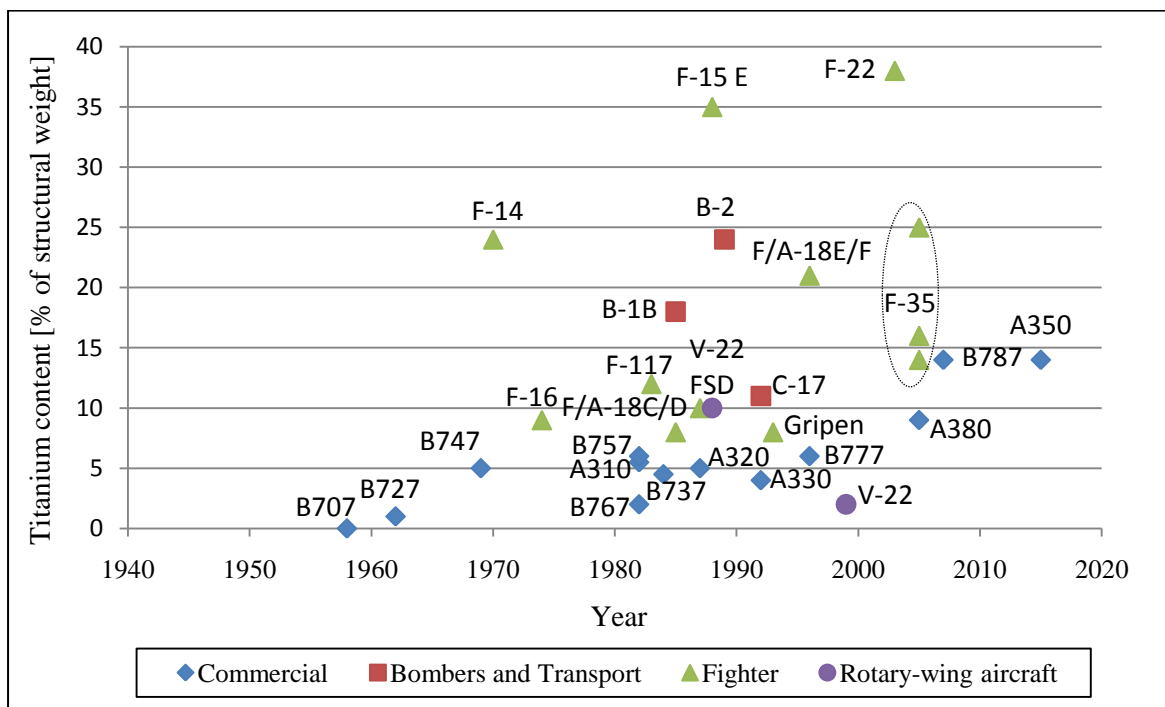
**Figure 1.1:** Teal Group's world aircraft forecast (Adapted from [9])

Rolls Royce forecasts that engine deliveries units are estimated to be 71,500 in 2017-2026 and that engine demand over the next 20 years could be worth US\$ 701 billion [10]. Additionally, world traffic is expected to increase by 4.9% p.a. [7]. Since 1970, air traffic has doubled every 15 years, and Airbus expects it to double again in the next 15 years [7]. These high growth rates together with the highly competitive environment in which aerospace companies operate, will necessitate an accompanying increase in machining effectiveness and capacity.

Fuel is the largest cost for all airlines and a major priority for profitable airline operation. For some carriers the fuel bill can account for up to 50% of direct operating costs. In the past (2003-2006) the fuel expense for most carriers, grew from 15% to more than 25% of total airline operating costs [10]. The aerospace market need will be driven by the need for more fuel and eco-efficient aircraft to cope with traffic growth, as well as for the replacement of older-generation equipment [8]. The CO<sub>2</sub> emissions are directly proportional to the amount of fuel burnt. According to the UN



Intergovernmental Panel on Climate Change, aviation accounts for 2% of global CO<sub>2</sub> emissions [7]. Therefore, the drive for fuel efficiency is vital in all airlines' operations. This is also reflected in the orders for newer type, fuel efficient aircraft. By 2026, the fuel consumption of the average world fleet is expected to be at three litres per 100 passenger kilometres (km), similar to the benchmark that the A380 set recently [8]. Cars currently marketed in Europe have an average of 6.5 litres per person per 100 km, while the average for US cars is 9.6 litres [7]. Whether if the fuel price will continue its long term upward trend only time will tell. Fuel efficiency will remain important to many airlines and fleet renewal is an essential part of this. The future trend is to fight climate change and to reduce the impact on the environment. Reducing the weight of the aircraft can contribute a significant amount. To increase aircraft efficiency and reduce lifecycle costs, aircraft manufacturers are using more composites and titanium alloys. Titanium alloys can increase airframe structural life up to 60% compared to that for aluminium alloys [11]. The forecast for the next 10 years is that there will be a general increase in titanium content (% of structural weight) in aircraft production as illustrated in Figure 1.2. Titanium's superior strength-to-weight ratio, corrosive resistance and superior compatibility with composites enable this alloy to become the material of choice in the aerospace sector [12].



**Figure 1.2:** Change in titanium alloy content (% of structural weight) use in aircraft over time [9]

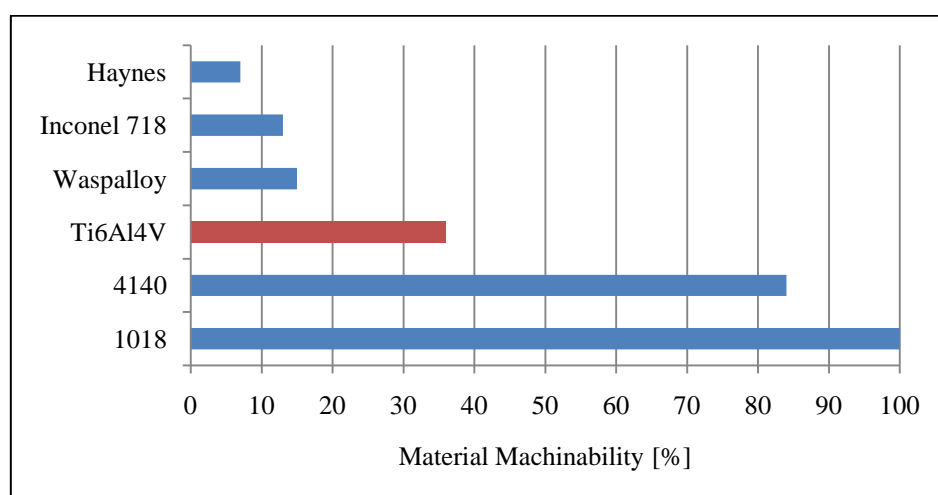
Today, the aerospace industry consumes roughly 42 percent of all titanium produced globally, with double-digit demand growth expected to continue throughout the rest of this decade [11]. The growing use of composites, titanium alloys and stacks containing both materials in structural applications is driving major change in the airframe industry. Ti6Al4V is the most popular titanium

alloys used in this sector and comprises about 45-60% of the total titanium products in practical use [13,14]. A good deal of current cutting technology development is focused on maximizing material removal rates ( $Q_w$ ) in order to reduce the machining costs to make Ti6Al4V components.

Ti6Al4V is formed by a blend of alpha- and beta favouring alloying elements. The alpha (hexagonal close packed) is hard and brittle with strong hardening tendency. The beta (body centred cubic) is ductile, easily formed with strong tendency to adhere [15]. This alloy can be produced in a variety of formulations, depending on the application. The aluminium content may reach up to 6.75% (by weight) and vanadium 4.5%. The oxygen [14] content may vary from 0.08 to more than 0.2% and the nitrogen may be adjusted up to 0.5%. Raising the content of these elements, especially oxygen [16] and nitrogen, will help to increase the strength. Equally, the lower additions of oxygen, nitrogen and aluminium will improve ductility, stress-corrosion resistance, fracture toughness and resistance against crack growth [16].

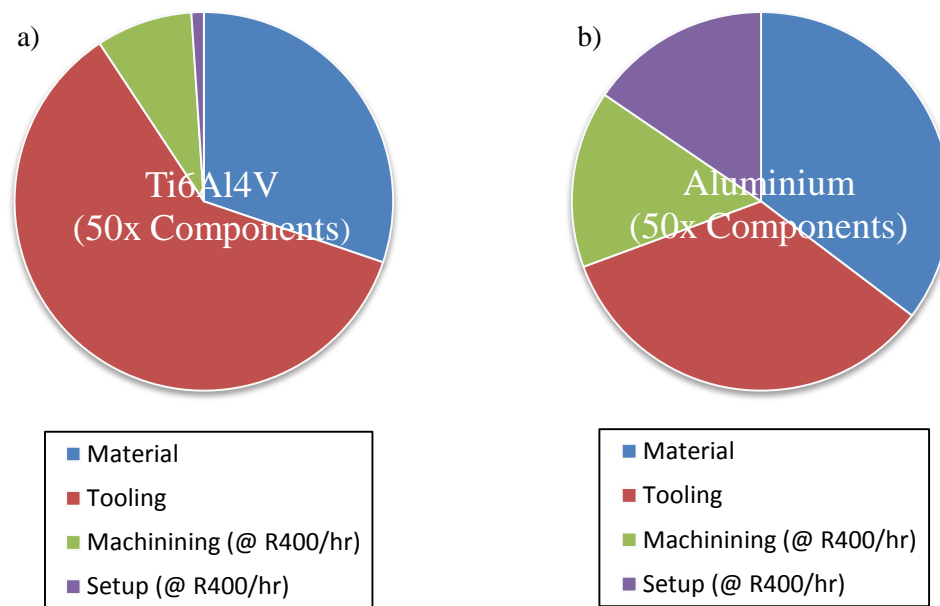
## 1.2 Requirements for the demand

These growing demands on aerospace manufacturers to machine more difficult-to-machine [12] titanium alloys, require manufacturers to increase their capabilities and capacities. This requires a better understanding of the tool demands and effective strategies for the milling of Ti6Al4V. Machining is a major cost contributor, but at the same time, a differentiating factor for a competitive advantage. Many of the same qualities that enhance Ti6Al4V's appeal for most applications, also contribute to its being one of the most difficult materials to machine [17]. Figure 1.3 illustrates Ti6Al4V's machinability by comparing it to the machinability ratings [18] of other materials with 1018 as benchmark.



**Figure 1.3** Comparison of the machinability ratings of some popular materials [18]

The key demand that distinguishes milling from turning is the interrupted cutting; and the related mechanical and thermal shock loading. Tool wear when milling Ti6Al4V may be modeled as a thermo-mechanical highly cyclic fatigue phenomenon. The thermal conductivity of Ti6Al4V (7 W/m.K) is approximately twenty five times lower than that of Aluminium (6061: 177 W/m.K) [15]. The result is a concentration of heat in the cutting zone, that cause complex wear mechanisms like adhesion, oxidation and diffusion [19,20]. Figure 1.4 illustrates the cost breakdown for fifty Ti6Al4V components and compares it to the cost for the same benchmark component machined out of Aluminium.

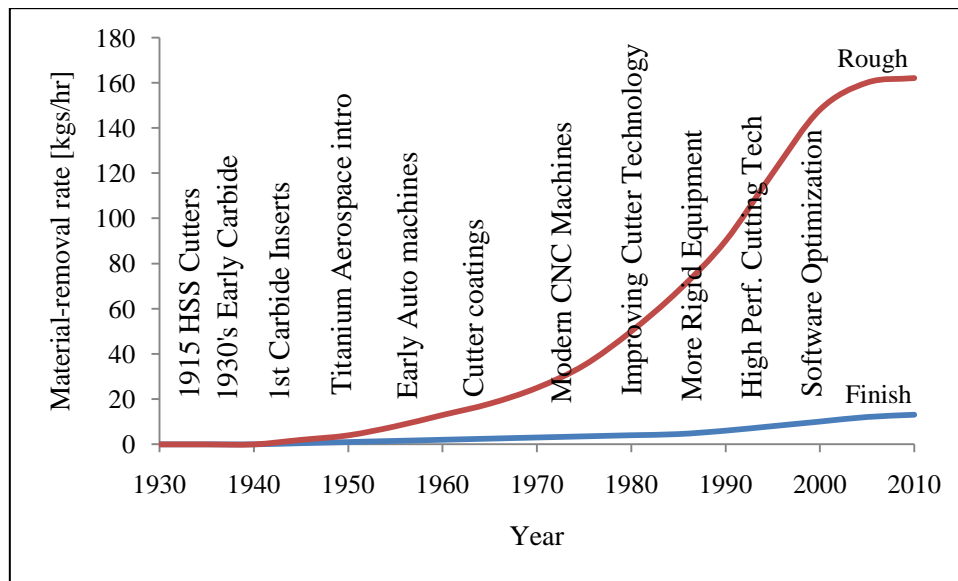


**Figure 1.4:** Comparison between the breakdown of costs for a) fifty Ti6Al4V- and b) Aluminium components (Adapted from [21])

A better understanding of the wear mechanisms found in the milling of Ti6Al4V, will help to enhance tool performance and reduce tool cost. As illustrated in the figure, this will have a pronounced effect on the total cost. Catastrophic tool failure, due to vibration while in cut, is caused by self-excited chatter [22] and forced vibrations due to the formation of shear localization [23] and the fluctuating friction force between the tool and chip flow. The combination of a low Young's modulus (114 GPa) [15], encourages chatter and work piece movement away from the tool. Work hardening, especially at a low maximum un-deformed chip load ( $h_{ex}$ ) and the re-cutting of hard chips can lead to catastrophic tool failure [24,25].

In order to get the most out of a machining centre cutting Ti6Al4V, “it is crucial to customize the way you use tools around the system you are dealing with,” said Ken DeRoche, senior program engineer, Kennametal Inc., Latrobe, Pa. “What works on one part doesn’t guarantee success on the next. What works on all parts is the complete understanding of the application,

or system” [26]. An optimised machining process is one where the maximum  $Q_w$  is obtained with the minimal amount of tool wear. Figure 1.5 illustrates the improvements in the  $Q_w$  for rough- and finish operations of titanium alloys over time as machining technology improved.



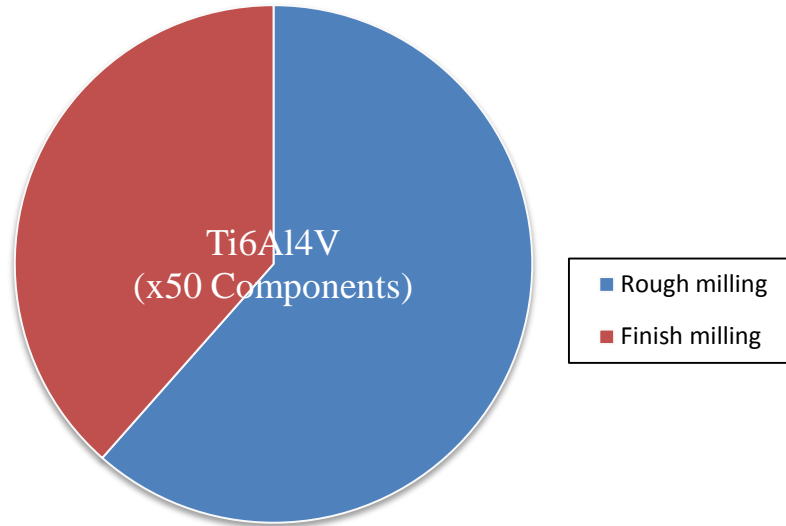
**Figure 1.5:** The effect of various machining improvements in titanium machining over time [9]

As shown in Figure 1.5 the role of titanium machining improvement has levelled off. Therefore there is a need for new technology to enable further improvement. According to various researchers [9,24,25] the following are the desirable properties for the ideal cutting tool material for Ti6Al4V:

- Small grain size to be able to produce a sharp cutting edge
- High hardness, including high hot hardness, to provide excellent abrasive wear resistance
- Good toughness (high transverse rupture strength and fracture toughness) to maintain a sharp cutting edge without chipping or deformation under a cutting force’s dynamic action,
- Good thermal conductivity to remove heat from the cutting zone,
- Thermal stability to maintain integrity at cutting temperatures, and
- Low chemical affinity or reactivity to the work piece material.

In *rough milling* also defined as first stage machining (FSM), the design or choice of the type of cutter selected will determine the  $Q_w$  possible [ $\text{cm}^3/\text{min}$ ] and the programming options. The aim is to have a strategy suited to the feature to be machined giving a maximum  $Q_w$  that can be balanced with an economic tool life (TL). The description  $\kappa_r$  of the insert style (round,  $45^\circ$  or  $90^\circ$ ) and the number of teeth selected will have a dramatic effect on the machining strategy and ultimately the TL and  $Q_w$  [27] Although cutting speed ( $v_c$ ) has the highest focus and is the easiest to change, it can be the most sensitive regarding the thermal load [12]. While a high percentage of the radial immersion increases the  $Q_w$  it has been found that the relationship of  $a_e/\phi$  is critical. The best balance of high  $Q_w$  and

economic TL is found with  $a_e/\phi$  between 30-40% [28]. While round and  $\kappa_r$  inserts have limited depth of cut,  $\kappa_r=90^\circ$  has a cutting depth as deep as the cutter diameter and a length that allows for stable cutting. Importantly for Ti6Al4V, an increase in  $a_p$  has no detrimental effect on tool life (for  $\kappa_r=90^\circ$  cutters) [29]. Figure 1.6 illustrates the cost for the rough- and finish milling operation to machine fifty Ti6Al4V benchmark components [21].



**Figure 1.6:** Comparison of the rough- and finish milling costs to machine fifty Ti6Al4V components (Adapted from [21])

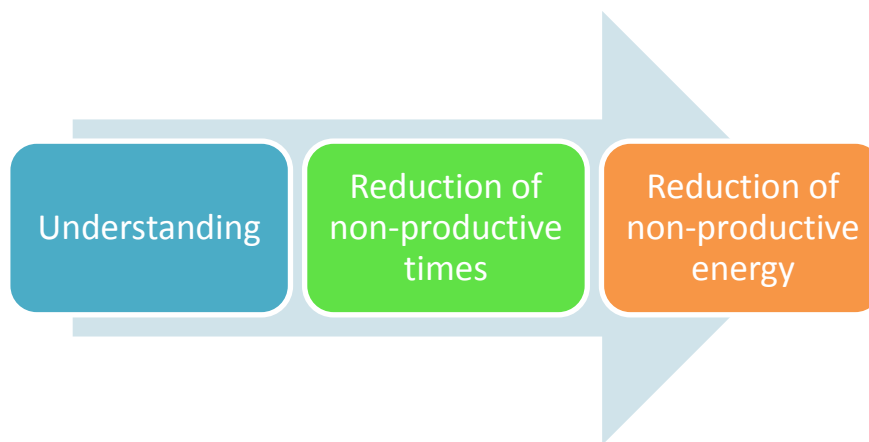
As illustrated in the figure both milling operations need to be considered. Although the costs for finish milling operations are found to be less for this Ti6Al4V component, work piece related failure in the final stages makes the machining company financially vulnerable.

In *finish milling* operations also defined as last stage machining (LSM), the surface finish is the main criteria and the productive driving factor is no longer  $Q_w$  [cm<sup>3</sup>/min], but finished surface area [cm<sup>2</sup>/min]. In order to maintain a good surface finish an increase in the feed rate is limited. Likewise the productivity can't be increased with  $a_e$ , as the radial cut is limited to 0.5-1 mm finishing stock [24,15]. Therefore, the critical parameters to optimize finish milling operations are the cutting speed ( $v_c$ ), axial depth of cut ( $a_p$ ) and the number of teeth ( $z$ ) that can be used to change the speed of area coverage. The  $a_p$  should be as high as possible (Max.  $2 \times \phi$ ), but is restricted by the stability of the cutter (high  $L/\phi$  %), which can be slender.

One way to select the most suitable machining conditions is to examine the trends of tool wear with varying machining conditions [1,20]. Wear maps representing the rates of tool wear in a two-dimensional space defined by the machining conditions in metal cutting have been found to assist in such an optimisation process [1]. It was found that cutting speed and maximum un-deformed chip load played a critical role in determining the extent of wear on cutting tool materials [20]. These

machining parameters ( $v_c$  and  $h_{ex}$ ) were chosen as the wear map's axes. These maps which describe the global wear characteristics of cutting tools can be used to achieve a certain degree of optimization of machining operations. These maps were taken a step further by Kendall [30], when a safe operating region was proposed for cutting tools by superimposing possible boundaries. It was suggested that as long as the machining parameters lay within this safe zone, the tools would not suffer catastrophic tool failure (failure before scheduled replacement time). It was noted that further work is necessary to incorporate work piece related failure and remedial actions into these maps for the milling of Ti6Al4V. The positive correlation in terms of wear-rate trends obtained with other work piece materials suggests that this is a viable approach to achieve the objective of developing an integrated predictive system for tool wear in metal cutting [1].

Since the 1980's there has been significant development in relation to the technical capabilities of cutting processes. As illustrated in Figure 1.7, right at the core of all cutting processes is the understanding of the mechanisms of material removal. Recent work [31,32] on the cutting edge engineering is showing us that significant benefits can be obtained by very careful analysis of the precise engagement conditions and of the precise mechanisms underlying material removal. Such an understanding allows us to assess the effectiveness of the energy conversion from the electrical power utilization at source to its conversion into useful work for the process.



**Figure 1.7:** Towards evaluating material removal rates per kW of power required [17]

It is evident that an understanding of the Ti6Al4V milling operation is a fundamental requirement as input to future models. This research work is to understand the mechanisms of the Ti6Al4V milling process better and to develop wear maps to reduce non-productive times. In the future we can consider non-productive energy and design our systems to reduce or eliminate it. To date there has been little consideration given to evaluating the  $Q_w/kW$  of power required. This is a direction that needs a central location on the future roadmap of cutting technologies [17].

## 2. Literature study

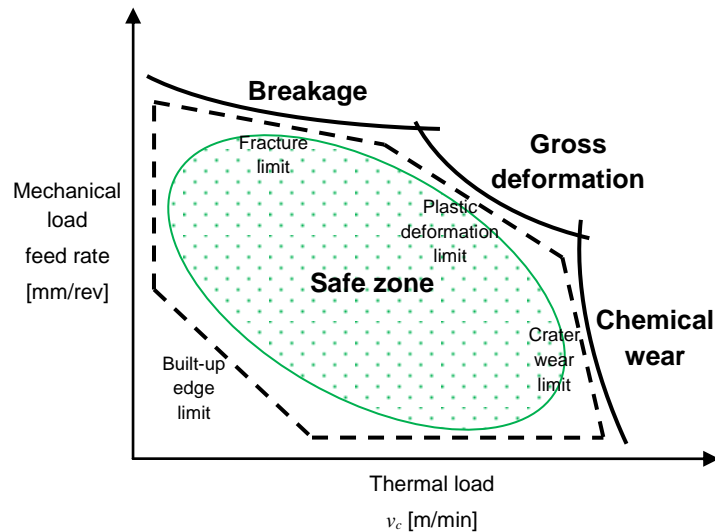
This section highlights the current understanding of the main factors [27] that influence machining performance. The tool failure modes and mechanisms are addressed and the competing chip theories are compared. The heat generation and dissipation differences of continuous- and segmented chip formation are discussed; and cutting force and surface integrity are evaluated for the milling of Ti6Al4V.

### 2.1 Tool wear

There are a number of possible modes by which a cutting tool can fail. Expected degradation (gradual wear) of the cutting tool is the only accepted form within the machining industry. Expected tool wear makes it possible to schedule tool replacements and to find the optimum cutting parameters, relative to the rate- and cost of production [33]. Figure A.1 in Appendix A, illustrates the factors which are considered to calculate the scheduled replacement time for different components. According to our research [21], literature [34] and tool suppliers [28] the tool life for the milling of Ti6Al4V should currently be at least 30 minutes (SRT) to ensure an economic viable solution. Therefore, if a cutting tool material withstands the cutting demands for longer, the cutting conditions define a safe operating zone.

Premature, catastrophic tool failure is the least desirable failure mode, because it is the most unpredictable, can be damaging to the work piece and cause costly downtime. This type of failure can be minimized through an understanding of the physical demands on the cutting tool and the effect of changing the operating conditions. Quinto [35] constructed a tool wear map in terms of the two variables, namely cutting speed and normalized feed rate (i.e. the product of feed rate and depth of cut) for turning operations. This map is derived from Kendall [36,30], the wear mechanism maps from Lim [2] and Trent's [37,38,39] machining charts.

The tool wear map is illustrated in Figure 2.1 and was used as basis to construct the tool wear map for the milling of Ti6Al4V. The safe zone depicted in the failure mode diagram is a region of gradual wear associated with reliable performance [35].



**Figure 2.1:** The failure mode diagram for a cutting tool material in machining (Adapted from [35])

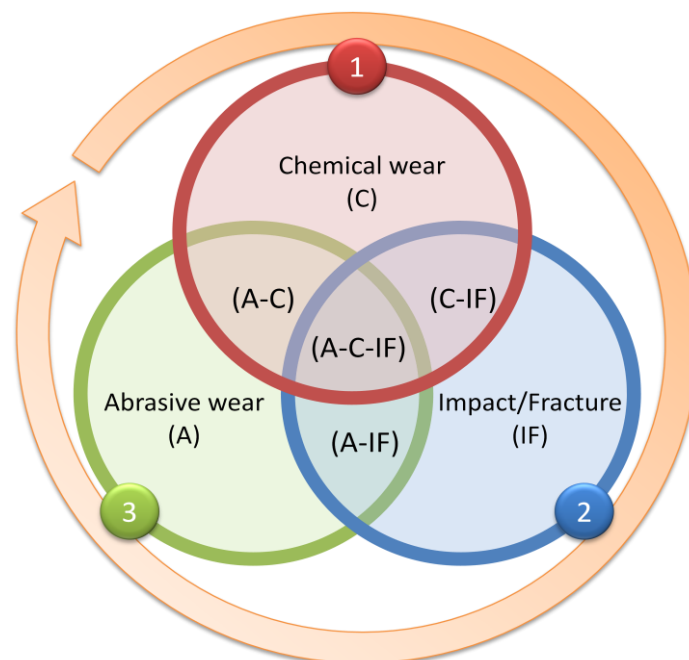
This wear map was also found to be the most appropriate map to construct and evaluate the failure modes for carbide tools under rough- and PCD tools under finish milling conditions. Machine engineering methods [40] to characterise the failure mode were also considered for this study to integrate into this wear map. This enables machining operators to understand the cause of failure, in order to take remedial action.

Tribo-chemical wear is a combination of chemical-mechanical wear; and may be considered a thermally activated process whereby the work piece material and tool material react in such a manner as to remove material from the tool on an atomic scale [40]. Thermal activation refers to the breakdown caused by high temperature cycling of the cutting edge between the heating and cooling stages in milling. Chemical wear is therefore caused by a reaction between the tool and the titanium alloy during cutting.

The cutting edge strength is the property that resists the breakdown of the cutting edge due to the cutting impact. Breakage by means of fracture is found when the mechanical load exceeds the physical properties of the tool material [40,24]. Abrasion wear is caused by the action of the sliding chips on the rake face of the tool, as well as by the friction phenomenon between the flank face of the cutting tool and work piece. Abrasion wear takes place primarily due to the hard grain orientations [16,14] in the Ti6Al4V alloy, which can act like hard inclusions in the work material; and is compounded by the part's hardness and strength properties.



Researchers [41] compared the cutting forces for the machining of Ti6Al4V and carbon steel (0.45%C) under similar cutting conditions. It was found that the cutting forces from the titanium alloy were reduced by 50% compared to that of carbon steel. Similar Machado [42] found that the magnitude of the cutting force to be equal to, or less than for steel. It can be argued that the tool demands for titanium alloys are quite reasonable when considering only the mechanical loading and abrasive wear. Therefore, the main objective is to design tool materials with a high tribo-chemical wear resistance, followed by strength and abrasion resistance [25]. Figure 2.2 illustrates the sequence of importance for the type of resistance needed of innovative tool material and coatings to withstand the different demands in the milling of Ti6Al4V. Research [25,12] confirmed that tool wear in the machining of titanium alloys is mainly due to high thermal loads localized in the vicinity of the cutting edge and the enhanced chemical reactivity of Ti6Al4V with different tool materials at elevated temperatures.



**Figure 2.2:** Importance of different modes of tool resistance when designing tool material for the milling of Ti6Al4V (Combined from [25,12,41])

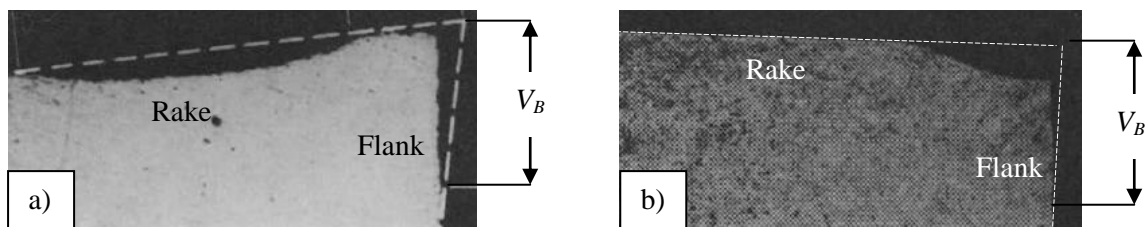
Premature (catastrophic) tool failures, due to an excessively high thermal load (mainly thermal shock or chemical wear [24,19,43]) or mechanical load (mainly chipping or fracture [20,44]) may be minimized by careful analyses and an understanding of the demands of the work piece material at different cutting conditions.

### 2.1.1 Flank wear

Flank wear on the clearance face of the cutting tool results from rubbing between the newly generated work surface and the tool; and has been observed in the milling of Ti6Al4V [20]. Flank wear is measured by the average width of the wear band ( $V_B$ ) on the clearance face as illustrated in Figure 2.3. In industrial application the failure criterion is set at a maximum  $V_B$  limit of 0.4 mm in rough- and 0.3 mm for finish milling [43], as accelerated wear follows. According to research [12,25,45,46,47,15] the  $V_B$  involves attrition, due to adhesion, diffusion- and abrasion wear in the milling of titanium alloys.

### 2.1.2 Crater wear

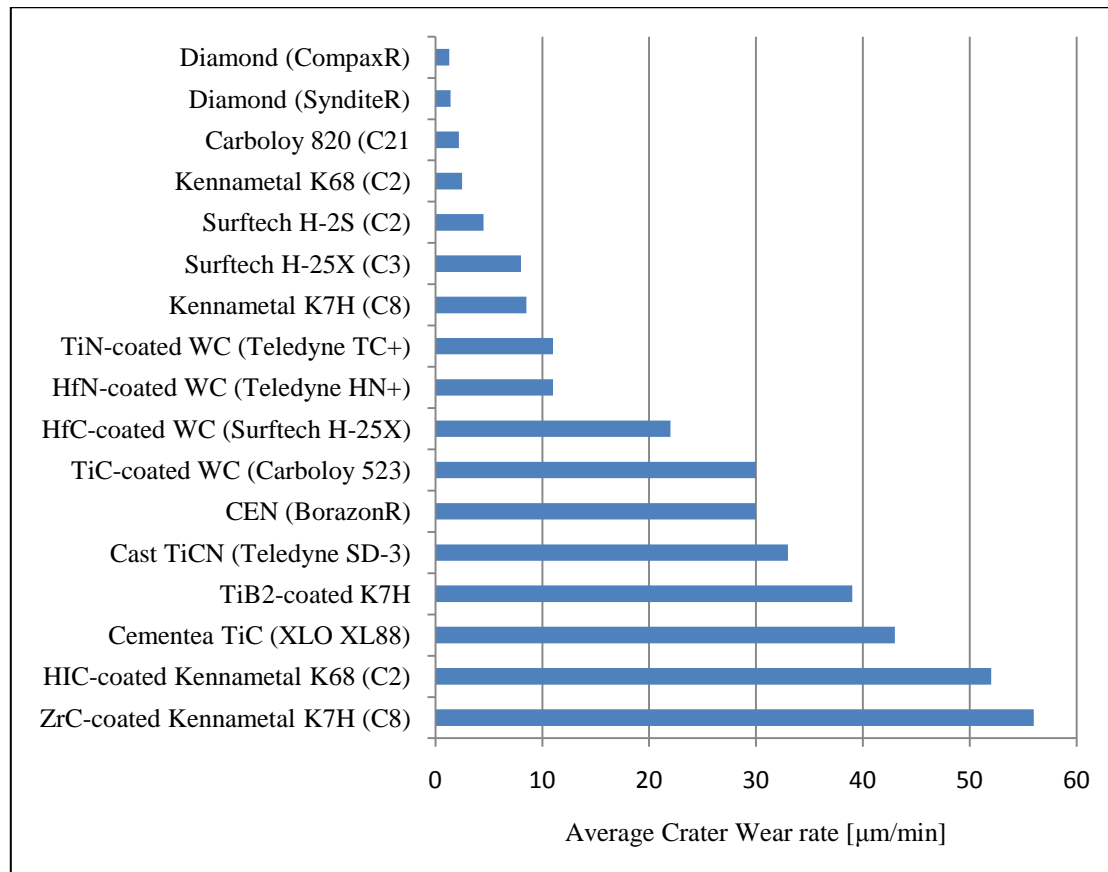
Crater wear is formed by the action of the chips sliding against the rake surface of the tool and mostly tribo-chemically removing the tool material on an atomic scale [40,20]. High temperatures and stresses characterize the tool-chip contact interface [48]. Most of the heat during the milling of Ti6Al4V is restricted in the primary zone [47]. Since the segment-just-formed rolls over and slides onto the rake face of the tool, during the upsetting stage of segmented chip formation, most of this heat is dissipated near the cutting edge. The resulting pattern is not conventional crater wear (see Figure 2.3 a), but rather the maximum crater depth occurs at what used to be the tip of the tool (see Figure 2.3 b) [49].



**Figure 2.3:** Location and shape of crater wear: a) conventional full wear away from the tool tip in machining steels and b) partial crater wear at cutting tool tip in the machining of Ti6Al4V [49]

In interrupted cutting at high thermal loads the tool material becomes more susceptible for catastrophic failure, due to the chipping of the cutting edge as a result of excessive crater wear [42]. It is expected for a tribo-chemical wear driven cutting environment that any reduction in crater wear will result in longer tool life [50,20].

Therefore, the comparison [19] of different crater wear rates [ $\mu\text{m}/\text{min}$ ] of different cutting tool materials was found to be interesting as illustrated in Figure 2.4.



**Figure 2.4:** The performance of various tool materials in the turning of Ti6Al4V [19]

It was found that when machining Ti6Al4V at  $v_c=61\text{m}/\text{min}$ , the PCD ( $1.4\mu\text{m}/\text{min}$ ) outperformed both Carbide ( $2.2\text{--}8\mu\text{m}/\text{min}$ ) and PCBN ( $30\mu\text{m}/\text{min}$ ). Research [42] shows that the rake face temperature is around  $900^\circ\text{C}$  ( $v_c=75\text{m}/\text{min}$ ) when machining Ti6Al4V; which causes rapid crater wear due to dissolution (mostly diffusion driven) [42,51,20].

### 2.1.3 Main wear mechanisms

A research study [51] indicates that the wear mechanisms brought into play when milling Ti6Al4V were diffusion and adhesion. Complementary other experiments [20] conclude that the main wear mechanisms machining this alloy include adhesion, diffusion and oxidation. They also made the remark that these mechanisms require a thorough study. According to Mishnaevsky [52] the mechanisms of tool wear can be classified as follow:

- *Mechanical wear*: Abrasive wear (roughnesses of contacting surfaces are cut, squeezed out or failed in friction), erosion, wear due to plastic deformation of surface layers, wear due to embrittlement of surface layers, fatigue wear (fatigue destruction of surface layers).
- *Molecular-mechanical wear*: Adhesion of contacting surfaces, which leads to the destruction of surface, layers of weaker material.
- *Corrosion wear*: Oxidation, Fretting and Diffusion

The mechanisms that cause wear at the tool-chip and tool-work piece interfaces in the milling of Ti6Al4V can be summarized as follows.

### **2.1.3.1 Abrasion**

As mentioned, abrasion wear happens primarily due to the hard grain orientations [16,14] in the Ti6Al4V alloy, which can act like hard inclusions in the work material. This mechanism normally occurs gradually on the flank (make it possible to estimate TL) during the break-in and initial part of the steady state wear regions. Thereafter the crater is weakened due to diffusion wear and crater formation also accelerated by the abrasion mechanism [43].

### **2.1.3.2 Adhesion**

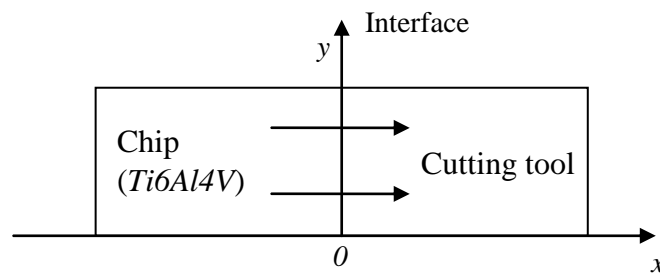
Adhesion is when two materials are forced into contact under high pressure and temperatures until they weld together. This results in attrition, as the sticky chips break away small particles on the surface [15] The critical temperatures for adhesion to occur during machining with PCD and CBN are 760°C and 900°C respectively and the nominal pressures approximately 0.142 and 0.146 GPa [51]. Adhesion of work piece material demonstrates a strong bond (no evidence of any gaps) at the work piece-tool interface, suggesting that seizure had taken place [49]. According to literature [53], adhesion takes place after the coating(s) has worn out or coating delamination has occurred when machining with coated carbide tools.

### **2.1.3.3 Diffusion**

A smooth wear scar on the flank- and rake face of the tool is an indication of diffusion wear [49,54]. Research [55] showed that high mechanical loads at conventional cutting speeds (similar to rough milling) the tool wear was mainly caused by abrasion and adhesion, but was dominated by a diffusion process at higher cutting speeds with low mechanical loads (similar to finish milling). Diffusion wear was also found for a cutting speed greater than 150 m/min in other experimental results [56]. These observations support the fact that diffusion is responsible for the crater wear on the rake face of the tool at elevated cutting speeds [57,58]. It is also supported by the fact that diffusion is controlled by

the cutting temperature [46] when particles move toward areas of low concentration [59]. Diffusion of the tool material at 700°C [60] supports the hypothesis to regard this temperature as critical for machining titanium alloys with CBN tools. Titanium can react with the Nitrogen in the CBN at temperature above 1100°C when inter-atomic diffusion of titanium and CBN accelerate significantly. This was confirmed [45] machining a titanium alloy with CBN and PCD tools. The cutting edge of the tool was bonded to the underside of the chips. Even at the lowest thermal load ( $v_c=55$  m/min with  $f_z=0.1$  mm/z), diffusion between the tool and the work piece material took place. Evidence of diffusion of cobalt and tungsten atoms into the work material was found with EDAX analysis on the adhered Ti6Al4V work piece at the flank- and rake face of the sectioned inserts [61]. Therefore, knowing that the diffusion mechanism plays a critical role in the corrosive tribo-chemical tool wear, studying this mechanism between Ti6Al4V and tool materials are required for a more comprehensive understanding of the mechanisms of diffusion. The chemical compatibility of WC-Co and PCD tool materials with Ti6Al4V have been evaluated by means of the static interaction diffusion-couples technique in this study.

If the boundary surface between the rake surface of the cutting tool and the chip are represented as a plane [62], the flow of elements has two major origins. The first one is diffusion between cutting tool and the chips; and the second one is the convective transport of material that moves on the tool surface [63]. As illustrated in Figure 2.5, in order to simplify the diffusion analysis at the tool–chip interface, it is assumed that the concentration gradient in the  $y$ -direction is small with respect to the gradient in the  $x$ -direction.



**Figure 2.5:** Coordinates in the tool–chip diffusion interface [59]

The diffusion flux and the concentration gradient ( $C$ ) vary with depth ( $x$ ) below the rake surface of the tool and with time ( $t$ ). According to Fick's second law [62], the concentration profiles for non-steady state diffusion can be expressed as follows,

$$\frac{\partial c}{\partial t} = \frac{\partial}{\partial x} \left( D \frac{\partial C}{\partial x} \right) \quad (1)$$

where,  $C$  is the concentration of material [ $\text{kg/m}^3$ ],  $x$  is the depth below the rake surface of the tool [m], and  $D$  is diffusion coefficient [ $\text{m}^2/\text{s}$ ]. To simplify the theoretical analysis of the diffusion process at the interface, we assume that the  $D$  is independent of chemical composition, eqn. (2) becomes

$$\frac{\partial c}{\partial t} = D \frac{\partial^2 C}{\partial x^2} \quad (2)$$

The concentrations of tungsten (W), carbon (C), and cobalt (Co) are held constant for the one-dimensional diffusion at the tool–chip interface. Table 2.1 illustrates the diffusion coefficient of the elements from the cutting tool into the Ti6Al4V work piece and chips.

**Table 2.1:** Diffusion coefficient of the elements from the cutting tool into the chip,  $R=8.315/\text{mol}\cdot\text{K}$  [64,38,65]

Elements	Frequency factor $D_0$ [ $\text{m}^2/\text{s}$ ]	Activation energy $Q_d$ [J/mol]	Diffusion coefficient $D$ [ $\text{m}^2/\text{s}$ ]
W	$2.475 \times 10^{-1}$	313,800	$D_w = 2.475 \times 10^{-1} \exp [-313,800/(RT)]$
Co	$9.0 \times 10^{-3}$	334,720	$D_{Co} = 9.0 \times 10^{-3} \exp [-334,720/(RT)]$
C	$1.5 \times 10^{-5}$	133,888	$D_C = 1.5 \times 10^{-5} \exp [-133,888/(RT)]$

The second-order partial differential diffusion equation requires two boundary or initial conditions to obtain a unique solution. These boundaries can be described as follow:

1. Initial state:  $C = 0$ , for  $x > 0$  and  $t = 0$ .
2. Boundary: At  $x = 0$ ,  $C_0$  is maintained for all  $t > 0$ .

Application of the above initial and boundary conditions to eqn. (3) yields the solution:

$$C(x,t) = \frac{C_0}{2} \left[ 1 - \operatorname{erf} \left( \frac{x}{2\sqrt{Dt}} \right) \right] \quad (3)$$

where,  $C(x, t)$  is the concentration at depth  $x$  after time  $t$ ,  $C_0$  is the initial concentration of tungsten, carbon and cobalt in tool material. The corresponding data used in eqn. (3) are listed in Table 2.1 [64,38,65]. The diffusion coefficient ( $D$ ) is assumed only a function of temperature but may change with time, as temperature gradually varies with time due to increasing wear. Furthermore, the diffusion rate of the constituents from the cutting tool into the chip is mainly determined by the concentration at the interface. From a thermodynamic and kinetic point of view, it is expected that the diffusion coefficient has a temperature-dependent Arrhenius [65] expression as per eqn. (4):

$$D = D_0 \exp \left( \frac{-Q_d}{RT} \right) \quad (4)$$

where,

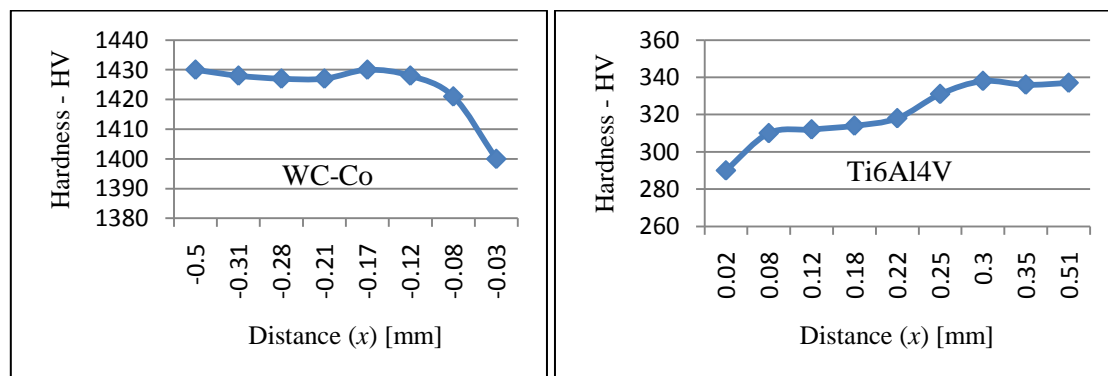
$D_0$  is a temperature-independent frequency factor [ $\text{m}^2/\text{s}$ ]

$Q$  is the activation energy for diffusion [ $\text{J}/\text{mol}$ ]

$R$  is the gas constant [ $8.315/\text{mol}\cdot\text{K}$ ]

$T$  is the absolute temperature [ $\text{K}$ ].

The activation energy is the energy required to produce the diffusive motion of one mole of the atoms. Relative large activation energy results in a relatively small diffusion coefficient (small diffusion flux). When time ( $t$ ), and depth ( $x$ ) are fixed, the final concentration  $C(x, t)$  depends on the initial concentration  $C_0$  and diffusion coefficient  $D$ . In a research study [46] the hardness near the interface of the diffusion couple was measured by Vickers indentation with a load of 10.0N for WC/Co carbide and 2.0N for Ti6Al4V. The Vickers hardness values along the interface of the diffusion couple are listed in Figure 2.6.



**Figure 2.6:** Hardness values along with the interface of the diffusion couple [46]

It is revealed that the Vickers hardness near the interface of the diffusion couple is lower than that far away from the interface. The hardness decreased owing to element diffusion [46].

### 2.1.3.4 Chemical reactions

Chemical wear (oxidation) is considered as a thermally activated process [66,30]. It's due to a reaction between the insert, the work piece and the surrounding elements. The rate of these chemical reactions increases with an increase in temperature, also resulting in the removal of the tool material on an atomic scale [40]. One of the most important physical properties of sintered PCD's is its resistance to oxidation. In cutting conditions where the tool is subjected to extreme cutting temperatures and relatively low pressure, sintered PCD undergoes irreversible changes. These irreversible changes include oxidation, grain boundary weakening, decrease in the density and

degradation of the mechanical tool properties. The reason for this is that at high temperature (above 950°C) and normal pressure the oxygen in the air diffuses into the PCD along the grain boundary; and the diamond is changed into graphite [19]. This oxidation (graphitization) can lead to a catastrophic form of wear on the flank of the tool, known as notch wear. Researchers [20] observed a notch at the limit of the cutting zone (situated a few tenths of millimetres from the tool nose) and realized that the cutting temperatures are close to those in the cutting zone (600°C-1000°C) [50,60], but the cutting pressures are significantly lower. This graphitization phenomenon was considered during the experimental design of the PCD-Ti6Al4V static diffusion-couples.

### **2.1.3.5 Thermal cracks**

Thermal cracks were found [24] with carbide tools in the finish milling of Ti6Al4V at cutting speeds of 152 m/min with flood coolant. Thermal cracking can be defined as the propagation of cracks on the surface of the cutting tool as a result of rapid temperature fluctuations [67]. As experienced in milling the cutting edges go through a cyclic heating and cooling process as the tool edge move in and out of the cut. As cutting speed (thermal load) is increased and is compensated for by means of higher power cooling, thermal shock can become predominant. Thermal crack development can be divided into following stages [44]:

1. *Comb-type* crack development initiate from the highest temperature zone on the rake face, then develop perpendicular to the cutting edge. These comb-type cracks have a close relationship with micro-chipping.
2. *Transverse crack* development initiates from a void or a comb-type crack and develops rapidly parallel to cutting edge.
3. *Crack crossing*. With the development of a transverse crack, its two ends reach two adjacent comb-type cracks.
4. *Tool fracture*. Closed cracks develop very fast under cutting conditions and cause fracture.

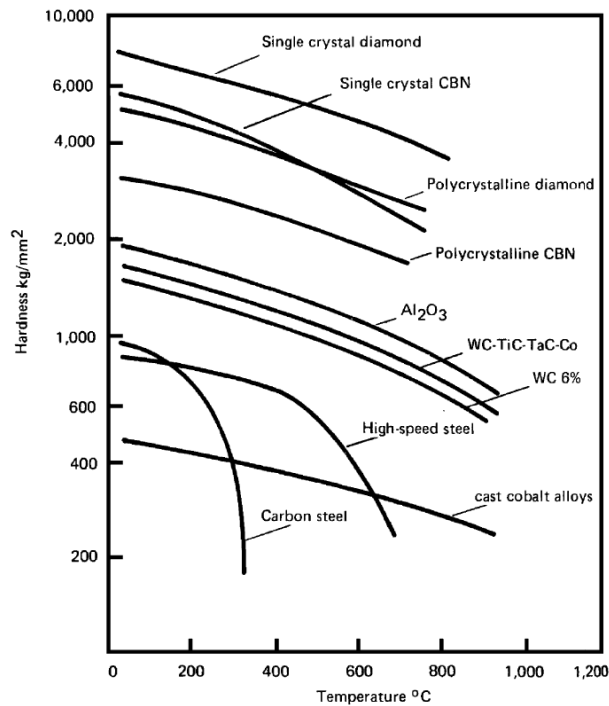
A research study [68] on the investigation of novel cooling methods for this alloy, found that gaseous cooling can be a promising technology to reduce thermal shock, but the placement (volume, location and directionality) of the gaseous cooling application onto the cutting tool still requires extensive investigation.

### **2.1.3.6 Plastic deformation**

In a research study [24] it was mentioned that most carbides exhibit plastic deformation with thermal loads in the excess of 60 m/min under rough milling conditions. The softening temperature (hot



hardness) [12] of commercially available cutting materials are illustrated in Figure 2.7. Most tools lose their hardness at higher temperatures, resulting in the weakening of the inter-particle bond strength [69].



**Figure 2.7** Typical hot hardness characteristics of some tool materials [12]

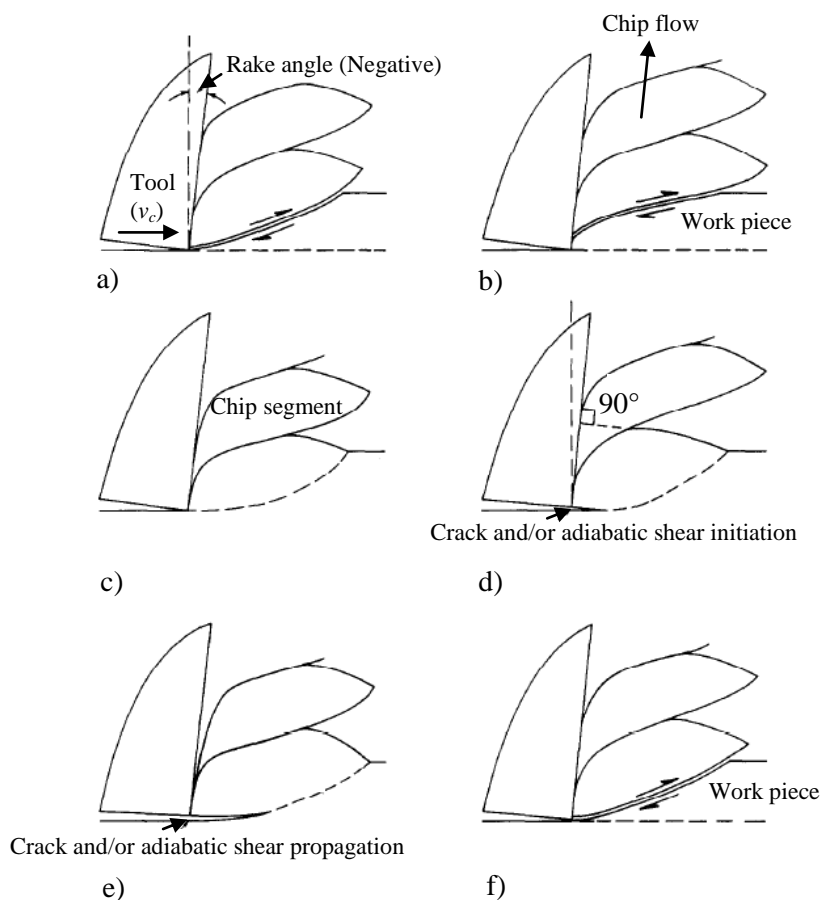
The forces acting on the edge at high temperatures cause the edge to deform plastically, which makes it more vulnerable to abrasion. Strong evidence of cracks and plastic deformation were found [48] under various cutting conditions that partly contributed to tool failure.

## 2.2 Segmented chips

Titanium alloys are known for the formation of *shear localised* [70,71] or *saw tooth* [23] chips. The term *segmented chip* is adopted in this paper, as it does not propound to the mechanism of chip formation. Segmented chip formation is believed to be due to either adiabatic shear band formation which is caused by the localized shear deformation resulting from the predominance of thermal softening over strain hardening [70,47,72]; or as a result of periodic crack initiation at the free surface of the work material ahead of the tool and propagation pathway toward the tool tip [73,74]. Another model [75,76] is based on an interesting phenomenon called strain softening. It has been introduced in a flow stress model in order to explain the segmented chip formation.

Komanduri [70,47] proposed the chip formation mechanism model (illustrated in Figure 2.8), that is consistent with most practical evidence in titanium machining. There are four possible cases of chip morphology arising from the shear localisation [77]. The first case corresponds to flow chip

morphology without shear localisation, due to any micro structural softening event. Merchant's model [78] applies to the first case with sliding tribology involving asperity contact at the tool-chip interface. Oxley's model [79] also applies to this case, but with the tribo-logical conditions of seizure involving atomic contact at the tool-chip interface. The second case is where shear localisation occurs only in the secondary shear zone and the third case is where shear localisation in the secondary shear zone is coupled to shear localisation in the primary shear zone. Komanduri [70] examined the fourth case which applies to shear localisation due to microstructural softening in the primary shear zone, but to the exclusion of shear localisation in the secondary shear zone. Figure 2.8 (a-f) illustrates the sequence of events, showing various stages involved in segmented chip formation according to Komanduri's segmented chip theory [70,47]. This sequence is based on the analysis of the videos of the chip formation process inside the scanning electron microscope.

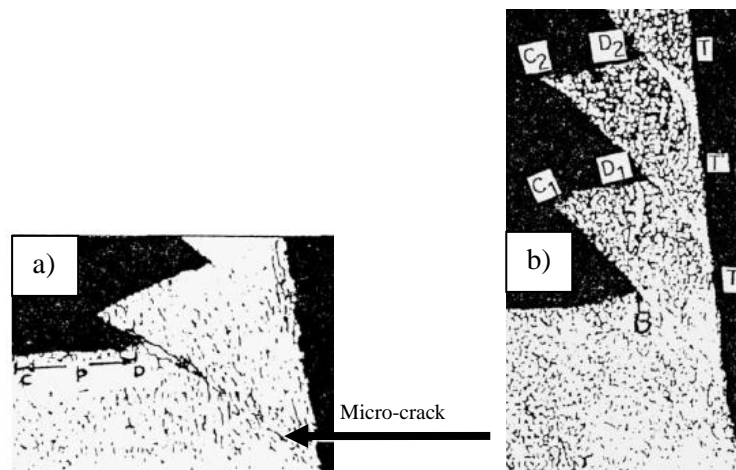


**Figure 2.8:** Schematic illustration of a sequence of events, showing various stages involved in segmented chip formation [80]

This mechanism of segmented chip formation in milling of Ti6Al4V, based on the occurrence of thermo-plastic instability within the primary shear zone, has been divided in two stages. The first stage involves the build-up of the segment with negligible deformation by the flattening of the wedge-shaped work material ahead of the advancing tool. The second stage involves plastic instability

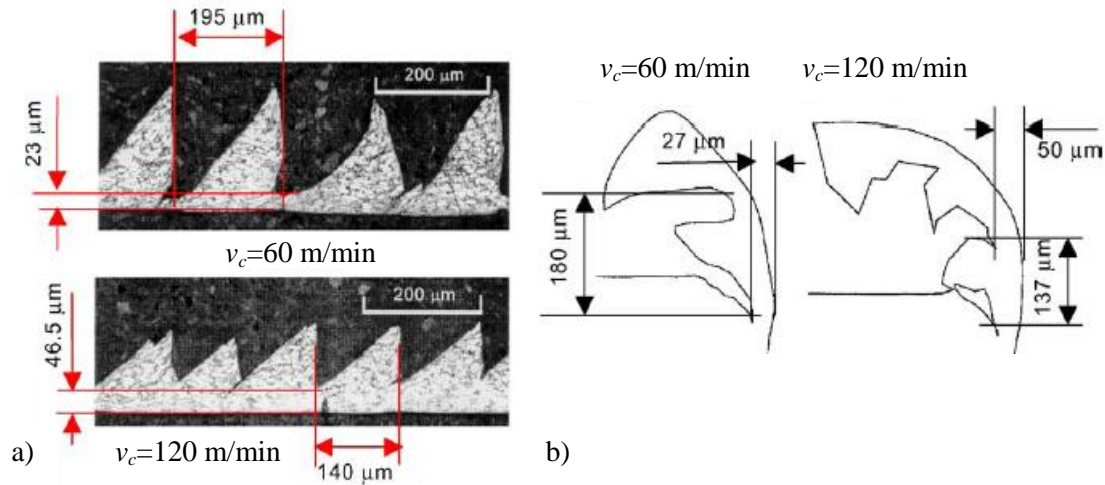
leading to strain localization along the shear surface, which originates from the tool tip parallel to the cutting vector and curves upwards until it meets the free surface [70,47].

Vyas and Shaw [73] maintain that segmented chips form as a result of periodic crack initiation at the free surface of the work material, ahead of the cutting tool with a propagation pathway towards the tool tip. As illustrated in Figure 2.9 it appears that the principal evidence to support this theory is the observation of cracks within titanium quick-stop specimens. However, the fact that tensile stresses evolve during the period of tool retraction in quick-stop tests was not considered [72]. Often, the magnitude of such stresses is sufficient to cause fracture within the cutting tool [37,72].



**Figure 2.9:** Quick-stop photomicrographs of Ti6Al4V chips a) shortly after formation of gross crack at free surface and b) about halfway between cyclic cracks [73]

Shivpuri's [75,76] periodic prediction of chip morphology is based on an implicit (Lagrangian), non-isothermal rigid-viscoplastic finite element simulation of orthogonal machining of Ti6Al4V, in which a dynamic flow stress model based on high strain rate and high temperature. A ductile fracture criterion based on the strain energy is applied to the crack initiation during the chip segmentation. This model is verified with dimension of the chip geometries gained from experimental results as illustrated in Figure 2.10.



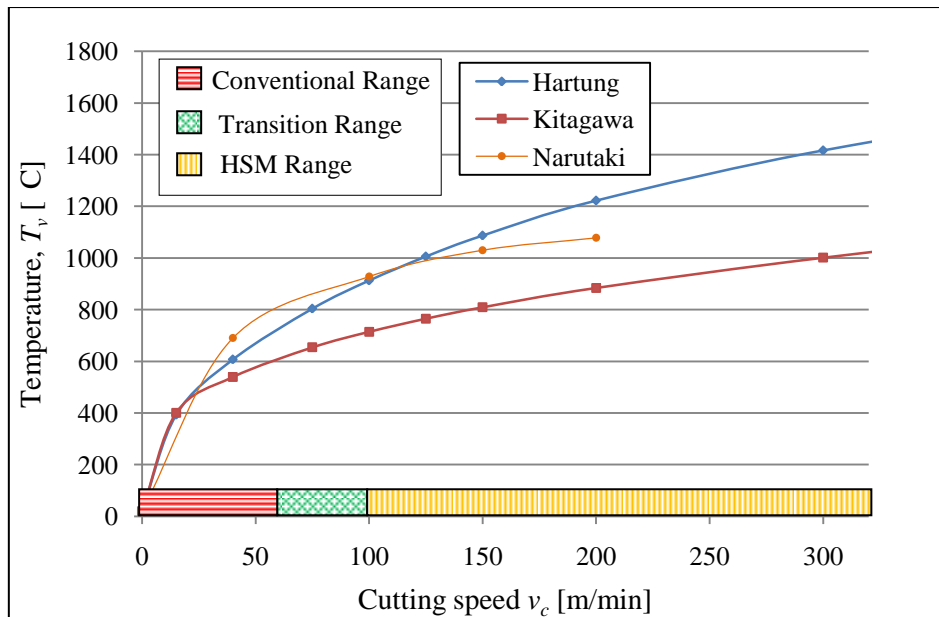
**Figure 2.10:** Chip morphology of a) experimental results and b) simulation results [75,76]

The simulation results [75,76] indicate that as the cutting speed is increased, the stress state near the tool tip changes, leading to the crack propagation shifting from the tool tip to the free surface of the deformed chip in the shear zone of the work piece.

Nevertheless the mechanism behind segmented chip formation results in a cyclic variation of the different force components (both cutting and thrust) [75]. The consequent vibration or chatter [22] in the milling process [47] limits the material removal rate; and makes the cutting edge susceptible to catastrophic tool failure. The significance of the magnitude in this variation is compared in this research study with the effect of the frictional phenomena between the chip, work piece and cutting tool. The characteristics of chip morphology can also provide useful information for simulation models and tool design.

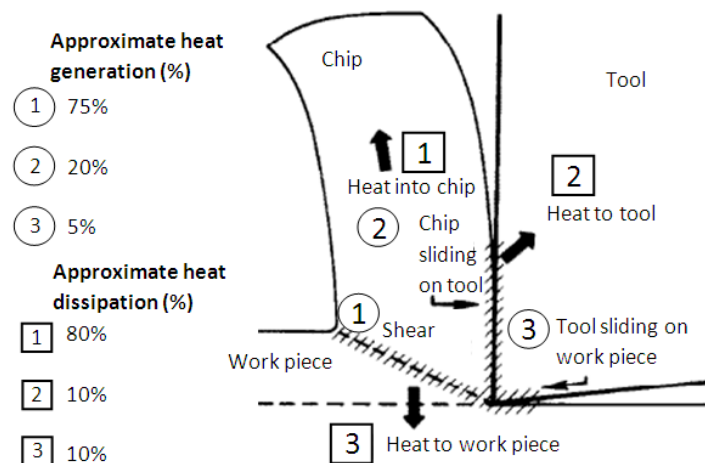
### 2.3 Cutting temperature

Ti6Al4V has high strength at high temperatures [25], a low thermal conductivity [15] and elasticity [14]. These properties together with the high frictional phenomenon between the cutting edge and the material [34], leads to a strong increase in the magnitude of the thermal load. In milling operations the tool is exposed to force fluctuation, and cyclic heating and cooling as the tool enters and exits the work piece. Although the temperatures measured in milling are found to be lower than those found in turning, the tool surface temperature ( $T_v$ ) demonstrated in Figure 2.11 from various research studies [19,81,41], is useful to identify the properties required for the tool.



**Figure 2.11:** Tool face temperatures machining Ti6Al4V relative to cutting speed (Adapted from [19,81,41])

The objective is to increase the  $v_c$  as high as possible without adversely affecting the surface integrity of the Ti6Al4V component. In view of the exposure time ( $\tau$ ) to these surface temperatures, it is critical to realize that the longer the duration of the exposure time, the higher the volume of the edge is exposed to harsh conditions. As illustrated in Figure 2.12, according to the traditional continuous-chip theory, heat is generated in three zones: the primary shear zone, the secondary shear zone and the interface between the flank and the machined surface [37].



**Figure 2.12:** Continuous chip formation: Heat generated and dissipated in continuous chip formation (Adapted from [70])

The specific energy flowing into the produced chip ( $U_c$ ), the cutting tool ( $U_t$ ) and the work piece ( $U_w$ ) are functions of the work piece shear ( $U_s$ ) and the friction ( $U_f$ ) energy from the sliding of the chip on the rake face of the cutting tool.  $R_1$  and  $R_2$  are the percentage (%) of heat to the chip from the shear-

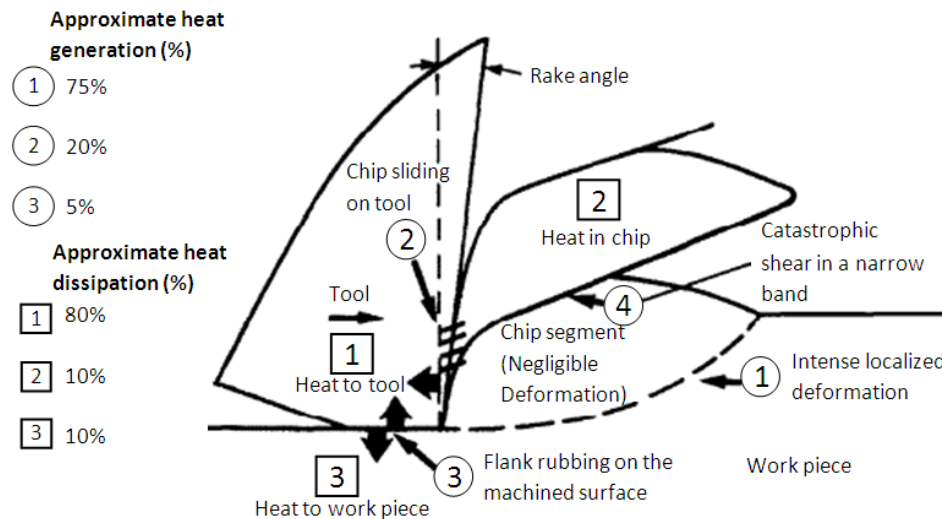
plane- and tool-chip interface respectively. Heat transferred on the flank of the tool sliding on the work piece may be neglected for sharp (new) tools.

$$U_c = R_1 U_s + R_2 U_f \quad (5)$$

$$U_t = (1 - R_2) U_f \quad (6)$$

$$U_w = (1 - R_1) U_s \quad (7)$$

Figure 2.13 illustrates the energy partition found in literature [70] for segmented chip formation. From eqn. (6) there is no contribution of heat to the tool from the primary shear zone, or from rubbing between the flank and the work piece. Owing to rapid flank wear and almost no secondary deformation on the rake face, the significance of zones 2 and 3 when milling Ti6Al4V is unlike that for materials yielding continuous chips.



**Figure 2.13:** Segmented chip formation: Heat generated and dissipated in segmented chip formation (Adapted from [70])

A significant amount of heat is generated at the clearance face, due to the rubbing between the flank of the tool and the work piece. The chip sliding against the rake face is found to generate an insignificantly small portion of heat ( $U_f$ ); and therefore the energy partition for titanium alloys are represented by the following equations:

$$U_c = R_1 U_s \quad (8)$$

$$U_t = (1 - R_1) U_s + R_3 U_{ff} \quad (9)$$

$$U_w = (1 - R_3) U_{ff} \quad (10)$$

where  $U_{ff}$  is the frictional energy per unit volume, due to the rubbing between the flank face of the tool and the work piece.  $R_3$  is the percentage of heat that is conducted into the cutting tool, due to the frictional phenomenon found at the flank face of the tool.  $U_f$  and  $R_2$  are assumed negligible since little secondary deformation at the chip-tool interface was observed. Heat input to the tool material [Eqn. (5)] combines the heat generated by the shear-failed surface and by the frictional phenomenon found between the flank face of the cutting tool and the work piece. Most heat generated in the shear band remains there and consequently its contribution to the work piece may be neglected.  $U_{ff}$  generates the only heat into the work piece in this type of chip formation.

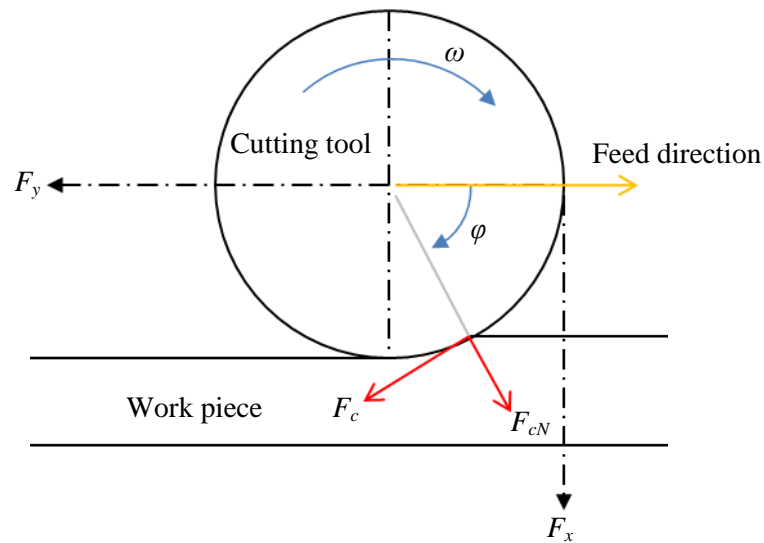
Comparing the equations for continuous chip formation [Eqn. (5) to (7)] with those for segmented chip formation [Eqn. (8) to (10)] the differences in heat partition are evident. This is consistent with some practical experience in that the heat removed in the segmented chips is known to be small, while the heat percentage removed by the cutting tool is found to be larger [69]. Conversely, the adhesive frictional phenomena and the separation of the chip from the rake of the tool were found to have significantly larger effect on the pulsating loads than chip shearing. These results are discussed in Chapter 6.1.

## **2.4 Cutting forces**

Cutting is a process of extensive stresses and plastic deformations, in which the high compressive- and frictional contact stresses on the cutting tool, result in the cutting force [66]. Ti6Al4V milling is characterised by an unusually small contact area where the chip is in contact with tool face [25]. The analysis of cutting force helps to determine the effect of altering certain cutting parameters. Cutting forces are mainly determined by the maximum un-deformed chip thickness ( $h_{eMax}$ ), the cutting speed ( $v_c$ ) and the average flank wear ( $V_B$ ).

A sound knowledge about the correlation between cutting force component variation and tool wear propagation can be vital to monitor and optimize the automatic manufacturing process. Exploring this correlation can be of great importance to the development of an effective tool condition monitoring strategy [82].

Figure 2.14 is a schematic view illustrating the different force components in a two dimensional view.



**Figure 2.14:** Schematic illustration of force components in a shoulder milling process

The entry angle of the cutting tool in the down milling operation, starting from the negative y-axis could be expressed by eqn. (11):

$$\varphi_{st} = 90^\circ - \cos^{-1}[(r - a_e) / r] \quad (11)$$

Once the force components in the x-, y- and z-directions were measured with a dynamometer,  $F_c$ ,  $F_R$  and  $F_a$  could be expressed by the following transformation [83], with  $\varphi_{st}$  being the entry angle and  $\varphi_{ex}$  the exit angle of the cutting tool

$$\begin{bmatrix} F_c \\ F_{cN} \\ F_a \end{bmatrix} = \begin{bmatrix} -\sin\varphi & \cos\varphi & 0 \\ \cos\varphi & \sin\varphi & 0 \\ 0 & 0 & 1 \end{bmatrix} \begin{bmatrix} F_x \\ F_y \\ F_z \end{bmatrix} \quad \text{when } \varphi_{st} < \varphi < \varphi_{ex} \quad (12)$$

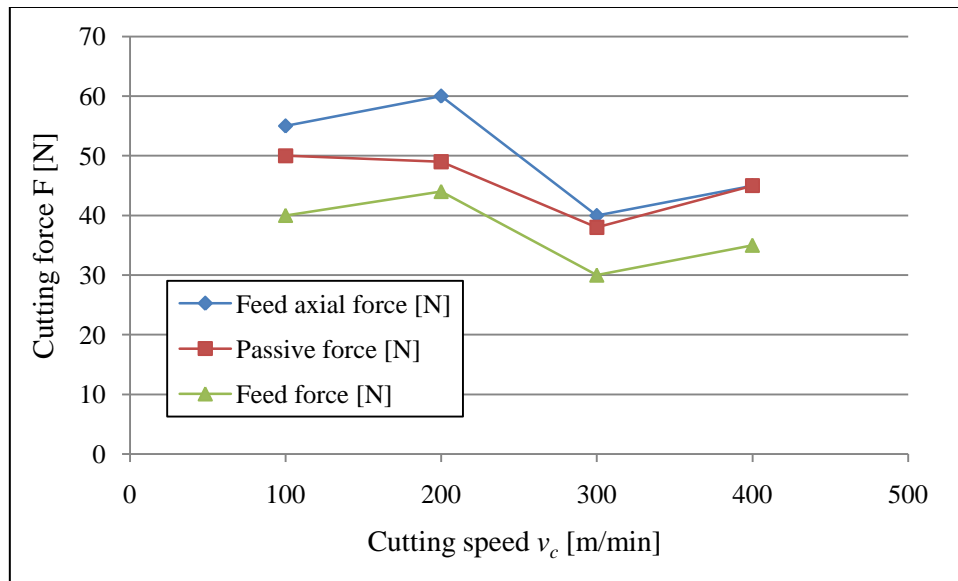
The single-tooth functions for partial cut (in which  $a_e < \varnothing$ ) are obtained simply by equating the relevant parts to zero. The cutting force components for a multi-tooth cutter are then calculated by summing eqn. (12) into eqn. (13):

$$F_{js}(\varphi) = \sum_{i=1}^z F_{ji}(\phi) \quad (13)$$

where  $F_{js}(\varphi)$  is the total force on the cutter in the  $j$  direction, as the leading tooth is at  $(\varphi)$  angle of rotation, with  $j=xyz$  and  $F$  as the functions of the different teeth lagging at a  $360^\circ/z$  (e.g.  $120^\circ$  for  $z=3$ ) behind each other. In literature [84] a clear minimum of all cutting force components is discovered when finish milling titanium with  $v_c=300$  m/min. The different force components are illustrated in



Figure 2.15. The passive force is represented by  $F_z$ ; and the feed axial- and feed force are represented by  $F_y$  and  $F_x$  respectively.



**Figure 2.15:** Cutting forces finish milling at elevated cutting speeds ( $v_c=100-400$  m/min) [84]

In another study [85] the authors studied the specific cutting force relative to cutting speed ( $v_c$ ) for different mechanical loads ( $h_{eMax}$ ). One of the most important objectives in manufacturing is the intelligent machining system. To come to such a solution, the tool wear has to be determined on-line during the cutting process on unmanned machining systems. The  $F_c$  should be measured for set cutting intervals and the tool wear ( $V_B$ ) measured throughout these intermissions. The flank wear land width  $V_B$  was measured by using the optical microscope after every run of the tool [86]. In general the cutting force and the power increase when the tool wear  $V_B$  increases. According to experimental work [87] there is a power increase of approximately 20–22%, when the tool is worn, in comparison to the power when the cutter is sharp. According to literature [88] with the analysis of variance of the mean cutting force ( $MF_c$ ), it is possible to develop a force model to investigate the effects of  $V_B$ . The  $MF_c$  during an operation is the product of the mean cutting force when the tool is sharp ( $MF_{c0}$ ) and the effect of  $V_B$  on the cutting force as per eqn. (14):

$$MF_c = MF_{c0} \times f(V_B), f(V_B) \geq 1 \quad (14)$$

The ratio of the actual mean cutting force ( $MF_c$ ) and of the mean cutting force when the tool is sharp  $MF_{c0}$  is the Normalized Cutting Force indicator ( $NCF$ ) [88] as per eqn. (15):

$$NCF = \frac{MF_c}{MF_{c0}} \quad (15)$$

In a research study [88] statistical analysis proves that 96% of the total variance of *NCF* is due to tool wear and that cutting conditions do not have an effect on *NCF*. However, tool wear has a significant effect on *NCF* indicator.

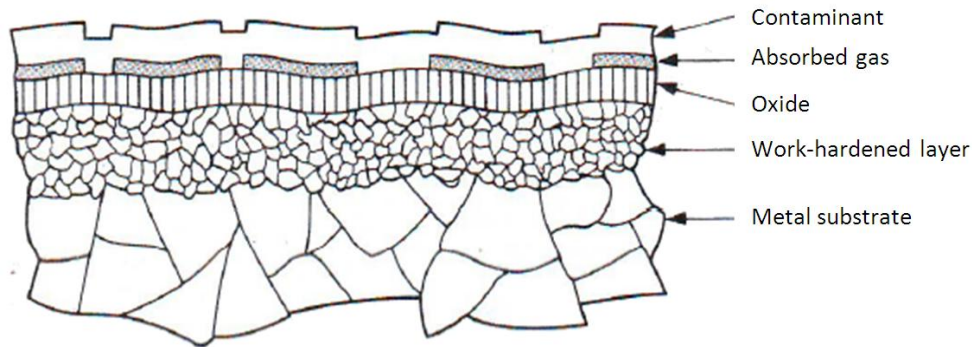
Still, only a few published articles [25,89] explore the variation in the dynamic cutting force components. Together, such results with research on the variation in both frequency and amplitude of these force components can form key to understand segmented chip formation and tool wear mechanisms. Research studies should be aimed to increase the understanding of the result in cutting force, with a change in  $v_c$  and  $h_{eMax}$ . There are also only a few [88] studies on the correlation between cutting force variation and tool wear propagation.

## **2.5 Surface integrity**

Since Ti6Al4V is used in the aerospace industry the characteristics of the machined surface have to conform to aerospace regulations [90,34]. If the work piece is exposed to oxygen and nitrogen at high temperature (high  $v_c$ ), these elements will diffuse into the base material and make the components brittle. This could lead to failure of the component before the end of its life [14,16]. Both oxygen and nitrogen stabilize the  $\alpha$ -phase and create a so called  $\alpha$ -case, on the surface of the work piece. This forms part of the effect known as *material burn* and a test called ‘Blue Etch Method’ has been developed [90] to detect the brittle parts. An anodization of the work piece in a Tri-sodium phosphate solution, followed by a partial removal of the anodized layer shows areas of alpha and beta segregation, and excessive grain growth [14,16].

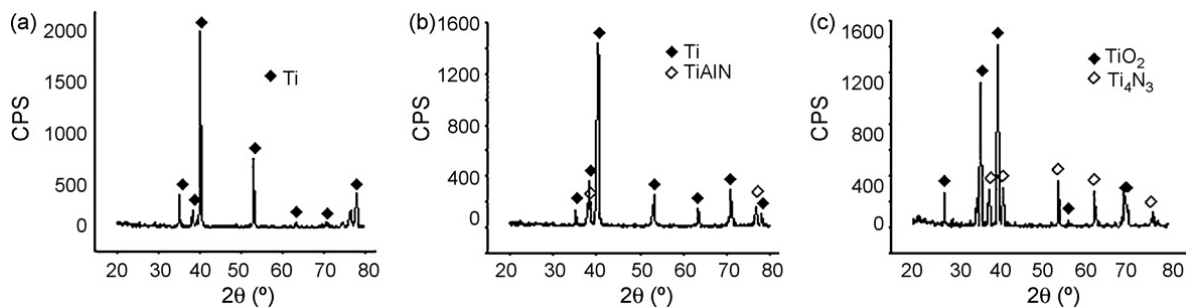
Surface integrity involves the outermost surface layers of a machined Ti6Al4V component. It consists of topography effects such as surface roughness ( $R_a$ ), changes in the metallurgy (phase transformations and inclusions) and the introduction of other surface layers such as oxides and contaminants. Mechanical effects such as voids and cracks; and deformation layers that influence the mechanical property changes (typically hardness) also play a role. These together with electrical (changes in conductivity) effects may be interrelated with one another, and have a major influence on the failure of the work piece [91].

As illustrated in Figure 2.16 assessment of a machined surface generally shows that it consists of multiple layers.



**Figure 2.16:** Typical cross section of a machined surface (Adapted from [92])

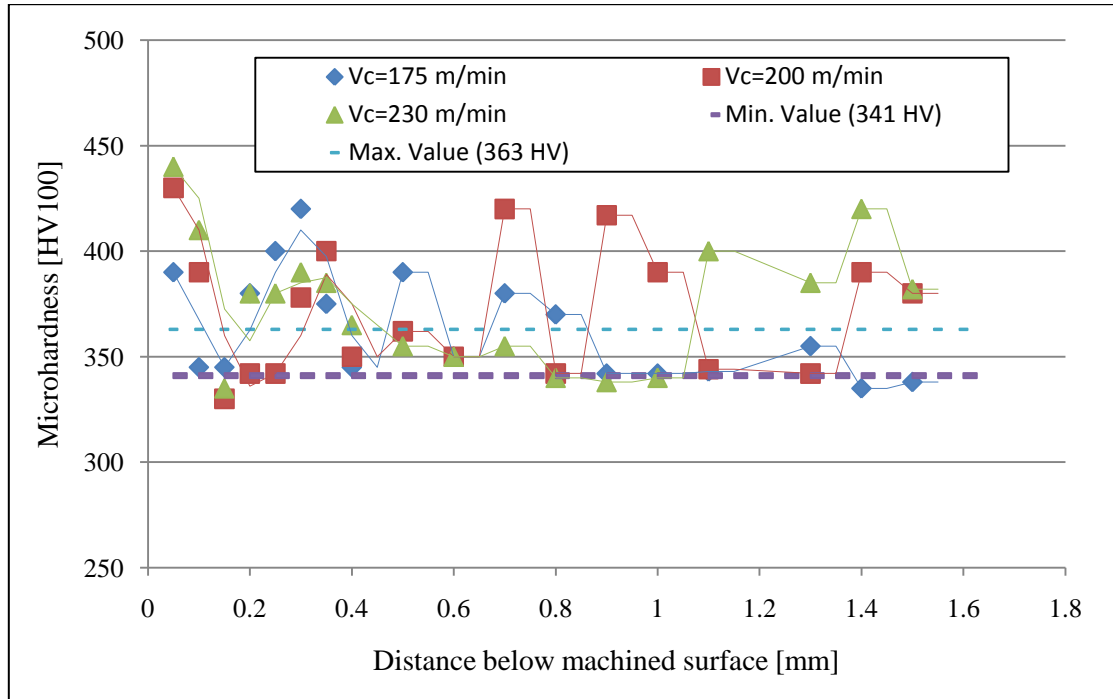
The depth and the properties of the work-hardened layer that lies above the substrate are a result of the milling conditions. Residual stresses occur in this layer of the surface, if the material is subjected to non-uniform deformation or severe temperature gradients [91]. A very thin oxide film, which is always created on a Ti6Al4V surface, forms above the work-hardened layer [93]. These oxide layers are generally much harder than the substrate making oxides brittle and abrasive [91]. If the  $\alpha$ -case exists, it is formed beneath this very thin oxide film. The  $\alpha$ -case formed is the base material with an exceptionally high oxygen content (up to ~10 wt. %) [94]. In a research study [46] Ti6Al4V samples were heated in air atmosphere for 90 minutes at 400°C, 600°C and 800°C. As illustrated in Figure 2.17 (c) no trace of Ti was found in the surface of the Ti6Al4V sample after heating it at 800°C, while TiO<sub>2</sub> and Ti<sub>4</sub>N<sub>3</sub> newly formed phases were detected with x-ray diffraction analysis.



**Figure 2.17:** X-ray diffraction analysis of the Ti6Al4V alloy after heating in air atmosphere for 90 min at (a) 400°C, (b) 600°C, and (c) 800°C [46]

This is primary due to the oxidation of Ti6Al4V and the reaction of Ti with the N in air. No oxidation took place at 400°C, but after heating at 600°C there are newly formed phases (TiAlN), which may be the result from the reaction of Ti, Al and N in air. This was taken into consideration with the experimental design for the experiments. Ezugwu et al. [95] investigated the surface integrity of a Ti6Al4V work piece after finish machining it with PCD tools as illustrated in Figure 2.18. The cutting speeds ranged from 175-230 m/min and conventional flood coolant was used. The surface roughness

( $R_a$ ) was found to be well below the work piece failure criteria of  $R_a=1.6\mu\text{m}$ . Similar results were found in other background studies [69] and other research work [91]. Micro-hardness analysis showed hardening of the top-machined surface and the microstructure below machined surface had minimum or no plastic deformation for this cutting speed range [95].



**Figure 2.18:** Hardness variation after machining Ti6Al4V with PCD tool material with a feed rate of 0.15mm/rev and depth of cut of 0.5 mm under conventional flood coolant [95]

Micro-pits and re-deposited work piece material were found to be the main factors behind surface damage. Micro-hardness analysis showed hardening of the top-machined surface and the microstructure below machined surface had minimum or no plastic deformation.

At a low cutting temperature the equilibrium spacing between the titanium atoms is less than the space required for the oxygen and nitrogen atoms to penetrate. As the temperature rises (increasing  $v_c$ ), the distance between the Ti6Al4V atoms will increase. This leads to easier penetration of oxygen and nitrogen into the Ti6Al4V. The hardness of the surface can reach over 1000 HV. In another research study [34] with PCD cutting tools the resulting surface finishes were inspected with the ‘Blue etch method’ for various cutting speeds ( $v_c=50-550$  m/min) to establish the thermal load limit. It was found that all test pieces milled at  $v_c$  above 300 m/min showed signs of *material burn*. This corresponds well with results [91] from another study. Therefore, due to the safety regulations, the high speed machining (HSM) process is currently limited to a cutting speed of 300 m/min. Results from literature [91,95,92] also made it clear that the heat treatment condition plays an important part and should be taken into account. Refer to Appendix D for a summary of the different categories of Altered Material Zones (AMZ’s).

### 3. Integration of current understanding of milling Ti6Al4V

As new cutting tool materials emerge, they may possess the properties to succeed in niche areas hitherto unexploited. The objective of this section is to expand ISO 513, the standard covering hard cutting tool materials. It can be achieved by illustrating the physical demands on the tool material in the rough- and finish milling of Ti6Al4V, other than simply *toughness* and *wear resistance*. This understanding of the demands enhances this process of continuous improvement in the development of innovative cutting tools for titanium alloys. There are several ways to classify metal-cutting applications. The most obvious is to classify the application by process type (e.g. milling). In order to support wear characterization this does not adequately capture the demands on the cutting tool material in terms of toughness and wear resistance. It is the Ti6Al4V work piece material that largely determines the behaviour of the tool materials during milling; and it is therefore the work piece materials that are the basis for the International Standard for the ‘Specification and Application of Hard Cutting Tool Materials’ (ISO 513:2004).

The term *toughness*, as used in ISO 513:2004, should be interpreted not necessarily as the engineering quantity, *fracture toughness* (Refer to Appendix C for a comparison of the different cutting tool properties), but more so as the resistance to chipping [40]. Likewise, *wear resistance* does not refer to the wear resistance to a specific wear mechanism. It is worth noting that any attempt to standardise cutting tool materials on the basis of composition and/or microstructure would be largely erroneous; not only because materials exhibit complex behaviours, but also because other factors such as cutting edge geometry and coatings can influence tool performance. This is particularly true for Carbides and PCD tool materials, where it also encompass a very large number of compounds and microstructures [28]. Notwithstanding these limitations, ISO 513:2004 is considered a valuable system for classifying the enormous range of processes and materials in use today. The system’s utility is evident in the fact that it has been adopted by all major suppliers of cutting tools [40].

The main issues considered in this section for the different demands are summarized and highlighted in Table 3.1. The objective of any cutting tool material is to resist plastic deformation and/or brittle fracture under the mechanical loads. Only when these criteria are fulfilled, does the notion of wear resistance assume any importance. If non-catastrophic tool failure for a given mechanical- and thermal load can be guaranteed with a high confidence level; optimizing work piece related (tool life in a Taylor fashion) failure inside these bounds becomes the only concern.

**Table 3.1:** Summary of the physical demands milling Ti6Al4V

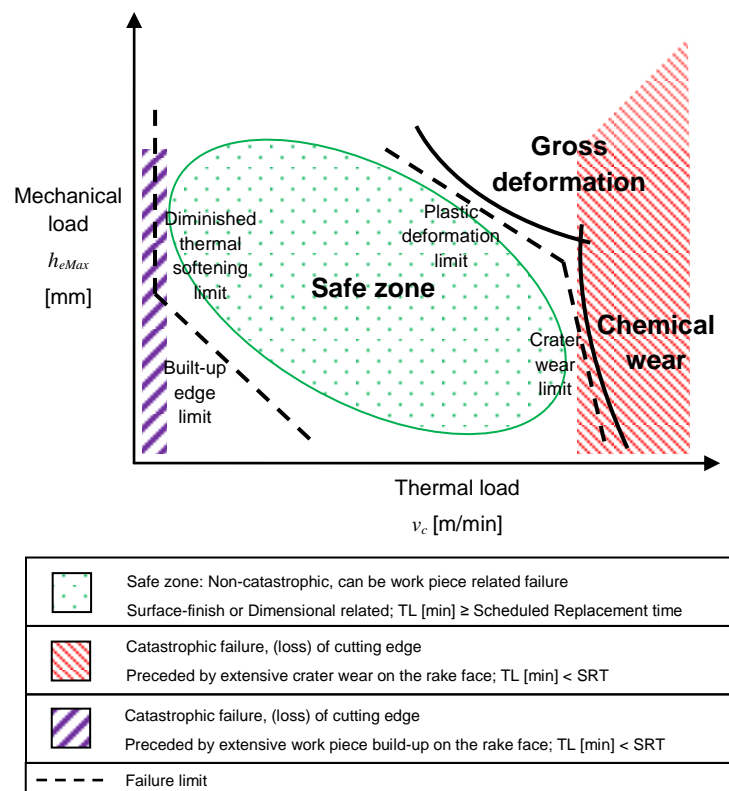
<i>Demand</i>	<i>Issue</i>	<i>Factor</i>	<i>Section</i>
Thermal	<i>Thermal load</i>	Cutting speed ( $v_c$ ) represents the magnitude of the thermal load	3.1.1

	<i>Exposure time</i>	Cutting speed ( $v_c$ ) and the ratio of radial immersion over tool diameter ( $a_p/\phi$ %) represents the exposure time to the thermal load	3.1.2
	<i>Thermal shock</i>	Thermal shock resistance factor ( $R_T$ ) represents the feature which parameters need to be maximized to avoid catastrophic chipping	3.1.3
Mechanical	<i>Mechanical load</i>	The mechanical load is a function of the maximum un-deformed chip thickness ( $h_{eMax}$ ) and the chip thinning factor ( $\kappa_r$ ) due to cutting insert geometry	3.2.1
	<i>Vibration</i>	Chatter and the forced vibrations due to chip formation, frictional phenomena and to more than one insert in cut are discussed	3.2.2

Currently it is virtually impossible and quite impractical to measure or model the stress distribution in the cutting edge [40]. This section describes the physical demands on the tool material and explains the most influential issues of these demands. This section also examines the effects of the different cutting parameters on the mapping of the tool failure limits.

### 3.1 Thermal demands

As discussed in section 2.1, chemical or more accurately ‘tribo-chemical’ wear may be considered a thermally activated process, whereby the Ti6Al4V and tool material react in such a manner as to remove material from the tool on an atomic scale [40]. Figure 3.1 illustrates the minimum and maximum thermal load limits for the cutting tool materials.



**Figure 3.1:** Tool failure constraints of tool due to the thermal demands on the cutting tool

As illustrated in the figure, the cutting tool will fail catastrophically when  $v_c$  is too low due to diminished thermal softening; or when the  $v_c$  is too high due to chipping preceded by extensive crater wear. As discussed in section 2.5 the thermal load ( $v_c$ ) is currently limited to 300 m/min in order to prevent *material burn*, due to the safety regulations. The effects that the thermal load, exposure time, thermal shock and milling strategy have on the thermal demands are discussed.

### 3.1.1 Thermal load

The tool face temperature ( $T_v$ ) in milling is generated as a function of  $v_c$ ; and will also determine the resistance to deformation of the work piece [37]. Temperature versus  $v_c$  is usually modelled as a power law relationship, which may rise to infinity with an increase in the cutting speed [20]. This is acceptable for interpolating temperature at conventional (rough) milling, but for high speed (finish) milling the  $T_v$  may approach the melting point ( $T_m$ ) of the work piece. Any  $T_v$  model suitable for High-Speed Machining (HSM) must limit the maximum cutting temperature to the  $T_m$  or a significant fraction thereof. Although data [19,81,41] of the temperatures for the machining of Ti6Al4V are limited, finding data for  $v_c > 200$  m/min is even more difficult. Research [40] and experience indicates that in purely interrupted cutting (milling), the temperatures generated are significantly lower than in continuous cutting operations (turning) under nominally the same conditions. Finish milling (more associated with HSM) may be defined as the  $v_c$  [96] range that will produce a tool-face temperature ( $T_v$ ) in the excess of  $1000 \pm 200^\circ\text{C}$  (Refer to Figure 2.11); and is used as reference temperature for PCD ( $T_{cPCD}$ ). Rough milling (more associated with HPM) [97] may be defined as the cutting speed range that will produce a tool-face temperature in excess of  $650 \pm 100^\circ\text{C}$  (Refer to Figure 2.11); which is used as reference temperature for carbides ( $T_{cCarbide}$ ).

### 3.1.2 Exposure time

In milling it is necessary to consider not just the severity of the thermal- and mechanical loads, but also the maximum period of engagement between the tool and Ti6Al4V work piece. Therefore, the tool temperature is not solely the  $T_v$ , but of equal importance is the exposure time ( $\tau$ ) of the tool material to and above critical temperature ( $T_c$ ) at a certain depth level below the surface. Stated concisely, it is the volume of the cutting edge that is exposed to the degrading (e.g.  $T_c = 800 \pm 100^\circ\text{C}$  [25]) conditions. The sweep angle ( $\beta$ ) is a function of the tool diameter ( $\phi$ ) and radial immersion ( $a_e$ ) as per eqn. (16).

$$\beta = \cos^{-1}\left(\frac{r - a_e}{r}\right) = \cos^{-1}\left(1 - \frac{a_e}{r}\right) \quad 0 < a_e < \frac{\phi}{2} \quad (16)$$

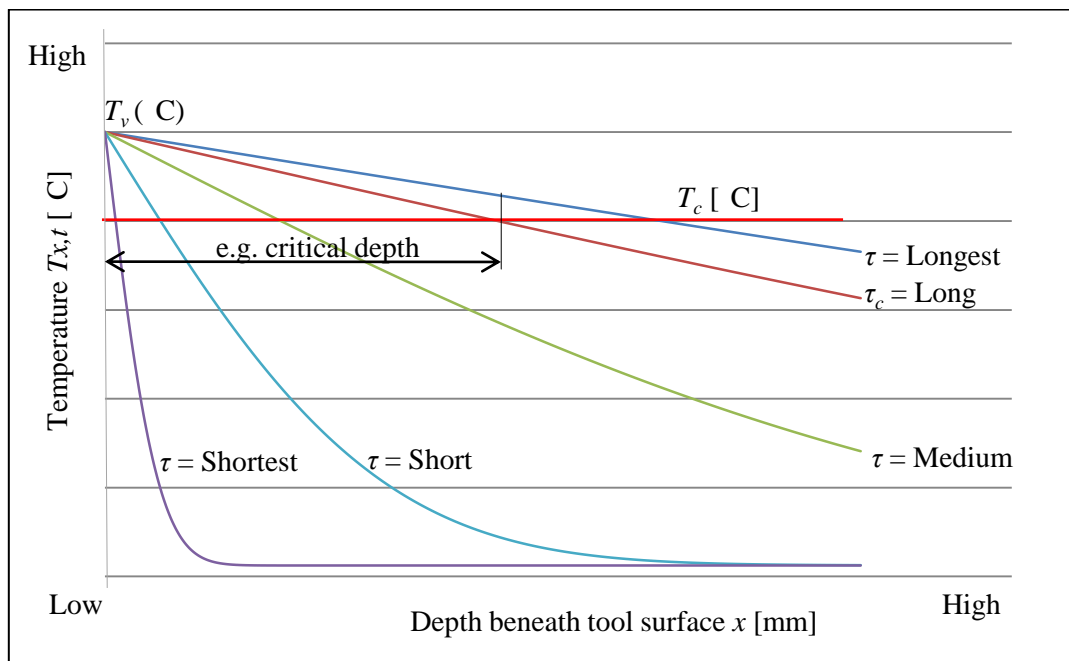
From eqn. (16) it is straightforward to convert the sweep angle ( $\beta$ ) to the sweep distance ( $\delta$ ) by multiplying  $\beta$  with pi ( $\pi$ ) and the tool diameter ( $\phi$ ). The exposure time ( $\tau$ ) is a function of sweep distance ( $\delta$ ) and cutting speed ( $v_c$ ) as per eqn. (17).

$$\tau = \frac{\delta}{v_c} = \frac{\pi\phi\beta}{360v_c} \quad (17)$$

Hence,  $\tau$  is a function of  $a_e$ ,  $\phi$  and  $v_c$ . The effect of the imposed temperature ( $T_v$ ) over time will increase the temperature in the body of the insert ( $T_{x,t}$ ) as per eqn. (18):

$$\frac{T_{x,t} - T_v}{T_i - T_v} = \text{erf}\left(\frac{x}{2\sqrt{\gamma\tau}}\right) \quad (18)$$

The effect of the equation is shown in Figure 3.2, where  $T_i$  is the initial insert temperature,  $x$  the distance beneath the tool surface, and  $\gamma$  is the thermal diffusivity ( $\gamma_{\text{Carbide}}=20 \times 10^{-6} \text{m}^2/\text{s}$  and  $\gamma_{\text{PCD}}=250 \times 10^{-6} \text{m}^2/\text{s}$ ) of the insert. The influence of temperature, due to the thermal load ( $v_c$ ) and duration of exposure to this temperature, on tool wear can be summarized as follows. For a given  $v_c$  a specific amount of heat is generated which defines the tool face temperature ( $T_v$ ). The maximum time (critical depth  $x$ ), that a point within the insert may remain at the  $T_c$ , will be noted as the critical exposure time ( $\tau_c$ ) for a surface exposure to  $T_v$ . The effects (temperature profiles) of different exposure times ( $\tau$ ) for a specific  $T_v$  are illustrated in Figure 3.2.



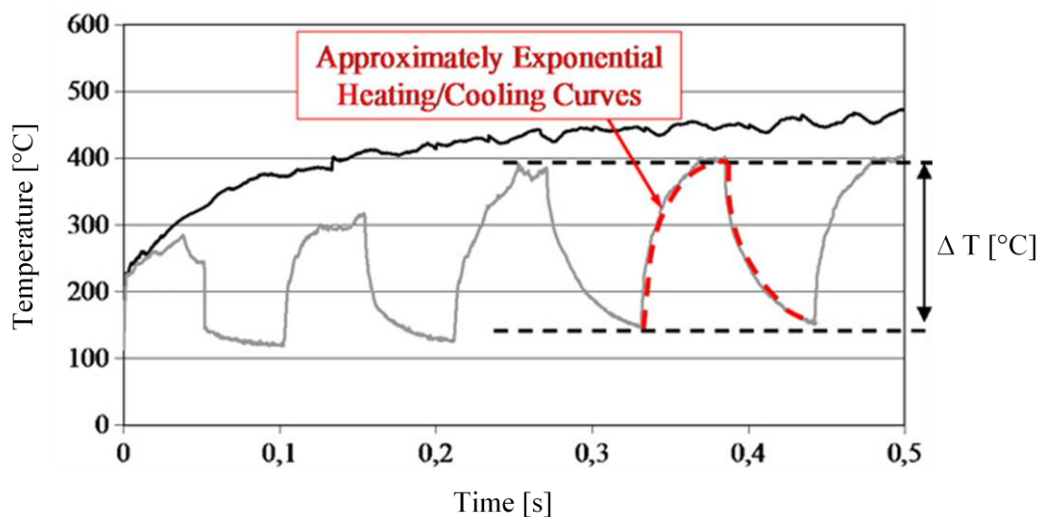
**Figure 3.2:** Insert surface temperature ( $T_v$ ) as a spatial function of exposure time, and depth beneath tool surface (lines are intended for concept explanation only) [24]



As shown in the figure it is evident that the longer the  $\tau$ , the higher volume of the edge is exposed to  $T_c$  (harsh conditions). Compared to turning, milling Ti6Al4V involves  $\tau$  for several tens of milliseconds at frequencies of several hundred to several thousand. Therefore the intermittent contact between the tool and the work piece serves to significantly lower the  $T_{\text{avg}}$ , but dramatically increase the strength demand on the cutting tool. Efficiency of the heat removal is a direct function of thermal transport properties of the tool material and the manner of their variation under realistic operation conditions [25].

### 3.1.3 Thermal shock

The tool is submitted to force fluctuation; and cyclic heating and cooling as the tool enters and exits the work piece. This cyclic temperature change is illustrated in Figure 3.3 [98]. The figure shows the steep temperature increase gradient followed by the decrease in the temperature, due to the absence of a heat source and forced convection conditions at the rake face of the tool.



**Figure 3.3:** Temperature fluctuation in continuous (black line) and 50% exposed intermittent (grey line) machining of Ti6Al4V [98]

The fluctuation is the temperature change defined by  $\Delta T$ , which can initiate a phenomenon known as thermal fatigue [44]. The most important properties of the cutting tools are transverse rupture strength ( $TRS$ ) and thermal conductivity ( $\lambda$ ). Transverse rupture strength (which controls crack initiation) must not be confused with fracture toughness ( $K_{IC}$ ) which controls crack propagation. In high-speed finish milling, where rapid tool wear nucleates from small cracks, high  $TRS$  is beneficial, while in high performance milling where the tools are over cooled and cracks always form, high *toughness* is beneficial. Thermal conductivity ( $\lambda$ ) is directly proportional to the thermal diffusivity ( $\gamma = \lambda / \rho C$ ) for the tool material. This determines the amount of heat that can be transferred per unit time. Refer to Appendix C for a comparison of these critical tool properties of various cutting tool materials. PCD

( $\approx 500$  W/m.K) has the thermal conductivity value 4-5 times that of unalloyed carbide ( $\approx 100$  W/m.K). Combining this increased thermal conductivity with a 3 times lower specific heat capacity ( $C$ ) value, allows PCD to transfer 12-15 times more heat per unit time. To avoid rake face chipping due to thermal shock, the appropriate parameter must be maximized. Depending on the heat flow conditions illustrated in Table 3.2 [24,99], the thermal shock factors in Table 3.3 are relevant [100,101].

**Table 3.2:** Range of values for heat transfer coefficient [24,99]

<i>Description</i>	<i>Heat Transfer Coefficient</i>	<i>Application</i>
Low speed air	$h=10-100$ W/m <sup>2</sup> ·K	Dry
High speed air	$h=100-2000$ W/m <sup>2</sup> ·K	TSA (10-100 psi)
Low speed water	$h=2000-5000$ W/m <sup>2</sup> ·K	Flood
High speed water	$h=5000-25000$ W/m <sup>2</sup> ·K	TSC (300-1000 psi)

Realizing the temperature of the insert is not constant (exhibits a maximum value at  $x=0$  mm that decreases with increasing  $x$ , as shown in Figure 3.2) and since only the tip of the insert is heated, the gradient of the heated/cooled surface is the area of primary interest. Hence, the cooling rate limit ( $R_\gamma$ ) should be the thermal shock resistance factor most relevant to milling. From a fundamental perspective, the magnitude of the Biot modulus ( $\beta_i=r_m h/\lambda$ ) controls the relevant factor for the application [100,101,44]. An exceedingly large heated depth or characteristic length ( $r_m$ ) for milling would be 0.001m. Table 3.3 illustrates the relevant thermal shock factors for different Biot modulus values. Typical  $\lambda$ -values for carbide (100 W/mK) and PCD (500 W/mK) will yield  $\beta_i$ -values of  $h/100,000$  to  $h/500,000$ . Utilizing the maximum heat transfer coefficient value estimate from Table 3.3 [24], yields  $0.05 < \beta_i < 0.25$ , which confirms the appropriate use of eqn. (21).

**Table 3.3:** Thermal shock resistance factors [24]

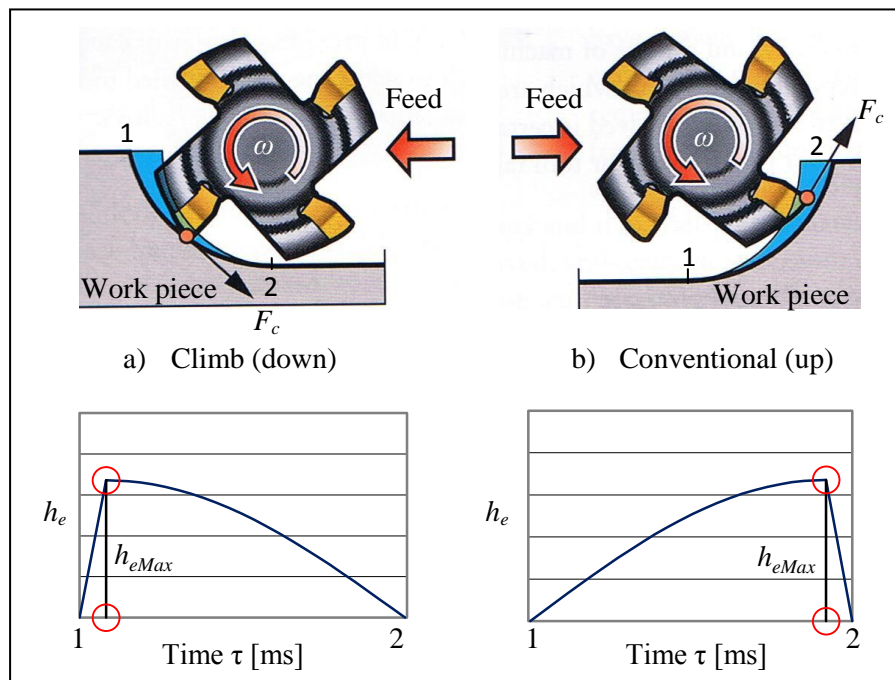
$R = \frac{TRS(1-\nu)}{E\alpha_{CTE}}$	$\beta_i \gg 1$	Maximum temperature difference under convective heating	Eqn. (19)
$R\lambda = \lambda \left( \frac{TRS(1-\nu)}{E\alpha_{CTE}} \right)$	$\beta_i < 1$	Maximum temperature difference under convective heating	Eqn. (20)
$R\gamma = \gamma \left( \frac{TRS(1-\nu)}{E\alpha_{CTE}} \right)$	$\beta_i \ll 1$	Maximum rate of surface cooling	Eqn. (21)

If  $T_v$  does not reach much lower values than that temperatures that are thermally transported to the inside of the tool, the thermal stress will decrease gradually into the tool between cuts. In order to avoid catastrophic tool failure due to thermal shock, the favourable material characteristics include high value of  $TRS$  and  $\gamma$  (or  $\lambda$ ), coupled with low values of  $E$  and  $\alpha_{CTE}$ . Thus, if the  $R\gamma$  is high enough

or the applied heat transfer coefficient ( $h$ ) low enough, then thermal shock may never be triggered as was found for PCD cutting tool material in the cutting speed range defined by the safe zone. As mentioned thermal cracks were found [24] with carbide tools at  $v_c=152$  m/min with flood coolant. Refer to Appendix C for a comparison of the main properties of different cutting tool materials.

### 3.1.4 Milling strategy

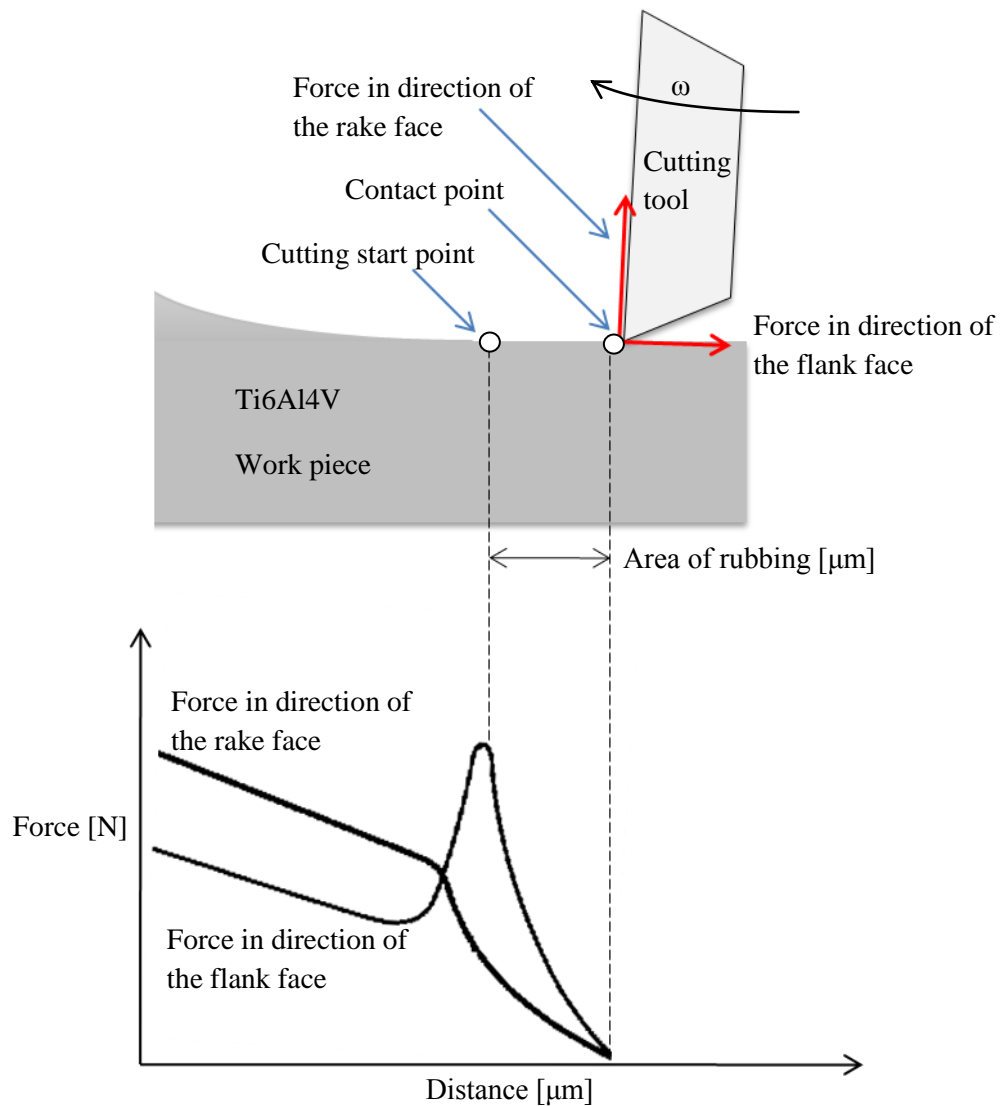
Although the milling strategy influences both the thermal- and mechanical demands, it was placed in this section due to its more profound thermal effects. In climb (down) milling the effective undeformed chip thickness ( $h_e$ ) rapidly increases to a maximum ( $h_{eMax}$ ); and then gradually decreases to zero as illustrated in Figure 3.4a. Climb milling is normally recommended, because the instant the cutting tool enters the work piece material it starts to cut, without much initial sliding [102]. While this generates less heat between the tool and work piece, more of this heat can also dissipate into the thicker chip, compared to conventional milling at the start (Point 1) of the cut [28]. Climb milling forces tend to push the work piece towards the fixture in the direction of the feed, and the chips are disposed of behind the cutter, leading to easier chip removal [66].



**Figure 3.4:** An illustration of a) climb (down) and b) conventional (up) milling [28]

As illustrated in Figure 3.4b, during conventional (up) milling the chip thickness ( $h_e$ ) starts at zero and gradually increases up to  $h_{eMax}$ , after which it decreases to zero. The cutting edge is more susceptible to tribo-chemical failure when exiting the work piece as the chip thickness is high [28]. In conventional milling of slender Ti6Al4V components, the cut at the start (Figure 3.4b, point 1) is so light, that the cutting tool could rather slide across the surface of the material than cut.

The tool will rub until sufficient pressure is build-up and the cutting tool suddenly bites and begins to cut as illustrated in Figure 3.5 [102]. This rubbing occurs more frequently as  $V_B$  exceed 0.15 mm [38].

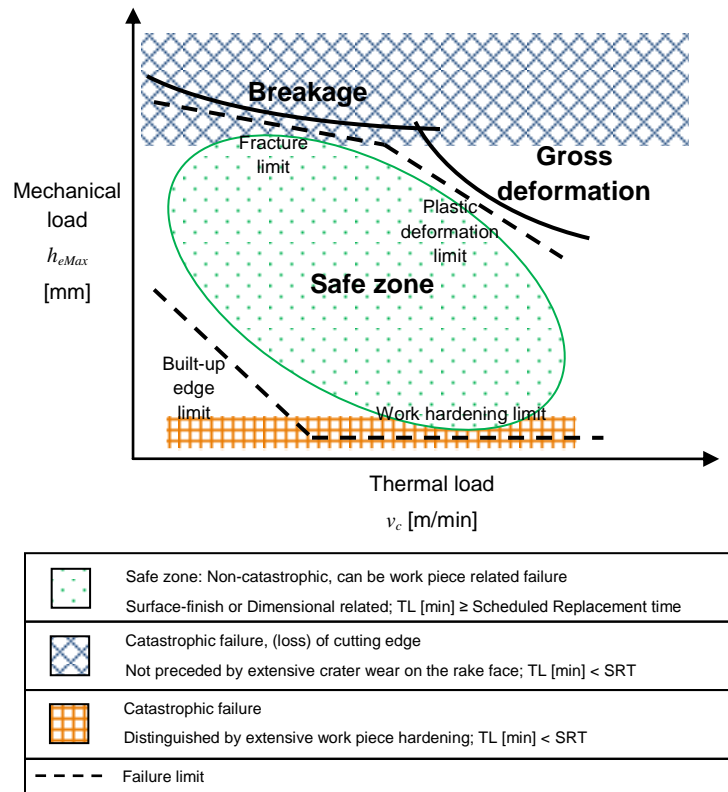


**Figure 3.5:** Rubbing in Conventional (Up) milling [102]

This sliding effect in conventional milling will generate more heat than climb milling between the cutting tool and work piece at the start of the cut. Most of this heat will dissipate into the tool (refer to section 2.3) as the chip is very thin at the start of the cut as shown in Figure 3.4 b.

### 3.2 Mechanical demands

The mechanical demands include the mechanical load ( $h_{eMax}$ ) and the influence of different types of vibration. The constraints imposed by the mechanical demands that are associated with catastrophic tool failure (earlier than scheduled replacement time) are illustrated in Figure 3.6.



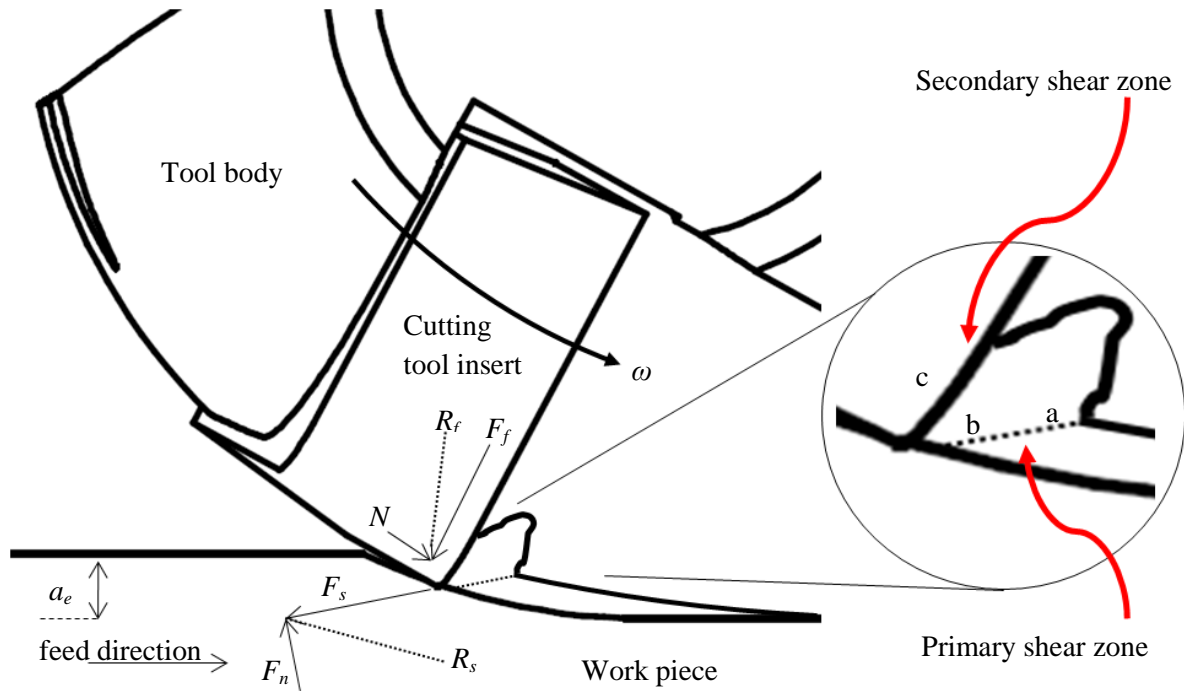
**Figure 3.6:** Tool failure constraints due to the mechanical demands on the cutting tool

As illustrated in the figure, the cutting tool will fail catastrophically when  $h_{eMax}$  is too low due to work hardening; or when the  $h_{eMax}$  is too high due to mechanical overload. The effects that the mechanical load, chatter and forced vibrations have on the mechanical demand are discussed.

#### 3.2.1 Mechanical load

In milling the mechanical load ( $h_{eMax}$ ) is a function of the tool diameter ( $\varnothing$ ), the feed rate ( $f_z$ ) and the radial immersion ( $a_e$ ) as per eqn. (26). The effect of the tool entering angle ( $\kappa_r$ ) is also considered and discussed later in this section. This load forms the vertical axis of the wear map illustrated in Figure 3.6. The forces acting in the primary and secondary shear zone are illustrated in Figure 3.7. The friction force ( $F_f$ ) between the tool and the flow of the chip along the rake face is largely influenced by the tool design and frictional phenomena, due to the periodical welding behaviour of the chip onto the tool [23].

The normal force ( $N$ ) is perpendicular to  $F_f$  in the secondary shear zone; and  $R_f$  is the resultant force of these two force components.



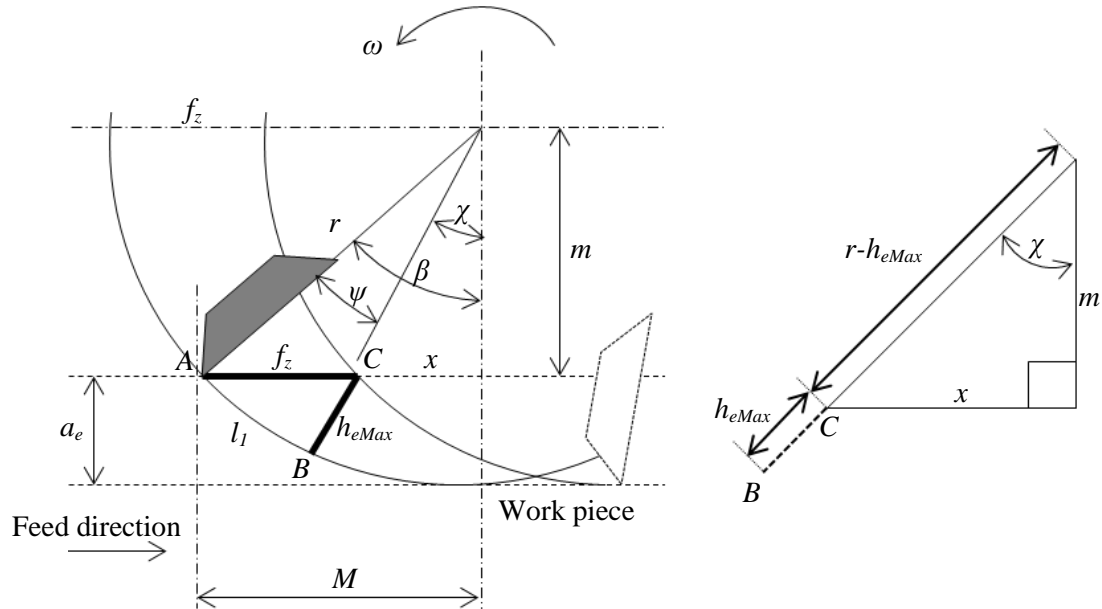
**Figure 3.7:** Schematic illustration of the forces acting in primary and the secondary shear zone; and the heat sources (a, b and c) during shear localization [23]

The two force components applied in the primary shear zone are the force ( $F_s$ ) that causes shear deformation to occur in the shear plane and the normal force ( $F_n$ ), which is perpendicular to  $F_s$ .  $R_s$  is the resultant force of  $F_s$  and  $F_n$ . The three primary heat sources [23] correlate with the acting forces.

The main shear band heat source [see Figure 3.7 (a)] will be the predominant heat source especially at higher cutting speeds. The secondary shear band heat source [see Figure 3.7 (b)] is the heat generated during the upsetting stage of cyclic chip formation, and the frictional heat source [see Figure 3.7 (c)] is the heat generated between the segment already formed and the rake face of the cutting tool.

Since doubling the  $h_{eMax}$  gives the same effect as tripling the radial immersion ( $a_e$ ), the effect of increasing the  $h_{eMax}$  on tool life is more evident than the effect of  $\tau$  [24]. Currently, no studies of the result of the effective feed ( $h_e$ ) along the cutting path on the different cutting force components in relation to the angular position ( $\omega$ ) exist. The line B-C in Figure 3.8 represents the maximum undeformed chip thickness ( $h_{eMax}$ ).

The arc length between A and B in Figure 3.8 is  $l_1$ . In order to calculate the contact time along the machining path and specifically to reach  $h_{eMax}$ , equations were derived from the figure to illustrate the effect along the rotation angle ( $\omega$ ).



**Figure 3.8:** Schematic illustrating the key kinematic quantities used in an equation to calculate the maximum effective feed ( $h_{eMax}$ )

The angle  $\beta$  can be calculated from eqn. (16) and the angle  $\chi$  illustrated in the figure can be calculated from the eqn. (23), assuming cutting takes place on the nose of the tool:

$$M = r \times \sin \beta \quad (22)$$

$$\chi = \tan^{-1} \left( \frac{x}{m} \right) = \tan^{-1} \left( \frac{M - f_z}{r - a_e} \right) \quad (23)$$

Thereby  $h_{eMax}$  could be calculated by re-arranging eqn. (24) into eqn. (25) or using eqn. (26) [72]:

$$\cos \chi = \left( \frac{m}{r - h_{eMax}} \right) = \left( \frac{r - a_e}{r - h_{eMax}} \right) \quad (24)$$

$$h_{eMax} = \frac{r \times \cos \chi - (r - a_e)}{\cos \chi} \quad (25)$$

$$h_{eMax} = r - \left[ f_z^2 + r^2 - 2 \times f_z \times r \cos \left( \sin^{-1} \left( \frac{r - a_e}{r} \right) \right) \right]^{1/2} \quad (26)$$

Considering eqn. (26) it is possible to see that  $f_z$  is the most influential cutting parameter on the mechanical load ( $h_{eMax}$ ), followed by  $a_e$ . The time period to reach the  $h_{eMax}$  and the associated angular

displacements can be calculated for a certain  $f_z$  and  $v_c$ . The angle ( $\psi$ ) between A (the point of impact) and B, illustrated in Figure 3.8, can be expressed as:

$$\psi = \beta - \chi \quad (27)$$

If angles  $\beta$ ,  $\chi$  and  $\psi$  are expressed in degrees as per eqns. (16), (23) and (27) and  $b$  is the angle  $\psi$  expressed in radians, the arc length  $l_1$  (AB) is given by:

$$l_1 = b \times r \quad (28)$$

The time ( $T_1$ ) needed for the tool to travel  $l_1$  can be calculated by:

$$T_1 = \frac{l_1}{v_c} = \frac{l_1}{\pi \times D \times \omega} \quad (29)$$

The axial angle ( $\gamma_a$ ) defined between the cutting edge and the tool rotation axis (helix angle), should also be taken into account in the time calculation. The length  $l_2$  could be expressed by eqn. (30):

$$l_2 = a_p \times \tan \gamma_a \quad (30)$$

$T_3$  is therefore the time it takes for the cutting edge to travel the distance from A to B ( $l_1$ ), and the distance due to the axial angle ( $l_2$ ).  $T_3$  can be expressed as:

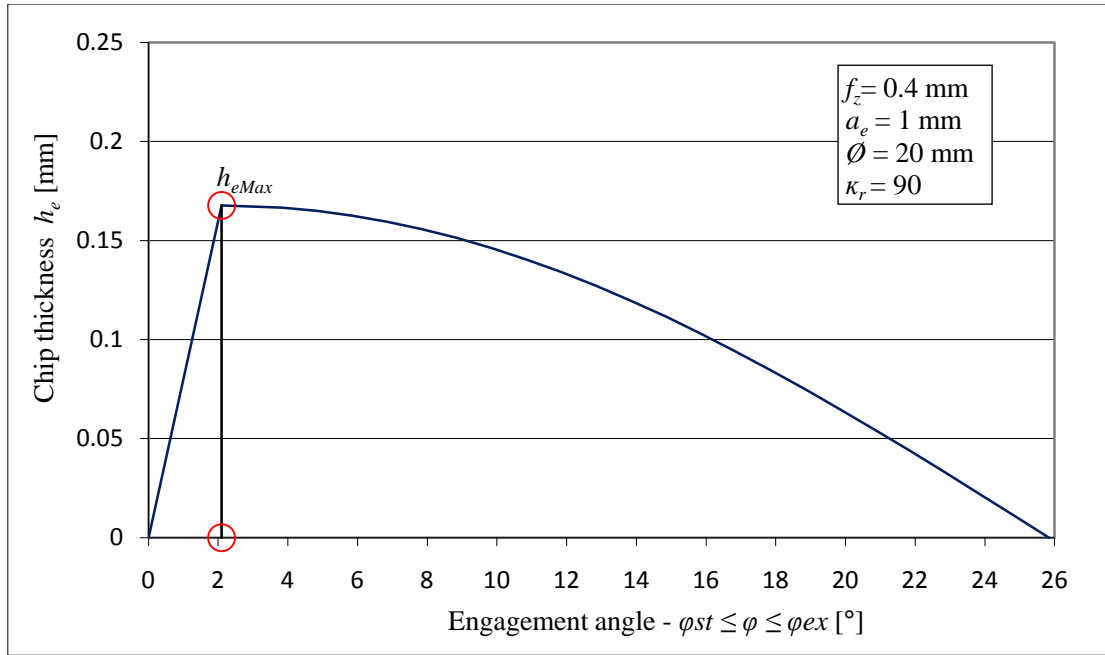
$$T_3 = \frac{l_1 + l_2}{v_c} \quad (31)$$

The segmentation frequency ( $f_c$ ) can be calculated by the ratio of the cutting speed ( $v_c$ ) to the length of the inner chip surface length ( $L_c$ ) and expressed as:

$$f_c = \frac{v_c}{L_c} \quad (32)$$

Therefore, the  $h_{eMax}$  is a  $f(r, a_e, f_z)$  as per eqn. (26). Figure 3.9 illustrates the varying effective chip load ( $h_e$ ) with the engagement angle for a specific milling condition and indicates the  $h_{eMax}$ .





**Figure 3.9:** Chip thickness ( $h_e$ ) as a function of rotation angle ( $\varphi$ )

From this figure the effect of  $\varnothing$  and  $a_e$  are significant, because although  $f_z=0.4$  mm the maximum  $h_e$  on the tool edge was only  $\approx 0.17$  mm. The second factor that influences the  $h_{eMax}$  is the chip thinning factor, due to the tool geometry (entering angle  $\kappa_r$ ). The chip thinning effect factors for  $30^\circ$ ,  $45^\circ$  and round inserts are illustrated in Table 3.4 [28].

**Table 3.4:** Considering the chip thinning factor for various cutting insert geometries [28]

<i>Insert geometry (Entering angle)</i>	<i>Chip thinning factor (e.g. <math>h_{eMax}</math> x factor)</i>
$90^\circ$	1
$30^\circ, 45^\circ$	$\sin \kappa_r$
Round	$\sqrt{\frac{4a_p}{iC} - \left(\frac{2a_p}{iC}\right)^2}$

Research [103] indicates that a lower entering angle may provide more stable cutting, as indicated by the regular tool wear instead of the micro-chipping resulting from the use of a higher value of this angle. Thereby, the effect of the chip thinning factor could be taken into consideration by multiplying  $h_{eMax}$  with the relevant factor from Table 3.4.

### 3.2.2 Vibration during milling

Milling is often susceptible to problems involving vibration of the tool and the clamped work piece, because of the proximity between their natural frequency harmonics and the frequency of tool entry on the work piece. Fluctuation in cutting forces cause tool breakage, while chatter results in very poor

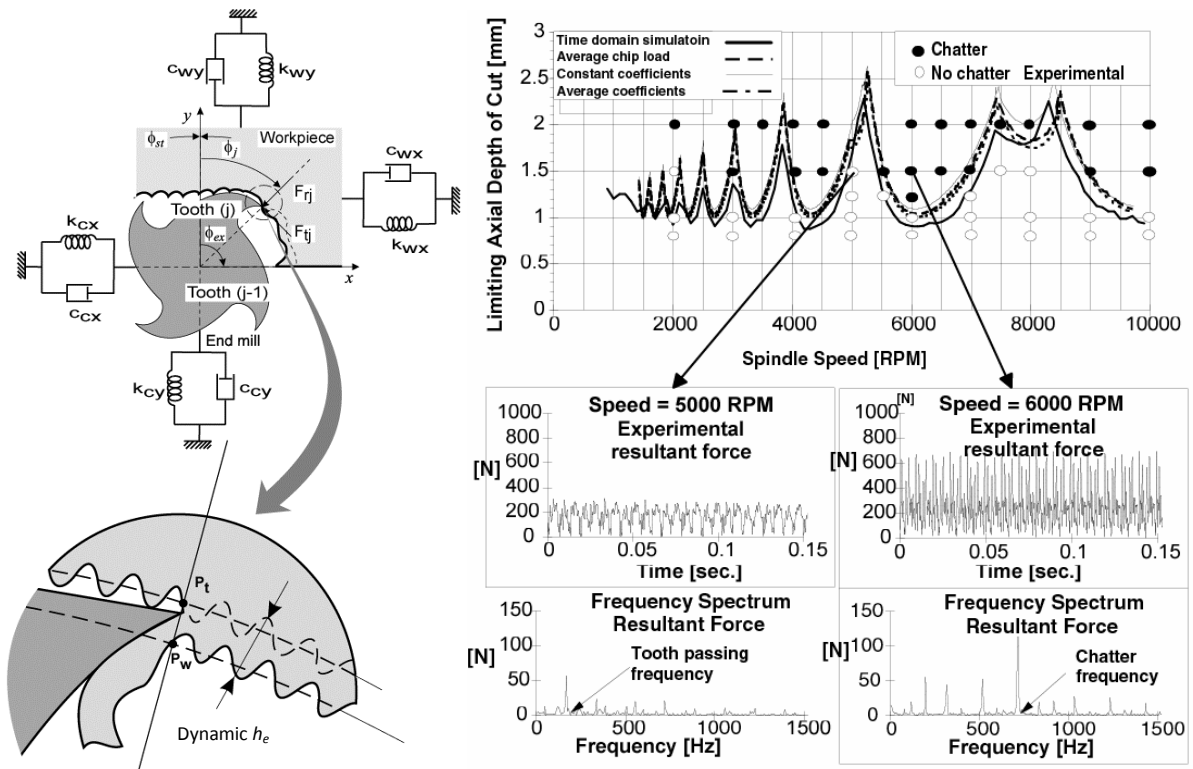
surface finish and reduced tool life [29]. Therefore, catastrophic tool failure through chipping is caused by pulsating loads due to shear localization [23]; self induced chatter [29] and altering cutting forces generated in the milling process. In order to avoid chipping from mechanical overload, the TRS of the tool material must be greater than the applied stress. Accurate prediction of the milling forces requires detailed information and an understanding of the influence of the different mechanisms. Precise data on cutting force coefficients, cutting tool geometry and cutting conditions are usually not available for all milling processes in production, particularly for 5-axis milling operations where the geometry of tool-work piece interface is relatively more complicated [29]. This section describes the vibration mechanisms that may cause tool failure and poor surface finish.

### **3.2.2.1 Chatter**

Chatter does occur at standard conventional cutting speeds, although it is more distinct and destructive with higher spindle speeds (RPM). This phenomenon is particularly important in the milling of Ti6Al4V alloys. This chattering can cause tool edge micro-chipping [25]. Self-excited (chatter) vibrations in milling develop due to dynamic interactions between the cutting tool and work piece which results in regeneration of waviness on the cutting surfaces, and thus variation in the chip thickness ( $h_c$ ) [104] as illustrated in Figure 3.10 [22].

Under certain conditions the amplitude of vibrations grows and the cutting system becomes unstable. The stability of milling process has been investigated using experimental, numerical and analytical methods [105,106] These methods can be used to generate stability diagrams from which stable cutting conditions, and spindle speeds resulting in much higher stability can be determined. Stability diagrams have been extensively used, particularly in high speed milling applications, to utilize the large stability pockets [16].

The diagram in the figure illustrates the regenerative effect of chatter on the dynamic chip thickness ( $h_c$ ) caused by the last cutting edge in cut and the ripple to be left by the cutting edge currently at work. Deep immersions ( $a_p$ ) result in very high cutting forces and severe chatter vibrations [29]. The chatter stability in milling is predicted either in time or frequency domains.



**Figure 3.10:** Analyzing the effect of self-excited chatter in the milling of Ti6Al4V [22]

From the figure it can be seen that spindle speed (RPM) and axial depth of cut are the most influential chatter causing mechanisms. Slow spindle speeds are used to stabilize the process by increasing the process damping [104]. The interface between the tool and the tool holder, and the interface between the tool holder and the spindle, both need to be as stiff as possible. A tool with an eccentric relief can offer process damping that wards off chatter. Milling cutters with irregular tooth spacing, or variable pitch, can be used to improve the stability [22]. Although these studies demonstrate the effectiveness of variable pitch cutters, there is a need for a practical method for the optimal design of pitch angles to maximize stability limits. As mentioned [103] a lower  $\kappa_r$  [°] may provide more stable cutting, as indicated by the regular tool wear instead of the micro-chipping resulting from the use of a higher value of this angle. The application of these methods in gas turbine milling resulted in significant improvements in productivity, surface quality and tool life [29]. In order to avoid chatter, very low  $a_e$  and  $a_p$  must be used. This small depth of cut limitation leads to the attempt to increase the spindle speed, to achieve an increased  $Q_w$ . This is the motivation for HSM. However, the loss of process damping complicates this strategy [75] strongly.

### 3.2.2.2 Forced vibration

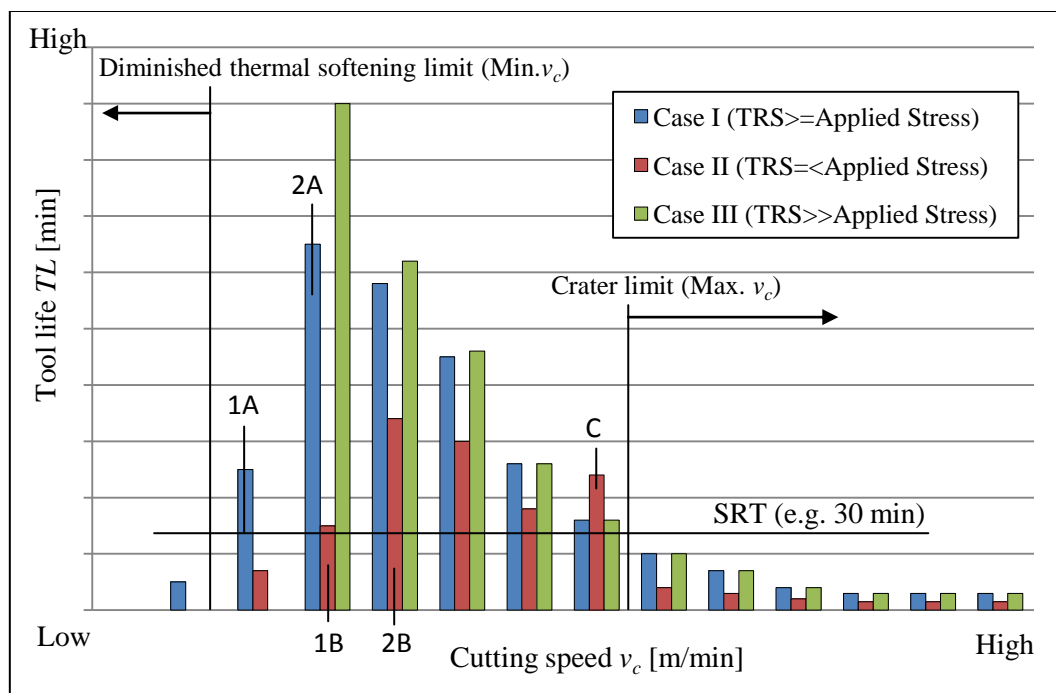
Research [107,23] indicates that vibration increases in response to the formation of serrated chips, which is also a consequence of low heat conductivity and further increases variations in the cutting force components. Catastrophic tool failure, due to vibration while in cut is due to this forced

vibration from the formation of shear localization [108,23]. According to published work [12] the chip segmentation phenomena significantly limits the  $Q_w$  and causes cyclic variation of the force components. The combination of a low [16] Young's modulus (114 GPa), coupled with a high yield stress ratio allows only small plastic deformations [15,12] and encourages deflections of the chip curling away from the rake of the tool while in cut. This results in a fluctuation of the  $F_f$ -component. The forced vibration of the result of the combined effect of the vibrations due to the fluctuation in  $R_s$  and  $R_f$  for more than one insert in cut should also be taken into consideration.

### 3.3 Influence of milling parameters on the cutting demands

#### 3.3.1 Effect of cutting speed ( $v_c$ )

Although this is the parameter which normally has the highest focus and is the easiest to change, it can be the most sensitive regarding tool life. Increased cutting speeds will generally decrease tool life until it results in catastrophic failure, preceded by extensive crater wear on the rake face. Figure 3.11 illustrates the effect of cutting speed on tool life for three different tool materials. In low TRS tool materials (Refer to Appendix C) there may be a minimum  $v_c$  below which mechanical overload may occur. This is due to increased forces due to diminished thermal softening. Similarly, a local tool life maximum may exist at a particular  $v_c$  if there is a phase change in the work piece material (Figure 3.11 C). Case III describes a tool material with excessive strength compared to the cutting stress applied by the work piece. In this case the tool life is entirely dependent on non-catastrophic, work piece related failure and the Taylor model applies.



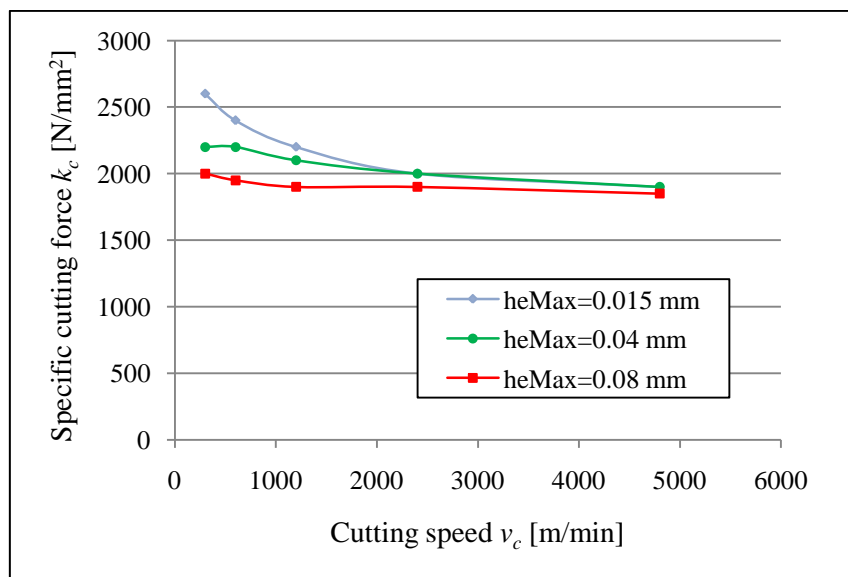
**Figure 3.11:** Schematic effect of cutting speed on tool life (points and trend lines are intended for concept explanation only) [38,24]

Case I illustrates the behaviour of a tool material that has reasonable, but not excessive strength compared to the cutting stress applied by the work piece. In the low cutting speed range (Figure 3.11: Point 1A to 2A) the resistance to deformation of the work piece exceeds the strength of the cutting edge, leading to catastrophic failure, not preceded by extensive crater wear.

Case II indicates the behaviour of a slightly lower strength tool material (weaker than case I) having a strength similar to the cutting stress applied by the work piece. In the low cutting speed range (Figure 3.11: Point 1B to 2B), the resistance to deformation of the work piece exceeds the strength of the cutting edge. This catastrophic failure, not preceded by extensive crater wear, for case II needs a more pronounced increase in  $v_c$  to overcome the work piece stress compared to case I [24]. In Figure 3.11 Points 2A and 2B represents the minimum thermal load constraints respectively, before diminished thermal softening. As  $v_c$  increases, strain rate hardening or thermal softening may act to increase or decrease the specific cutting force ( $k_c$ ) value as per equation eqn. (33) [109]

$$k_c = \frac{F_c}{h_{eMax} \times a_p} \quad (33)$$

The specific cutting force value ( $k_c$ ) decreased with an increase in cutting speed as illustrated in Figure 3.12.



**Figure 3.12:** Specific cutting force ( $k_c$ ) at elevated cutting speeds ( $v_c=300-4000$  m/min) for TiAl6V4 [85]

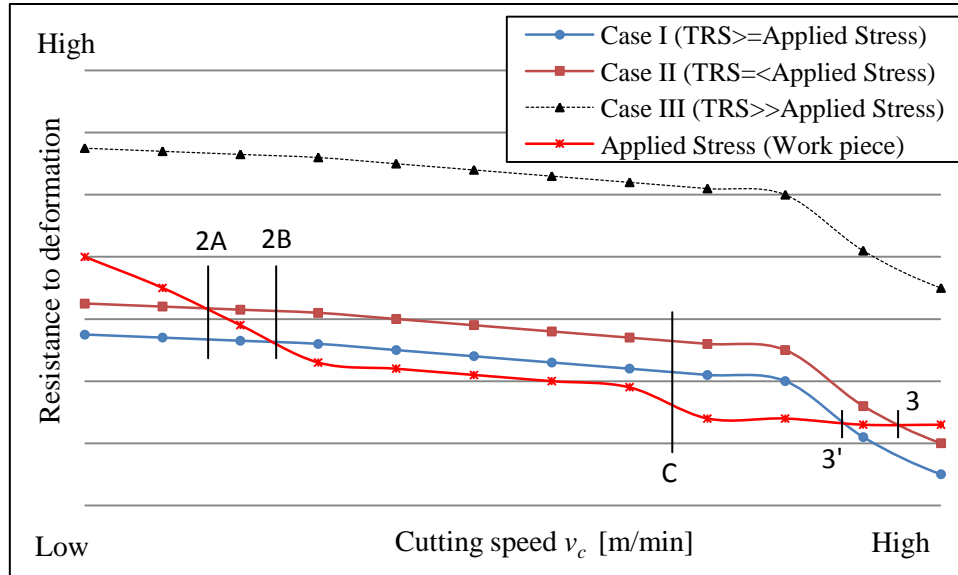
These results illustrated in Figure 2.15 and Figure 3.12, show that the cutting force ( $F_c$ ) should be determined for each application in particular; and is not easy to be specified in general. Phase changes may introduce a step increase or decrease in the value depending on the strength of the new slip system. The  $\alpha$  phase (hexagonal close packed) of Ti6Al4V is hard and brittle, with a strong hardening tendency. The  $\beta$  phase (body centered cubic) is ductile and can be cut more easily, but also has a

strong tendency to adhere [15]. If such phase transformation occurs (refer to Figure 3.11, Point C), the reduced stress may result in a local increase in tool life until the increased wear rate at an increased  $v_c$  overcomes this effect due to the cutting tool's loss of hardness. This leads to catastrophic failure preceded by extensive crater wear. In a background study [69] a slower wear progression was found at  $v_c=200\text{m/min}$ . This was complemented with the cutting force measurements that reduced by a significant amount when increasing  $v_c$  from 150 to 200 m/min. Table 3.5 illustrates the recommended cutting speeds range for rough - and finish milling in order to prevent catastrophic tool failure, preceded by extensive crater wear on the rake face of the cutting tool.

**Table 3.5:** Recommended cutting speeds ranges for non-catastrophic tool failure

<i>Condition (Tool material)</i>	<i>Thermal load (<math>v_c</math>) region</i>	<i>References</i>
Roughing (Carbide)	30-60 m/min	[81] [54]
Finishing (PCD)	175-300 m/min	[24] [28] [110] [41] [69]

For roughing, the recommended cutting speeds range from 30-60 m/min. However for finish milling, where very light radial cuts and thin chips are produced, the cutting speeds range from 175-300 m/min. Figure 3.13 illustrates the work piece applied stress versus  $v_c$  to demonstrate the various effects. The cutting tool's TRS and the deformation resistance of the work piece are scaled to explain the concept.

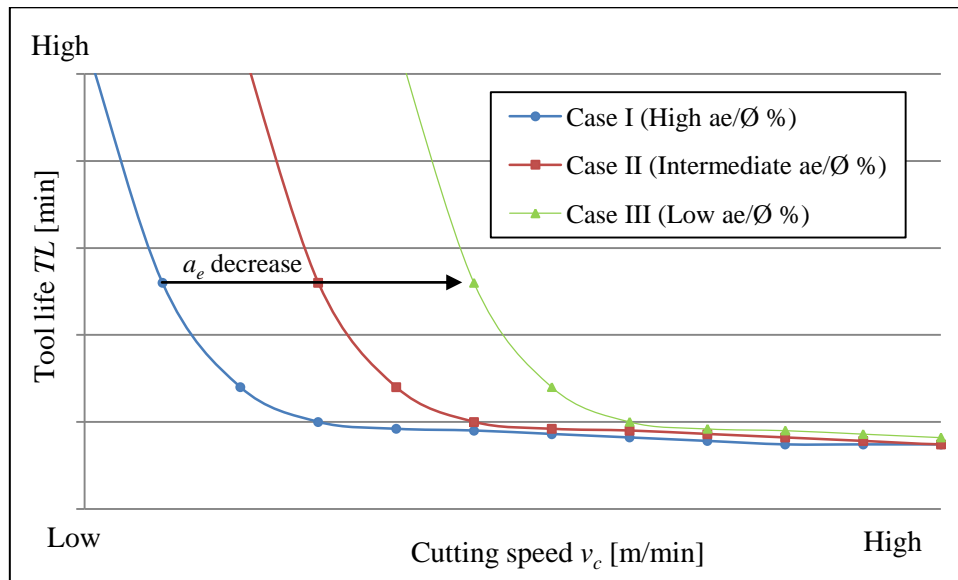


**Figure 3.13:** Schematic effect of cutting speed on applied stress (points and trend lines are intended for concept explanation only) [16,30,24]

Lines 2A and 2B in Figure 3.13 represents the maximum TL points in Figure 3.11. If the tool material strength is below the cutting stress applied by the work piece (Figure 3.13: Point 3 and 3'), catastrophic failure will result.

### 3.3.2 Effect of radial immersion ( $a_e$ )

Radial immersion is also a parameter that can affect both tool life and the material removal rate. Increased radial immersion ( $a_e$ ) will generally decrease tool life until it results in catastrophic failure. Values must be kept below a critical  $a_e$  for a specific  $\phi$ . This critical  $a_e$  decreases with an increase in  $v_c$  as illustrated in Figure 3.14.



**Figure 3.14:** Schematic effect of radial immersion % on tool life (trend lines are intended for concept explanation only) [98,38,24]

While a high percentage of radial immersion increases the  $Q_w$  it has been found [28] that the relationship of  $a_e/\phi$  is critical. The best balance of a high  $Q_w$  and economic TL is found with  $a_e/\phi$  between 30 to 40% [28] for roughing as illustrated in Table 3.6.

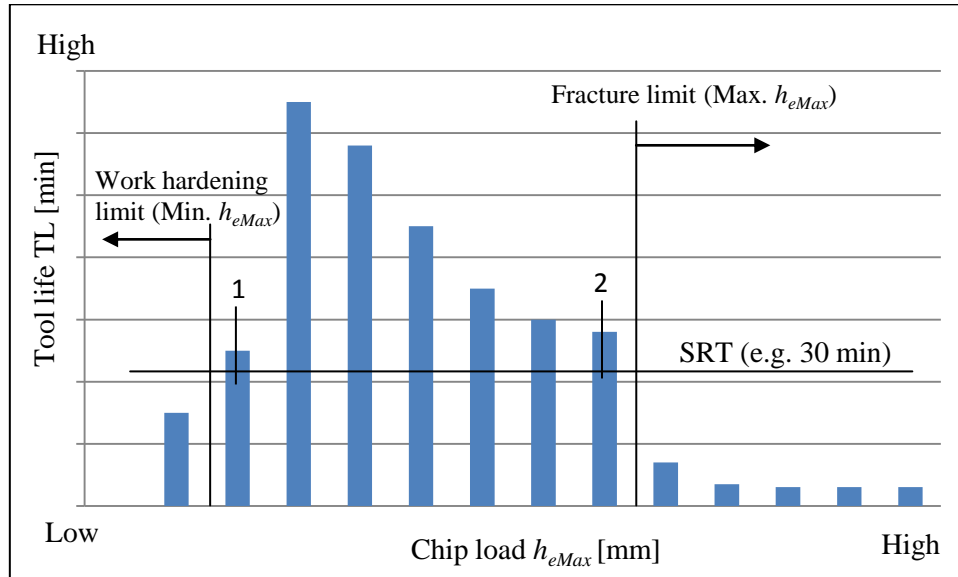
**Table 3.6:** Recommended  $a_e/\phi$  (roughing) and  $a_e$  (finish) ranges for non-catastrophic tool failure

<b>Condition (Tool material)</b>	<b>Radial immersion region</b>	<b>References</b>
Roughing (Carbide)	30-40% ( $a_e/\phi$ %)	[28]
Finishing (PCD)	0.5-1 mm ( $a_e$ )	[69] [24] [28]

In finish cuts where the radial cut ( $a_e$ ) is small in relationship to the  $\phi$ , the chip thickness is reduced. The recommended radial immersion range for finish milling is limited to 0.5-1 mm.

### 3.3.3 Effect of maximum un-deformed chip thickness ( $h_{eMax}$ )

Increased  $h_{eMax}$  will generally decrease tool life until it results in catastrophic failure. This failure mode is in the form of fracture, not preceded by extensive crater wear on the rake face. However,  $h_{eMax}$  must be kept below a maximum critical value (Figure 3.15: Point 2) to avoid mechanical overload, but above a minimum critical value to avoid piece hardening (Figure 3.15: Point 1).



**Figure 3.15:** Schematic effect of chip load on tool life (bars are intended for concept explanation only)

A weaker tool will also be very sensitive to fluctuations in the cutting force applied by the work piece. Only a perfectly sharp tool with adequately high strength will exhibit classical Taylor tool life over the entire region.

Table 3.7 illustrates the recommended chip load ranges for rough- and finish milling in order to prevent catastrophic tool failure, not preceded by extensive crater wear on the rake face.

**Table 3.7:** Recommended maximum un-deformed chip thickness ranges for non-catastrophic tool failure

<i>Condition (Tool material)</i>	<i>Max. un-deformed chip thickness (<math>h_{eMax}</math>) region</i>	<i>References</i>
Roughing (Carbide)	0.1-0.25 mm	[81] [54]
Finishing (PCD)	< 0.03 mm	[24] [28] [110] [41] [69]

As illustrated in the table the  $h_{eMax}$ 's are still limited to 0.25 mm for rough- and 0.03 for finish cuts before the mechanical load exceeds the fracture limit.



### 3.3.4 Effect of axial immersion ( $a_p$ )

In the milling of Ti6Al4V an increase in  $a_p$  has no detrimental effect on tool life as illustrated in Figure 3.16. Table 3.8 illustrates the recommended axial immersion ranges for rough and finish milling.

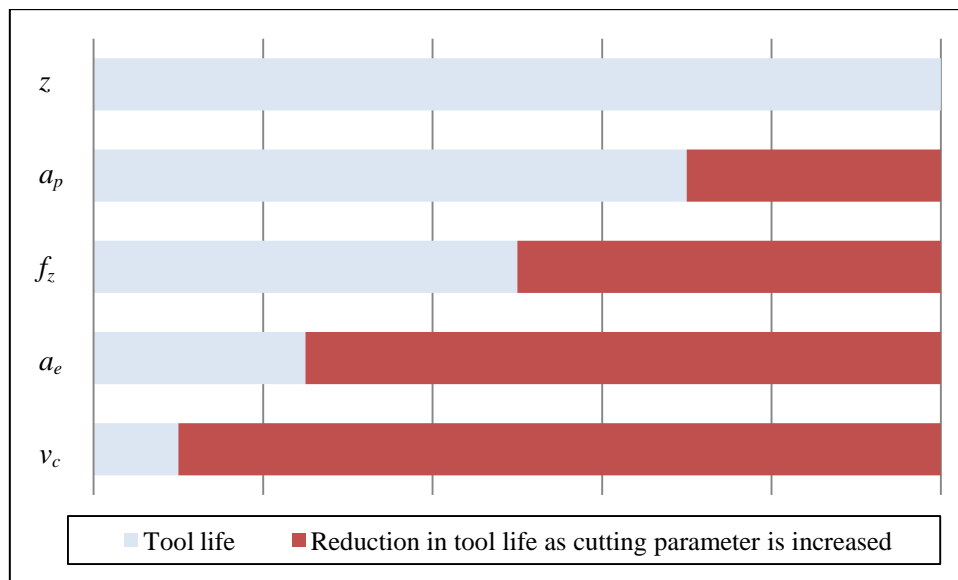
**Table 3.8:** Recommended chip load ranges for non-catastrophic tool failure

<i>Condition</i>	<i>Axial immersion [mm]</i>	<i>References</i>
Rough and finish milling	$\kappa_r=90^\circ$ : Depth that allows for stable cutting $\kappa_r=45^\circ$ : 2-10 mm Round: $(0.3 \text{ to } 0.4) \times iC$	[28] [22]

Although an increase in  $a_p$  has no detrimental effect on the tool life, it is still crucial to ensure the cutting is stable and the tool-work piece interface is rigid to diminish chatter. Remedies to minimize chatter are discussed in section 3.2.2.1.

### 3.4 Influence of milling parameters on the wear phenomena and wear mechanisms

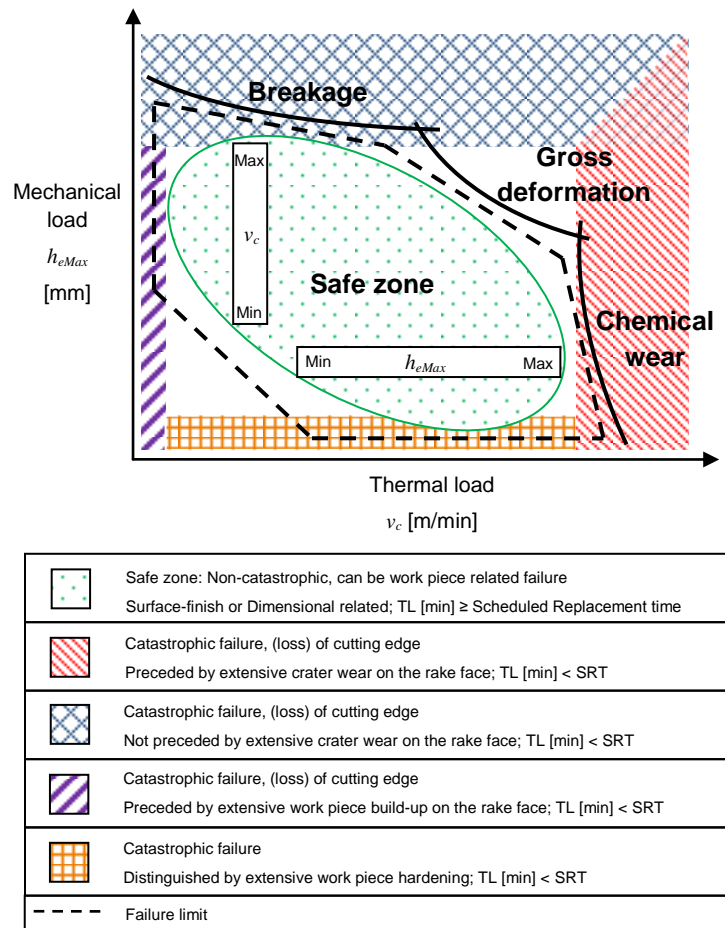
The effects of the different cutting parameters on the tool life [28] are illustrated in Figure 3.16. From this it is evident that an increase in the  $v_c$  has a significant reduction in tool life compared to an increase in  $a_p$ . An increase in exposure time ( $a_e$ ) has the second largest influence followed by an increase in  $f_z$ .



**Figure 3.16:** Illustration of the reduction in tool life as parameters are increased [28]

The amount of inserts ( $z$ ) on the tool life is not influential. As discussed earlier  $f_z$  is the most influential cutting parameter on  $h_{eMax}$  as per eqn. (26) followed by  $a_e$ . It is evident from the above figure that the main thermal demand cutting parameters ( $v_c$  and  $a_e$ ) have a greater effect on tool life

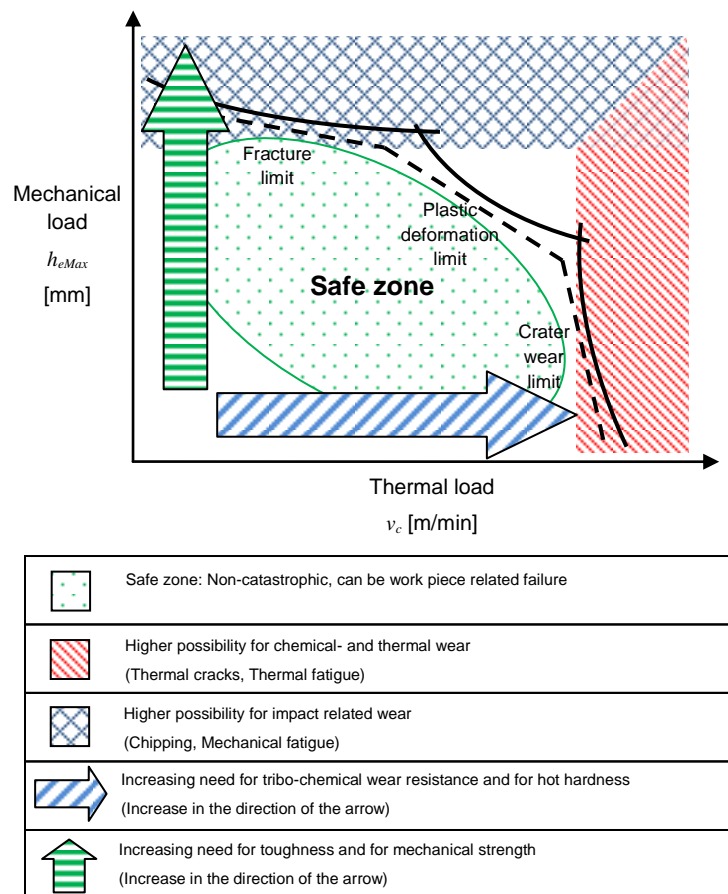
than the main mechanical load cutting parameter ( $f_z$ ). These support earlier studies [12,25,45] that tool life is mainly limited due to the high cutting temperature localized in the vicinity of the cutting edge. Knowing the effect of these cutting parameters, it is possible to understand the influence of these cutting parameters on the layout of the different failure regions as illustrated in Figure 3.17.



**Figure 3.17:** Influence of cutting parameters on the generic mapping of catastrophic- and non-catastrophic failures (areas are intended for concept explanation only)

As discussed in section 3.3.1, a tool life in a Taylor model fashion is possible between minimum and maximum  $v_c$ -values on the thermal load-axis, for a specific  $h_{eMax}$  range. Similarly, a tool life in a Taylor model fashion is possible between minimum and maximum  $h_{eMax}$ -values (refer to section 3.3.3) on the mechanical load-axis for a specific  $v_c$  range. Thereby, it is possible to establish the non-catastrophic tool failure area, also known as the safe zone [36]. This zone is the area enclosed by the fracture-, plastic deformation-, work hardening-, crater wear- and diminished thermal softening limits. The safe zone is regarded as the area where the best balance of a high  $Q_w$  and economic tool life is found. Increasing the radial immersion, hence exposure time, will shift the crater limit to a lower thermal load (refer to section 3.3.2). The effect of exposure time was considered in the tool wear maps by constructing a wear map for both rough- and finish milling of Ti6Al4V. In this study the exposure

time in rough milling are defined by 30-40% tool immersion and by  $a_e=0.5-1$  mm for finish milling. The axial immersion ( $a_p$ ) does not have a significant effect on tool life as shown in Figure 3.16, but can influence the milling strategy [22]. Considering the different tool material needs according to this constructed map, Figure 3.18 illustrates the increasing need for tool toughness and mechanical strength, with an increase in the mechanical load. The figure also illustrates the increasing need for tribo-chemical wear resistant tool materials with an increase in the thermal load.



**Figure 3.18:** Illustration of the tool material property needs and the mechanisms under different physical demands (Arrows and markers are for concept explanation purposes only)

Independent of the tool material properties and tool geometry, there is a higher possibility for catastrophic tool failure by fracture with a relative high mechanical load. In contrast, there is a higher possibility for catastrophic tool failure, preceded by extensive crater wear, with a relative high thermal load. This current understanding of the physical demands on tool materials helps establish cutting conditions for new experimental tool entrants as it is possible to be aware of the effect of these parameters on the physical demands of the cutting tool. This mapping makes it possible to develop and to understand remedial actions (Refer to Appendix B) for different tool failure modes and serves as a basis to understand the different wear mechanisms in the milling of Ti6Al4V.

## ***4. Experimental approach and output***

This research study explores the cutting demands found in rough- and finish milling of Ti6Al4V, in order to construct and validate tool wear maps for both conditions. The tool wear map serves the purpose of clarifying the complex interaction between the machining parameters to process designers. Thereby, a knowledge based iterative process improvement is facilitated, simultaneously enhancing machining knowledge needed in South Africa. Prior to this work, a map for the milling of Ti6Al4V were neither created nor remedial actions to optimize the production process, integrated. This framework has been used to discuss the observed effects and remedial actions that are developed by tool suppliers. Refer to Appendix B.

### **4.1 Experimental approach**

Several broad steps were taken to construct the maps describing the wear characteristics of carbide cutting tools in rough and PCD in finish milling of Ti6Al4V. The following describe briefly the steps adopted by the author.

#### **4.1.1 Defining the field of interest**

The pair of materials of interest, their mode of contact, the environment in which they are to interact in and lubrication condition were first identified. The cutting tool materials were restricted to carbide cutting tools for rough- and PCD cutting tools for the finish milling of Ti6Al4V. Thereby, the additional complications brought about by the different complex wear mechanisms are minimized. Flood lubrication was used throughout, unless stated otherwise. The milling experiments were done under normal atmospheric condition with flood lubrication. It was decided to do the additional static interaction diffusion-couple experiments to study and understand the chemical interactions at different temperatures better.

#### **4.1.2 Collecting experimental data and information**

Experimental data from background studies, literature and industry on wear rates and wear mechanisms pertaining to the milling conditions specified in the previous step was gathered and studied. An economic viable SRT value of 30 minutes was used to group this data into catastrophic or non-catastrophic tool failure modes. The tool life (TL) was examined through an extended Taylor model with boundary conditions found in literature [24]. Mathematical models describing the wear behaviour for these conditions were investigated. Wear data obtained from other types of machining operations, such as turning and drilling was also taken into consideration. Wear data of Ti6Al4V

obtained from laboratory-type experiments, such as pin-on-disk, were excluded from the present work.

### 4.1.3 Constructing the tool wear maps

Various tool wear maps from literature were considered. It is possible to construct two- or three dimensional tool wear maps. The majority of these wear maps are of the two-dimensional type. The parameters used as axes for the two-dimensional maps used in this research study were decided to be  $v_c$  and  $h_{eMax}$ . The effect of  $a_e$  was considered in the tool wear maps by constructing a wear map for both rough- and finish milling of Ti6Al4V. It was desirable to select the ranges of these parameters as wide as possible. In rough milling with carbide tools data of  $v_c$  ranged from 25-250 m/min with  $h_{eMax} < 0.4$  mm. In finish milling with PCD tools data of  $v_c$  ranged from 100-800 m/min with  $h_{eMax} < 0.1$  mm. The collected wear data were then introduced into this two-dimensional plane. The results were classified into catastrophic- or non-catastrophic tool failure. Catastrophic define tool failure earlier than 30 minutes of the cutting time, while non-catastrophic describes a longer tool life. In all cases the depth of cut, a cutting parameter not reflected in the map due to its relative minor effect on tool wear, varied from 1 mm to 3 mm.

### 4.1.4 Superimposing the data

The empirical wear maps were constructed by grouping the wear data according to the failure mode and mechanism of wear. The field of dominance of each mechanism was identified using field boundaries. At this stage, the wear map was sufficiently informative and it provided a summary of the tool wear behaviour for the rough- and finish milling maps. The work piece failure maps were then superimposed onto the tool wear maps constructed, to understand the global failure boundaries. Remedial actions that are developed by tool suppliers [102,28] were considered and integrated into the tool wear maps. Refer to Figure B.3 in Appendix B.

### 4.1.5 Experimentation

In order to check the validity of the map, carefully executed milling experiments were carried out. In the rough milling experiments, TiAlN (PVD) carbide tools were used to mill the Ti6Al4V work piece. In a background experiment, the dynamics of chip formation is studied to understand the significance of chip formation on tool vibration. As chipping is a major, catastrophic failure mechanism of carbide tools machining titanium, a clearer perspective of force synchronisation with shear localization is pursued. Real force component measurements with their dynamic component of the signal are analyzed together with chip segmentation. In the rough milling experiment different sets of thermal ( $v_c$ ) and mechanical ( $h_{eMax}$ ) loads were investigated. The effect of  $V_B$  of cutting force was also evaluated. Additional static interactions of WC-Co/Ti6Al4V diffusion-couple experiments at different

temperatures were conducted. This helped to reveal the potential for chemical interaction between Ti6Al4V and WC-Co. It was decided on uncoated carbide diffusion couples, in order to avoid various other chemical reactions between the coating and Ti6Al4V.

In the finish milling experiments, PCD tools were used to mill the Ti6Al4V work piece. As background work different (fine-, medium and coarse) materials were tested. A 3-factor, 3-level design was used in Statistica (Version 8) to analyze the data. In the finish milling experiment different sets of thermal ( $v_c$ ) and mechanical ( $h_{eMax}$ ) loads were also investigated. Additional static interactions of PCD/Ti6Al4V diffusion-couple experiments at different temperatures were conducted. This also helped to understand the chemical interaction between Ti6Al4V and PCD better.

The properties of the work piece and the tool materials, equipment, experimental setup and design for both the rough- and finish milling experiments are explained in the following chapter.

## **4.2 Experimental output**

The goal of this research study is to develop a body of knowledge to enable machining of titanium to be executed in such a way that local machining suppliers may be able to compete in the first world. Contribution to knowledge would be the development of an integrated CNC process design competency base to plan and execute the machining of the majority of smaller aerospace components in a competitive manner.

The construction of wear maps for the rough- and finish milling of Ti6Al4V will form the basis to these outputs. The wear characterisation of carbide cutting tools in the rough milling of Ti6Al4V and PCD tools in the finish milling of Ti6Al4V contribute to the understanding of these complex wear mechanisms. Scanning electron microscopy, energy dispersive X-ray analysis and optical microscopy were employed to assist in the identification of the various dominant wear mechanisms under various milling conditions. The different forms of chip formation and measured cutting forces will also enable to improve simulation models of the milling of titanium alloys.

Publications in journals and articles in peer reviewed conferences were prepared from these experimental outputs. Refer to Appendix F for the list of publications.

## 5. *Experimental work*

In general, experimentations are carried out to determine whether theories hold in practice. The Ti6Al4V and the different tool materials are expensive. Therefore, it is not cost effective to do the final experiments until the concepts have been refined and fully understood. This refinement phase is paramount in the development of tool wear maps. During the conceptual phase background experimentation was carried out to refine several concepts. The dynamics of chip formation was studied to understand the significance of chip formation on tool vibration. Different PCD materials were tested to establish which is most appropriate for the milling of Ti6Al4V, as relevant information is limited.

In the rough milling experiments, TiAlN (PVD) carbide tools were used to mill the Ti6Al4V work piece. This was followed by WC-Co/Ti6Al4V diffusion-couple experiments to reveal the potential for chemical interaction between Ti6Al4V and WC-Co.

In the finish milling experiments, PCD tools were used to mill the Ti6Al4V work piece. Moreover, possible interactions of PCD and Ti6Al4V during milling were studied to shed the light on the chemical interactions between Ti6Al4V and PCD.

### **5.1 *Rough milling with carbide tool material***

These experiments were designed to evaluate the constructed wear map for the rough milling of Ti6Al4V with carbide tools. Initially, dynamics of chip formation were studied to understand the significance of chip formation on tool vibration. Conventional- and transition-speed milling experiments followed to assess the maps. Thereafter, diffusion-couple experiments were conducted to reveal the truthful potential for chemical interaction between Ti6Al4V and WC-Co.

#### **5.1.1 The effect of chip dynamics**

The investigation of the fluctuation in the force components with a rigid milling setup is important for a detailed understanding of the main causes of forced vibration during a cut. This forms part of the basis for wear characterization and more effective FEM modelling. In a research study [75], it was found that the chip segmentation phenomena *significantly* limit the material removal rates in titanium machining. This observation was complimented with the remark found in literature [111], that the shear localization results in a cyclic variation of forces (both cutting and thrust) with a *significant* magnitude variation. As a result, the author was interested to study the effect of chip formation of force vibration in order to understand the mechanisms behind tool failure.

Therefore, one of the objectives of this experiment is to analyse the dynamic changes in the cutting force components relative to the effective un-deformed chip thickness ( $h_e$ ). The second goal is to further enhance the understanding of mechanical related tool failure mechanisms related to mechanical factors, by comparing the effect of forced fluctuations caused by shear localization ( $R_s$ ) and by the frictional force phenomena ( $R_f$ ) between the cutting tool, work piece and chip flow. Dynamic force measurements were analyzed in a synchronised fashion together with the chip segmentation phenomena by using a Kistler dynamometer and high-speed photography.

### 5.1.1.1 Experimental setup and design

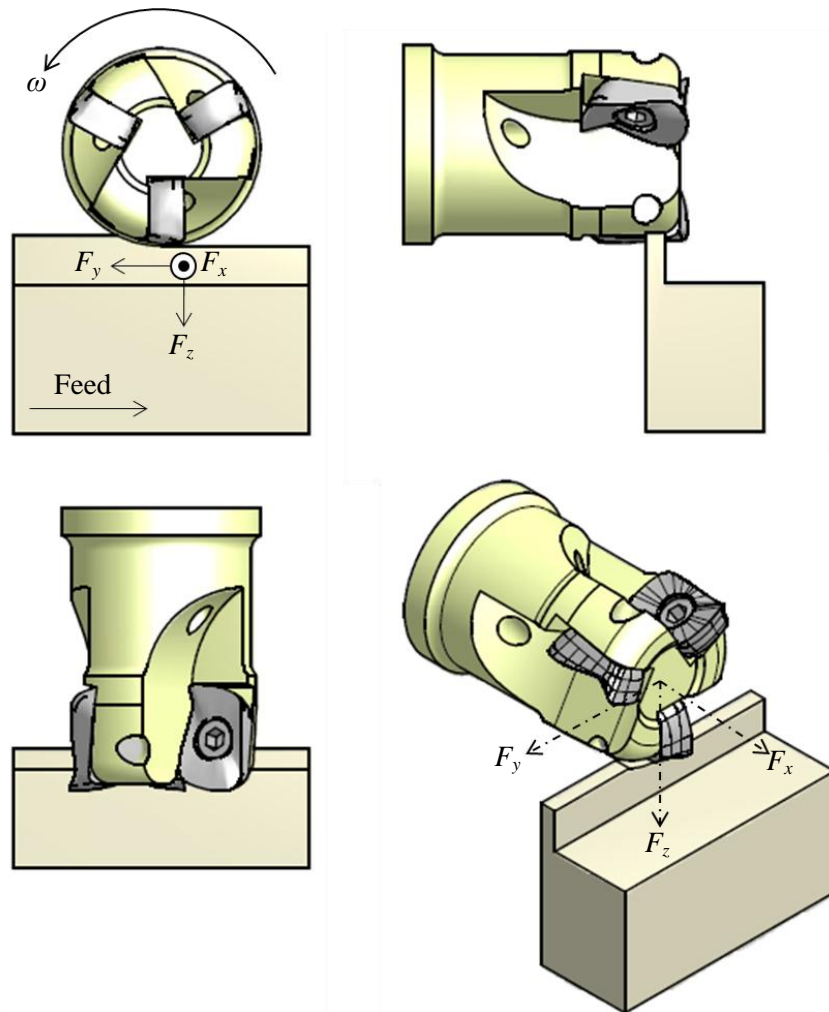
The experiment was designed so as to permit observation of the 2D chip formation during milling Ti6Al4V. Table 5.1 details the experimental equipment and the milling parameters used. The spindle axis was positioned horizontally with the well-balanced cutting tool over the thin ( $a_p=2\text{mm}$ ) work piece as illustrated in Figure 5.1. Although this setup was specifically designed with the thin work piece in order to minimize the fluctuation of  $R_f$  in the  $F_x$ -component, it was rigid enough to prevent self-excited vibration. Doing this it is possible to illustrate that both factors ( $R_s$  and  $R_f$ ) influencing forced vibration are active during the cut; and it is possible to compare the effect of both analyzing force components  $F_y$  and  $F_z$ . A FASTCAM SA 1.1 high-speed camera, that is capable to capture 10.000 images per second at a resolution of 512x512 pixels, was synchronized with the Kistler 3D dynamometer (Type 9255B). The table 9255B, that because of its size (260x260 mm) and force range (-20 to 20 kN in X and Y, -10 to 40 kN in Z) is currently the most adequate to measure forces in milling [112]. It shows a natural frequency mounted on flanges of 1.7 kHz in X, Y axes and 2 kHz in Z axis. It must be also taken into account that parts of a certain weight are mounted on the table, and this produces a decrease in the natural frequency of the system to values around 1 kHz [112]. The natural frequencies for most cutting tools are found to be above 2 kHz [103]. The valid range for measuring is below this natural frequency.

**Table 5.1:** Experimental equipment

Machine tool	DIGMA 850 HSC
Tool and inserts	HM90 E90A-D20-3W20 with $\gamma_a=7^\circ$
	Cemented carbide: APKT 1003R8T-FF (TiAlN PVD coated)
Coolant	Dry machining
Force measurement	Kistler 3D dynamometer type 9255B
High-speed camera	FASTCAM SA 1.1
Charge amp settings	Type 5011 (+/-10V)
	Measuring range +/-2000 N
Lighting arrangement	HTI 700 Watt (GK Lichttechnik, Hechingen)
Cutting speed ( $v_c$ )	40 m/min
Feed per tooth ( $f_z$ )	0.25 mm
Axial depth of cut ( $a_p$ )	2 mm
Radial depth of cut ( $a_e$ )	1 mm



The signal of the dynamometer was converted by three charge amplifiers (type 5011) into a proportional voltage signal (+/-10V). The amplifier's measuring range was set to +/-2000 N with a time constant of 1s (medium). The experiments were conducted at a radial depth of cut of 1 mm and  $v_c=40\text{m/min}$  at a  $f_z=0.25\text{ mm/z}$  as recommended by the tool supplier. Dry machining and a 700W spotlight were used so as to provide a clear view of the cutting zone during the filming. The rotation angle of the tool and the formation of the chip could be related to visual observations and the cutting force component measurements. The direction of the cutting force components, the rotation direction of the spindle ( $\omega$ ) and the feed direction are illustrated in Figure 5.1.



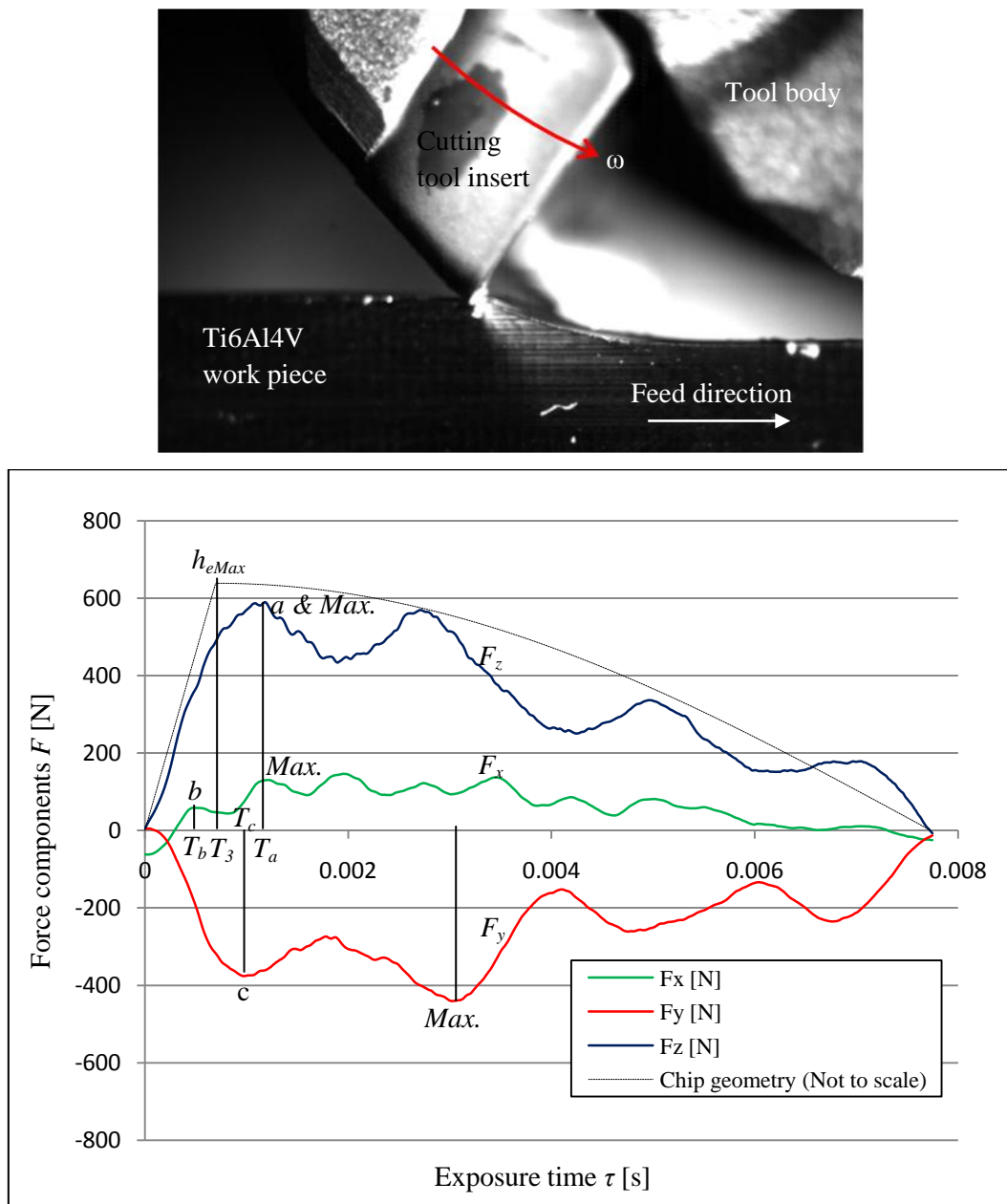
**Figure 5.1:** Experimental setup of the cutting tool over the Ti6Al4V work piece and the directions of the force components

The cutting forces are determined by the machined cross section width and thickness, the cutting speed and the tool wear.

### 5.1.1.2 Experimental results

The result of the experiments is presented as time domain plots of force progressions. The high-speed video footage showed in most of the experiments that hot chips adhere to the rake of the tool and are

only removed at the re-engagement point ( $\varphi_{st}$ ) between the cutting edge and the work piece. This adherence behaviour is considered to be the underlying mechanism causing the high friction forces. The frequency components in the force fluctuations were analyzed to compare to the segmented chip formation and video footage. Figure 5.2 illustrates the cutting tool at the point of impact with the Ti6Al4V work piece. After initial impact, there is a large increase in  $F_z$  and  $F_x$  to a maximum after which a gradual decline is observed. The maximum in  $F_y$  was encountered last. The increase in the effective chip load led to the increase in the cutting force components. The dotted line in the figure illustrates the effective un-deformed chip thickness relative to the tool position in cut. Data of the first variation of the cyclic force component in direction  $x$ ,  $y$  and  $z$  was collected from 25 different cuts at Point a, b and c indicated in the figure.



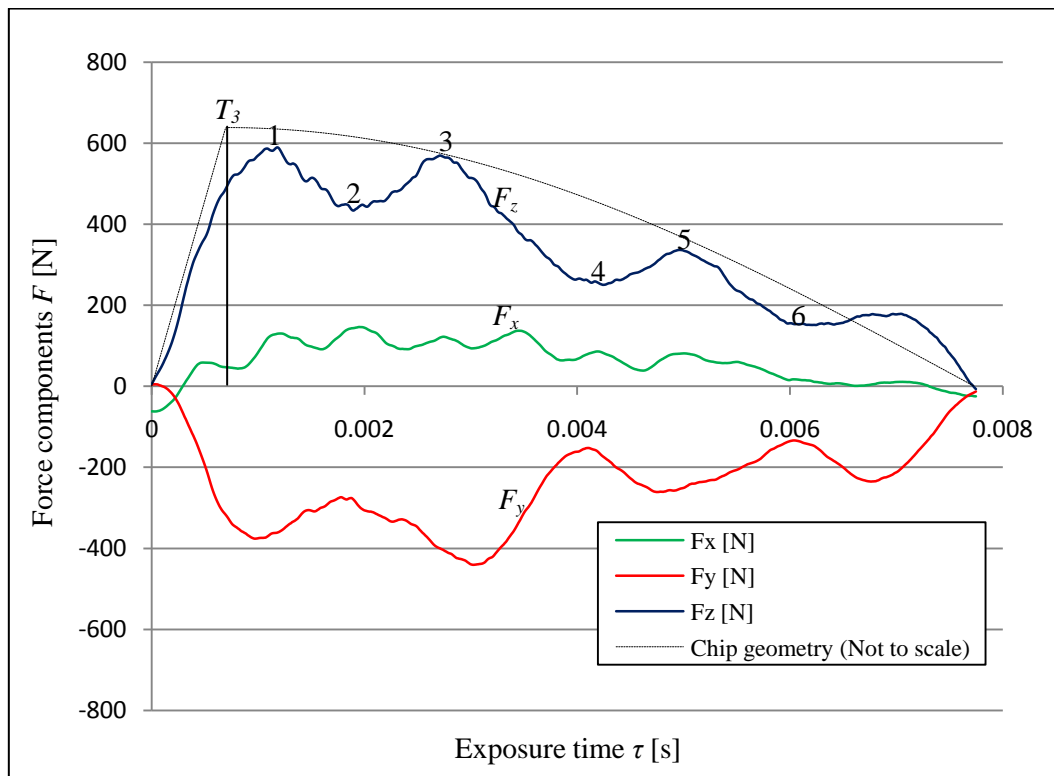
**Figure 5.2:** Tool and deformation at initial impact ( $\varphi_{st}$ ) of cut ( $v_c=40$  m/min and  $h_{eMax}=0.106$  mm)

The time periods ( $T_1$  and  $T_3$ ) are calculated using eqns. (16) and (23-31) and revealed in Table 5.2 are less than the measured time periods it took to reach the first variation of the cyclic  $F_y$  (Point c) component (Point c = 1.2205 ms) and  $F_z$  component (Point a = 1.3225 ms).  $T_3$  (0.708 ms) and the time required to encounter the first variation in  $F_x$  component (Point b = 0.7065 ms) are very similar.

**Table 5.2** Calculated and measured time periods for different force components

a		b		c		Calculated values	
$F_z$ [N]	$T_a$ [ms]	$F_x$ [N]	$T_b$ [ms]	$F_y$ [N]	$T_c$ [ms]	$T_1$ [ms]	$T_3$ [ms]
569.525	1.3225	55.98	0.7065	-328.54	1.2205	0.34	0.708

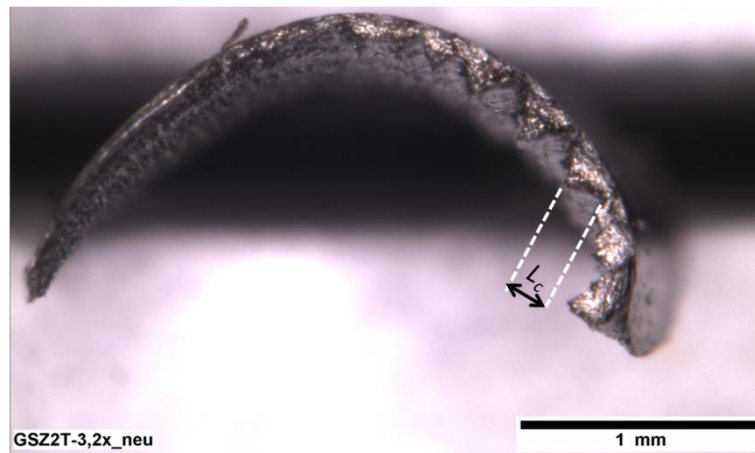
Therefore, the time it took to encounter the maximum in  $F_y$  ( $T_c$ ) and  $F_z$  ( $T_a$ ) was not at the time ( $T_3$ ) when the tool encountered  $h_{eMax}$  of the chip segment. The time it took to encounter the maximum in  $F_x$  and  $F_y$  is longer than for the tool to pass by  $h_{eMax}$ . Therefore the *real* maximum effective feed (Point 1, Figure 5.3) takes longer to encounter than the maximum theoretical value (when  $T_3=h_{eMax}$ ) calculated from eqn. (31). This could be due to the deformation of the work piece, and the frictional phenomena between the cutting tool and work piece. Figure 5.3 (Points 1-6) illustrates the position of the tool edge for the visual images shown Figure 5.5.



**Figure 5.3:** Illustrating the time difference in the *real* maximum effective feed and the maximum theoretical value ( $T_3=h_{eMax}$ ) with  $v_c=40$  m/min and  $h_{eMax}=0.106$  mm

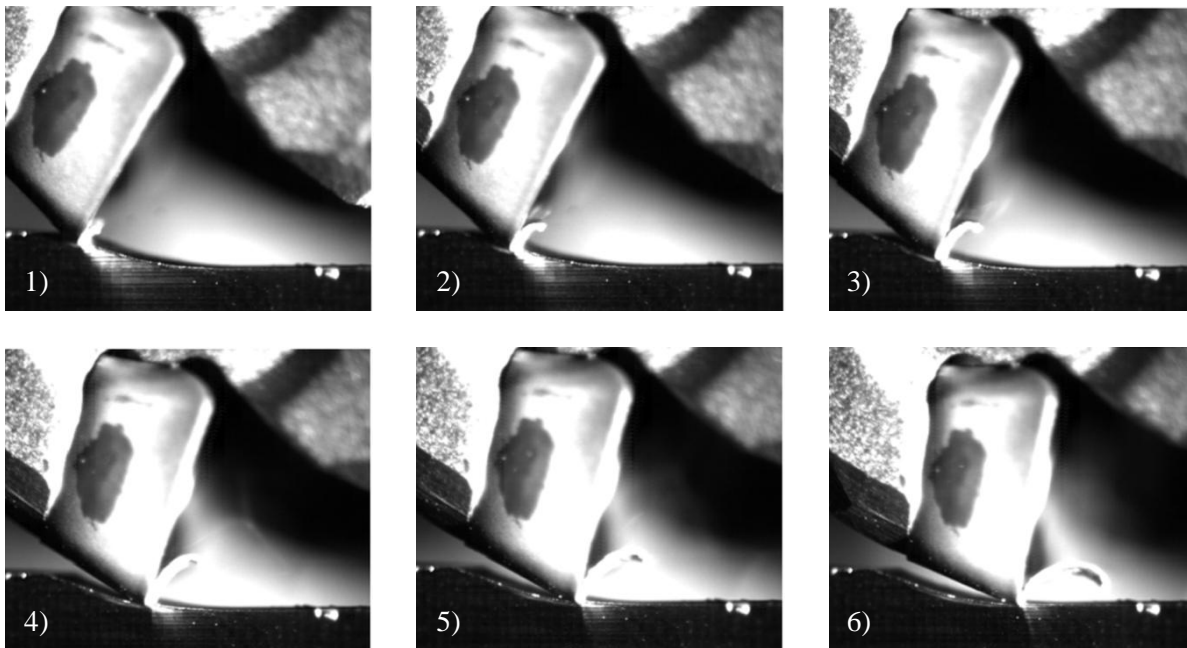
As illustrated in the figure above, there is a difference in the frequency of the variation for the three force components.  $F_x$  had more variations than  $F_y$  and  $F_z$  in the same period of time. The amount of

segmentations counted from the collected chips clearly correlates with the force variation frequency of  $F_x$ . In addition to this, the deformed chip surface length for the first few segments was also studied; and it was found that its chip frequency ( $f_c$ ) corresponded with the force variation frequency in  $F_x$ . The cutting tool has  $\gamma_a=7^\circ$  and therefore the cutting edge does not lie in the plane ( $x$ - $z$ ) normal to the feed direction. Thus, there is a force ( $F_x$ ) in the  $x$ -direction that corresponds to the chip frequency. The Ti6Al4V chip in Figure 5.4 illustrates the segmented chip formation and deformed chip surface length ( $L$ ).



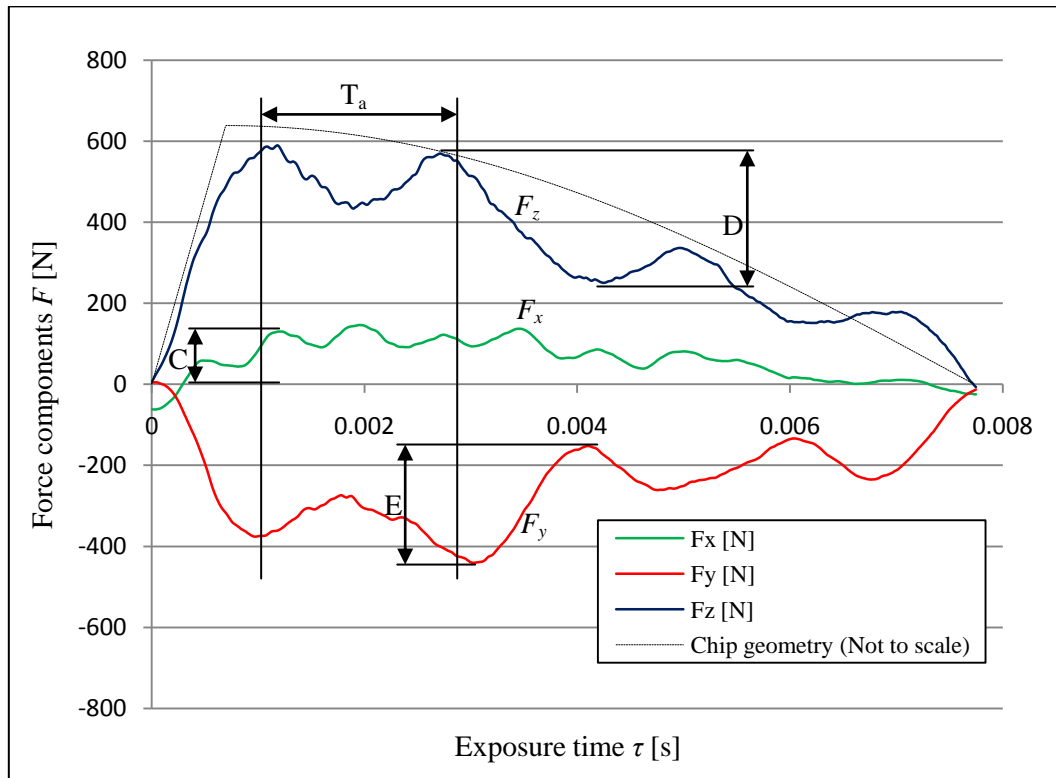
**Figure 5.4:** Deformed Ti6Al4V chip surface length of the segmented chip

As illustrated in Figure 5.5, the high-speed visual images of the experiments clearly indicate that the force fluctuations in  $F_y$  and  $F_z$  correlate with the deflections caused by the chip curling on the rake of the tool when measured at the peak value points [see Figure 5.3, Points (1-6)] in  $F_z$  and  $F_y$ .



**Figure 5.5:** Illustration of the chip curling on the rake of the tool (Points 1-6 are shown in Figure 5.3)

Although the forces declined due to the decreasing  $h_e$ , it was also interesting to note that the period ( $T_a \approx 1.9\text{ms}$ ) in the force fluctuations in  $F_y$  and  $F_z$  corresponded as illustrated in Figure 5.6. The fluctuation frequency (around 500 Hz) of these force components is found to be significantly lower than the supplied natural frequencies of the dynamometer and the cutting tool. From this analysis, another explanation for this fluctuation could be that a critical contact length on the rake is reached, before the chip separates from the tool. Nevertheless, the effect of the chip serration is found to be insignificant in the  $F_z$ - and  $F_y$ -components. This finding was also the main purpose of the experiment.



**Figure 5.6:** Tool rotation angle at final part of segment cut ( $v_c=40$  m/min and  $h_{eMax}=0.106$  mm)

Although titanium machining is characterised by an unusually small contact area where the chip is in contact with the rake of the tool, the results indicated that the force fluctuation of  $F_z$  and  $F_y$  (the 2D-plane) were caused mainly by the frictional phenomena between the chip flow, cutting tool and work piece. This could be due to the deflections caused by the curling of the chip on the rake face of the tool as illustrated in Figure 5.5 or due to vibration caused by the milling equipment. As illustrated in Figure 5.6, the amplitude (C) in the fluctuation of  $F_x$  was less than the amplitude (D and E) in the fluctuation of  $F_z$  and  $F_y$ .

Therefore, the effect of shear location on tool failure is found to be insignificant compared to the combined effect of the frictional phenomena between the cutting tool, chip and work piece; and the vibrations caused by the milling equipment.

## 5.1.2 Conventional- and transition-speed milling tests

Rough milling of Ti6Al4V with carbide cutting tools is still limited to a  $v_c$  ranging from 30-60 m/min and  $h_{eMax}$  ranging from 0.1-0.25 mm [25,28]. This experiment was to compare different rough milling parameters and to evaluate the effect on tool failure mode and wear mechanisms. Cutting force and chip formation within and outside the safe zone limits constructed from literature [24] were evaluated. The effect of tool wear on cutting force was examined with a normalized cutting force indicator. The goal was to validate the constructed tool wear map and to re-examine the thermal ( $v_c$ ) and mechanical ( $h_{eMax}$ ) limits. The safe zone for this experiment is defined by a TL > 30min.

### 5.1.2.1 Experimental setup and design

A Ti6Al4V (ASTM B265: Grade 5) sample was used, with a hardness measured to be 360 HV and a high ultimate tensile strength (1080 MPa) as indicated in Table 5.3. This grade of material was chosen to produce the most demanding conditions achievable when machining this alloy.

**Table 5.3:** Mechanical and physical properties of the work piece at room temperature

Test specimen	Ti6Al4V
Hardness	360 HV
Ultimate tensile strength	1080 MPa

The tests were done on the Heckert HEC 500 D with tough TiAlN PVD coated carbide, familiar to the South African industry. A Kistler 3D dynamometer (Type 9255B) was used to measure the cutting forces and Emulsion Hebro 565B (10%) coolant was used in a flood condition. The equipment used is summarized in Table 5.4.

**Table 5.4:** Experimental machines and equipment used in the conventional- and transition speed milling tests

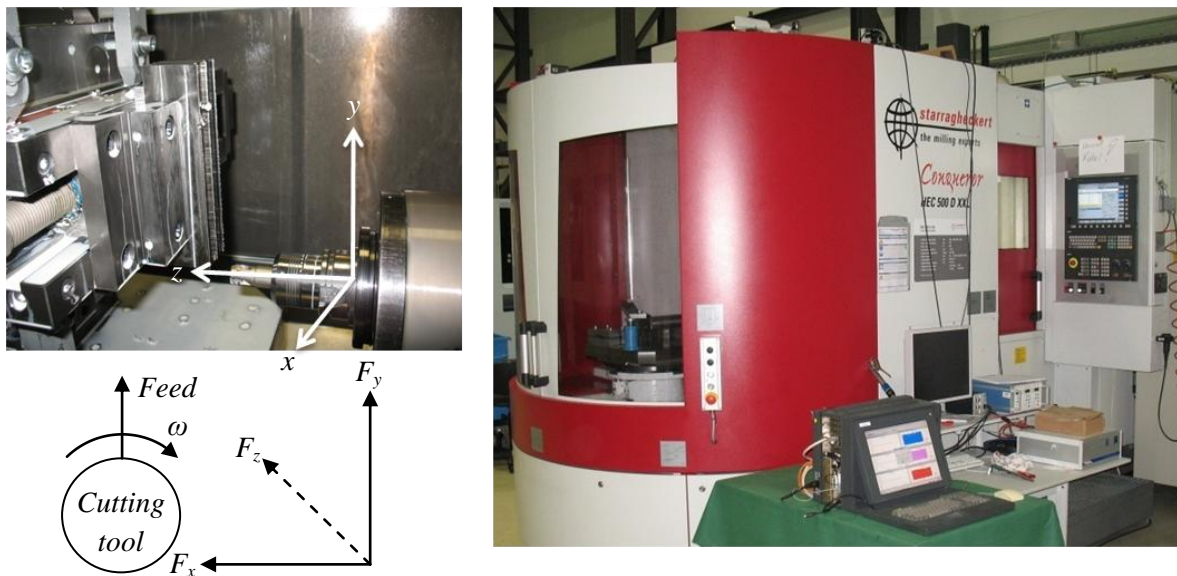
Machine tool	4-axis machining center Heckert HEC 500 D
Milling tool	HM90 E90A-D20-3W20 (Iscar), $z = 3$
Cutting insert geometry	APKT 1003R8T-FF (Iscar)
Cutting material	Cemented carbide: TiAlN (PVD)
Coolant	Emulsion Hebro 565B, 10%, inner coolant supply, flood
Force Measurement	Kistler 3D dynamometer type 9255B
Optical Microscope	Dell Computer with Zeiss AXIOVISION4

The coated carbide tools were analysed at conditions similar to that during high performance machining with cutting speeds ranging from 40-100 m/min and chip loads from 0.1-0.4 mm. Relatively high  $v_c$  and very high  $h_{eMax}$  were chosen for the tests with the carbide. The experimental conditions are shown in Table 5.5.

**Table 5.5:** Experimental cutting conditions of the conventional- and transition speed milling tests

Cutting speed ( $v_c$ )	40-100 m/min
Feed per tooth ( $f_z$ )	0.1-0.4 mm/z
Axial depth of cut ( $a_p$ )	2 mm
Radial depth of cut ( $a_e$ )	20 mm (Full immersion)

The flank wear land ( $V_B$ ) was analyzed with an optical microscope for dimensional measurements. The failure criterion due to wear on the flank [11] was set for a maximum when  $V_B=0.4$  mm. Figure 5.7 illustrates the setup and illustrates the direction of the cutting force components, the rotation angle ( $\omega$ ) and feed direction.



**Figure 5.7:** The experimental setup with the direction of force components, rotation angle ( $\omega$ ) and feed direction

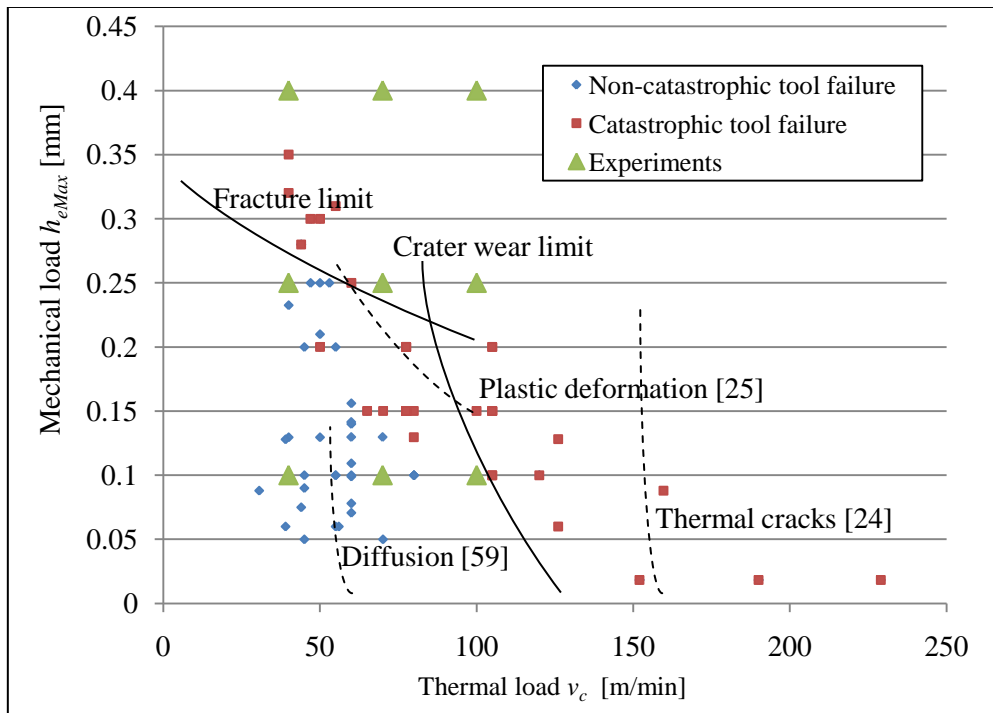
Once the force components in the  $x$ -,  $y$ - and  $z$ -directions were measured with a Kistler 9255B dynamometer,  $F_c$  could be expressed using eqns. (7-9). The carbide tool experiments were done with a full radial immersion ( $h_{eMax}=f_z$ ). Therefore entry angle for the carbide tool is given by  $\varphi_{st} = 0^\circ$  and the exit angle by  $\varphi_{ex} = 180^\circ$ .

### 5.1.2.2 Experimental results

Figure 5.8 illustrates the mapping of trials from literature [12,24,113,20] and industry and illustrates the experimental parameters for this study. The figure illustrates which cutting experiments failed catastrophically due to too high chip load (exceeding the fracture limit) and cutting speeds (exceeding the crater wear limit). Thermal cracks were found [24] for carbide tools  $v_c=152$  m/min. In another research study [25] carbides were found to plastically deform at  $v_c \leq 60$  m/min with a relative high chip load. The stipple-lines indicate the various failure limits according to the type of wear found in

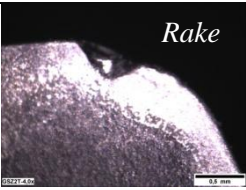
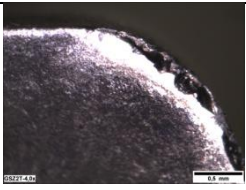
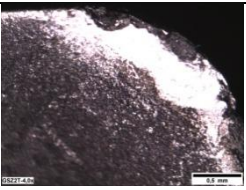
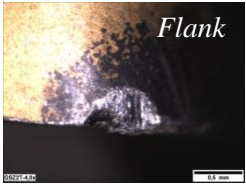
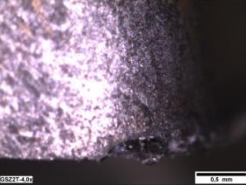
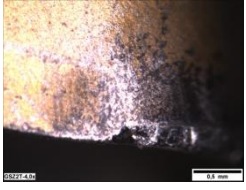


literature [24,25,59]. The solid fracture- and crater wear limit lines were given by tool suppliers [28,102] and complemented in background studies [114].

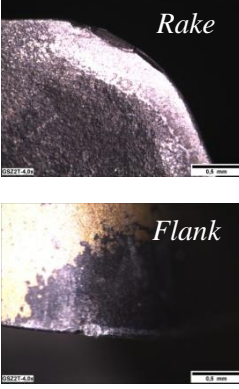
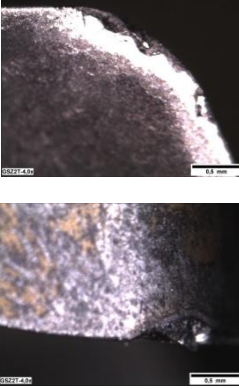
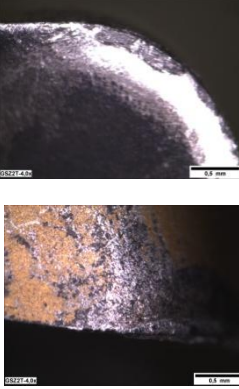

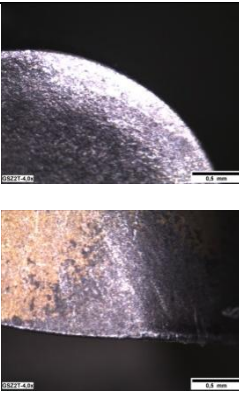
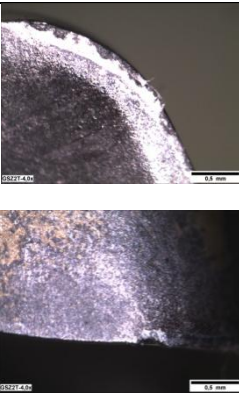


**Figure 5.8:** The constructed wear map for rough milling of Ti6Al4V with carbide tools

The catastrophic tool failure points in the safe zone were taken into account, but were found to be the result of experimental tool materials and improper milling machines. The experimental results of the carbide tools that were used for rough milling experiments are illustrated in Figure 5.9. The tools were examined with optical microscopy imaging and were characterized to categorize into a failure region.

 <p><i>Rake</i></p>		
 <p><i>Flank</i></p>		
<p><math>v_c=40</math> m/min; <math>h_{eMax}=0.4</math> mm; <math>TL&lt;30</math> min Catastrophic tool failure: Not preceded by extensive crater wear on the rake face</p>	<p><math>v_c=70</math> m/min; <math>h_{eMax}=0.4</math> mm; <math>TL&lt;30</math> min Catastrophic tool failure: Not preceded by extensive crater wear on the rake face</p>	<p><math>v_c=100</math> m/min; <math>h_{eMax}=0.4</math> mm; <math>TL&lt;30</math> min Catastrophic tool failure: Preceded by extensive crater wear on the rake face and deformation</p>

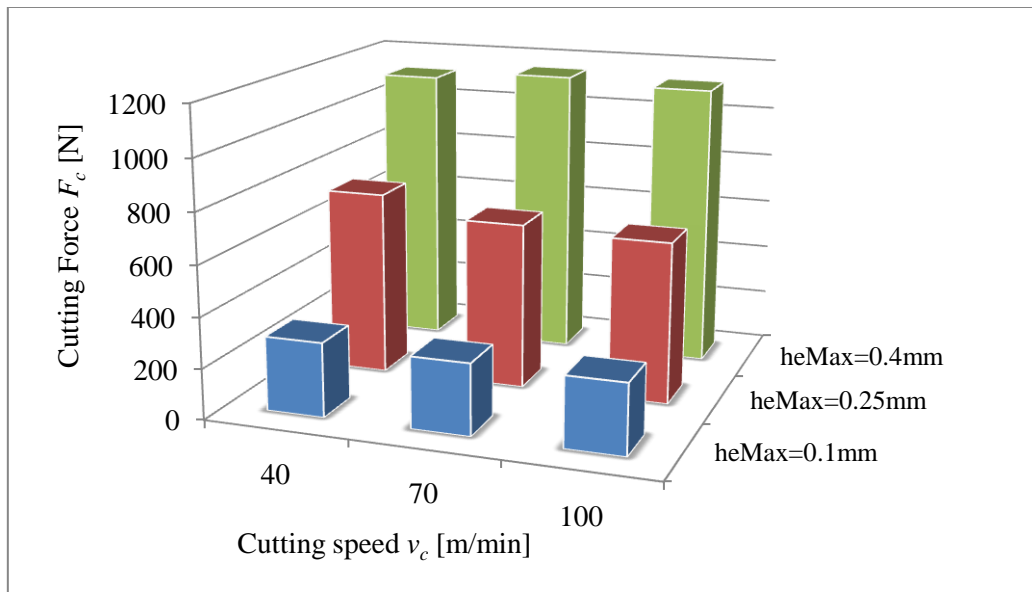


 <p style="text-align: center;"><i>Rake</i></p> <p style="text-align: center;"><i>Flank</i></p>		
<p><math>v_c=40</math> m/min; <math>h_{eMax}=0.25</math> mm; <math>TL&gt;30</math> min Safe zone: Non-catastrophic tool failure</p>	<p><math>v_c=70</math> m/min; <math>h_{eMax}=0.25</math> mm; <math>TL&lt;30</math> min Catastrophic tool failure: Not preceded by extensive crater wear on the rake face</p>	<p><math>v_c=100</math> m/min; <math>h_{eMax}=0.25</math> mm; <math>TL&lt;30</math> min Catastrophic tool failure: Preceded by extensive crater wear on the rake face</p>
 <p style="text-align: center;"><i>Rake</i></p> <p style="text-align: center;"><i>Flank</i></p>		
<p><math>v_c=40</math> m/min; <math>h_{eMax}=0.1</math> mm; <math>TL&gt;30</math> min Safe zone: Non-catastrophic tool failure</p>	<p><math>v_c=70</math> m/min; <math>h_{eMax}=0.1</math> mm; <math>TL&gt;30</math> min Safe zone: Non-catastrophic tool failure</p>	<p><math>v_c=100</math> m/min; <math>h_{eMax}=0.1</math> mm; <math>TL&gt;30</math> min Safe zone: Non-catastrophic tool failure</p>

**Figure 5.9:** Failure modes for carbide tools in rough milling of Ti6Al4V

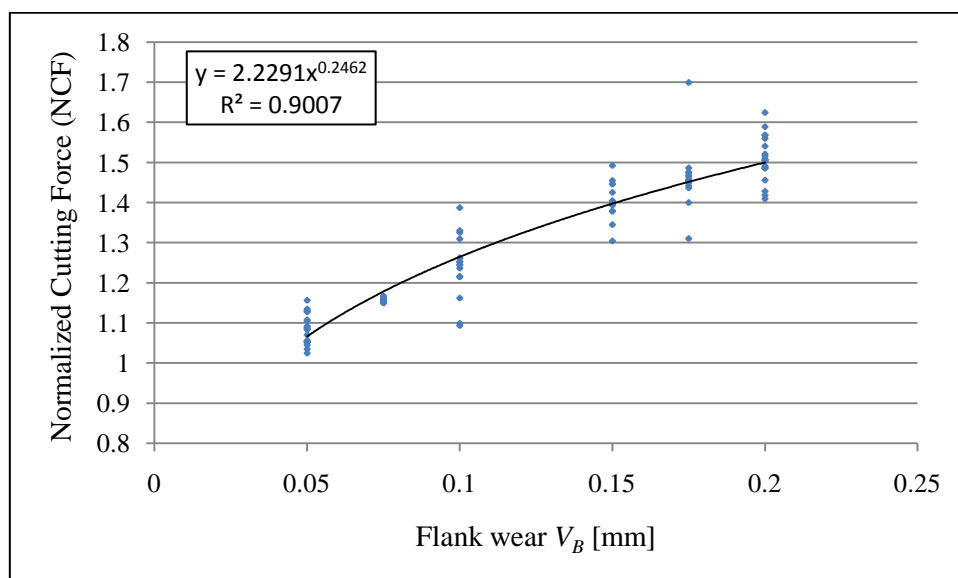
As illustrated in Figure 5.8, results from industry and experimentation indicate that rough milling operations are limited to cutting speeds of 30-60 m/min with  $h_{eMax}$  ranging from 0.1-0.25 mm [28]. As a complementary perspective this experimental results proved that the cutting speeds (thermal load) for carbide tools in rough milling conditions can be increased to 100 m/min under a low mechanical loading ( $h_{eMax}=0.1$  mm), while  $h_{eMax}$  is still limited to 0.25 mm at  $v_c=40$  m/min. No thermal cracks were observed, but plastic deformation was found at  $v_c=100$  m/min and  $h_{eMax}=0.4$  mm.

Figure 5.10 illustrates the cutting forces for the different rough milling conditions. The cutting forces were generally influenced by  $h_{eMax}$ , while the  $v_c$  showed no significant influence.



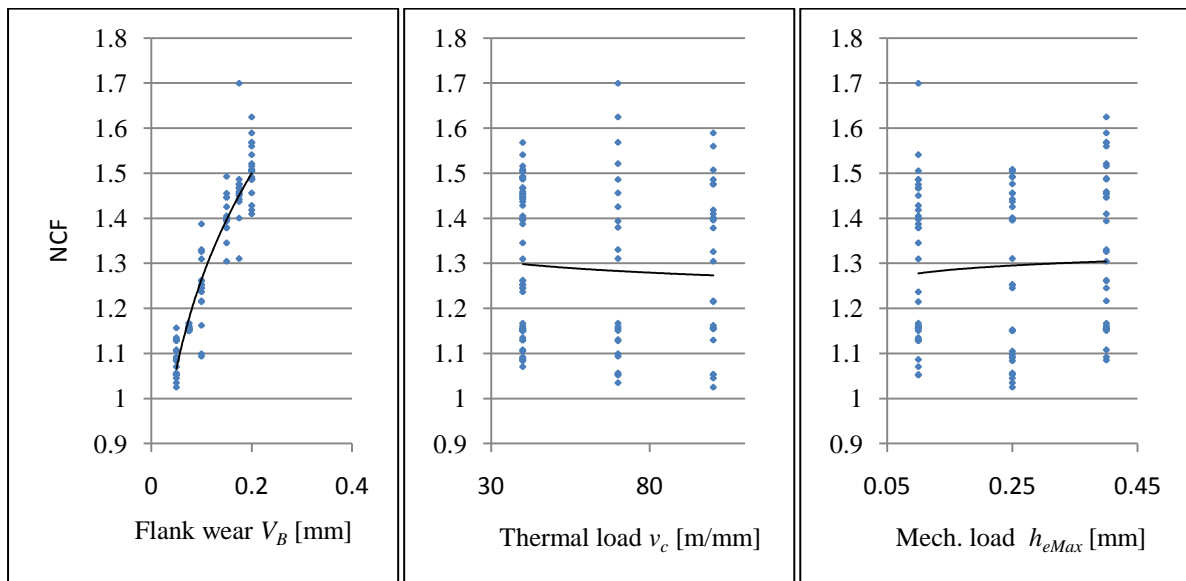
**Figure 5.10:** Cutting forces for carbide tools in rough milling of Ti6Al4V

The segmented chip formation and the frictional phenomenon caused cyclic variations in the force components as evaluated in the previous experiment. The cutting force was measured for set cutting intervals and the tool wear ( $V_B$ ) measured throughout these intermissions. The flank wear land width  $V_B$  was measured by using the optical microscope after every run of the tool [86]. The selected tool wear criterion, in order to avoid the effect of fractured cutting edges, was set at  $V_B=0.2$  mm for this analysis. In general the cutting force and the power increase when the tool wear  $V_B$  increases. These characteristics illustrated in Figure 5.11 and Figure 5.12 was developed using eqns. (14) & (15).



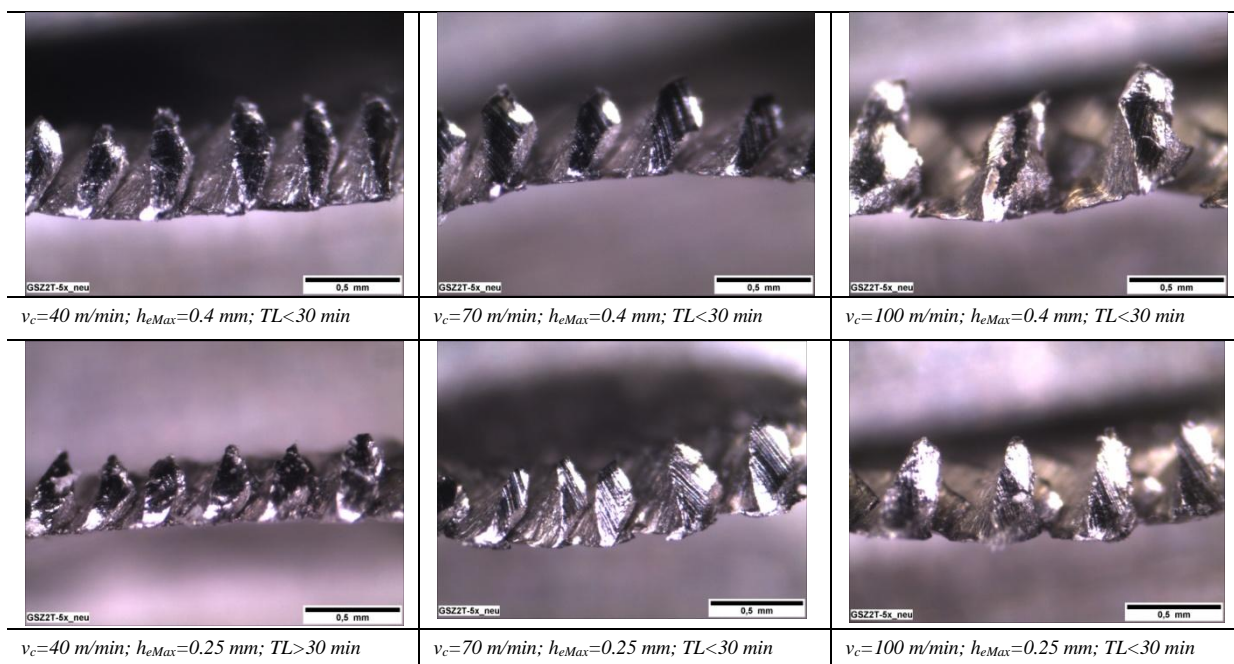
**Figure 5.11:** Normalized Cutting Force (NCF) relative to flank wear ( $V_B$ )

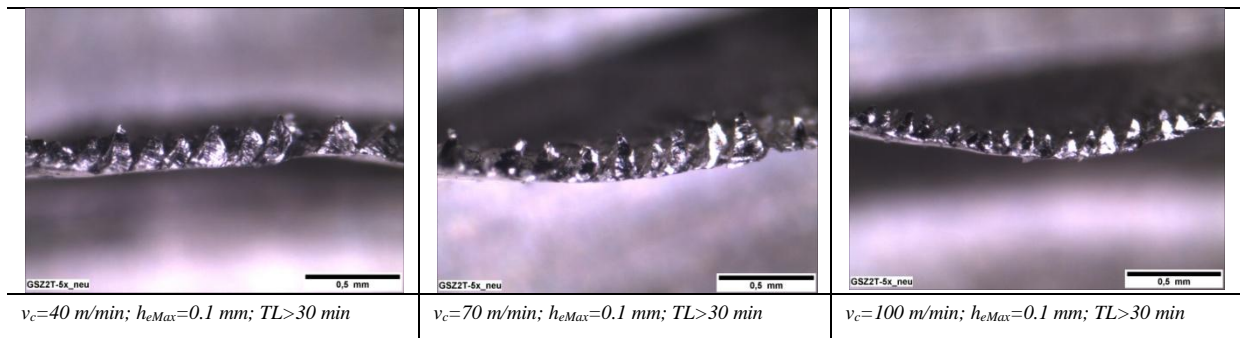
The results showed a confidence level of 90% to fit the power function. From this figure the tool wear can be estimated by measuring the increase in  $F_c$  (e.g.  $NCF = 1.5$  corresponds to  $V_B=0.2$  mm). The influence of other factors such as  $v_c$  and  $h_{eMax}$  was also studied and are illustrated in Figure 5.12.



**Figure 5.12:** Comparing the influence of  $V_B$ ,  $v_c$  and  $h_{eMax}$  on the increase of the NCF

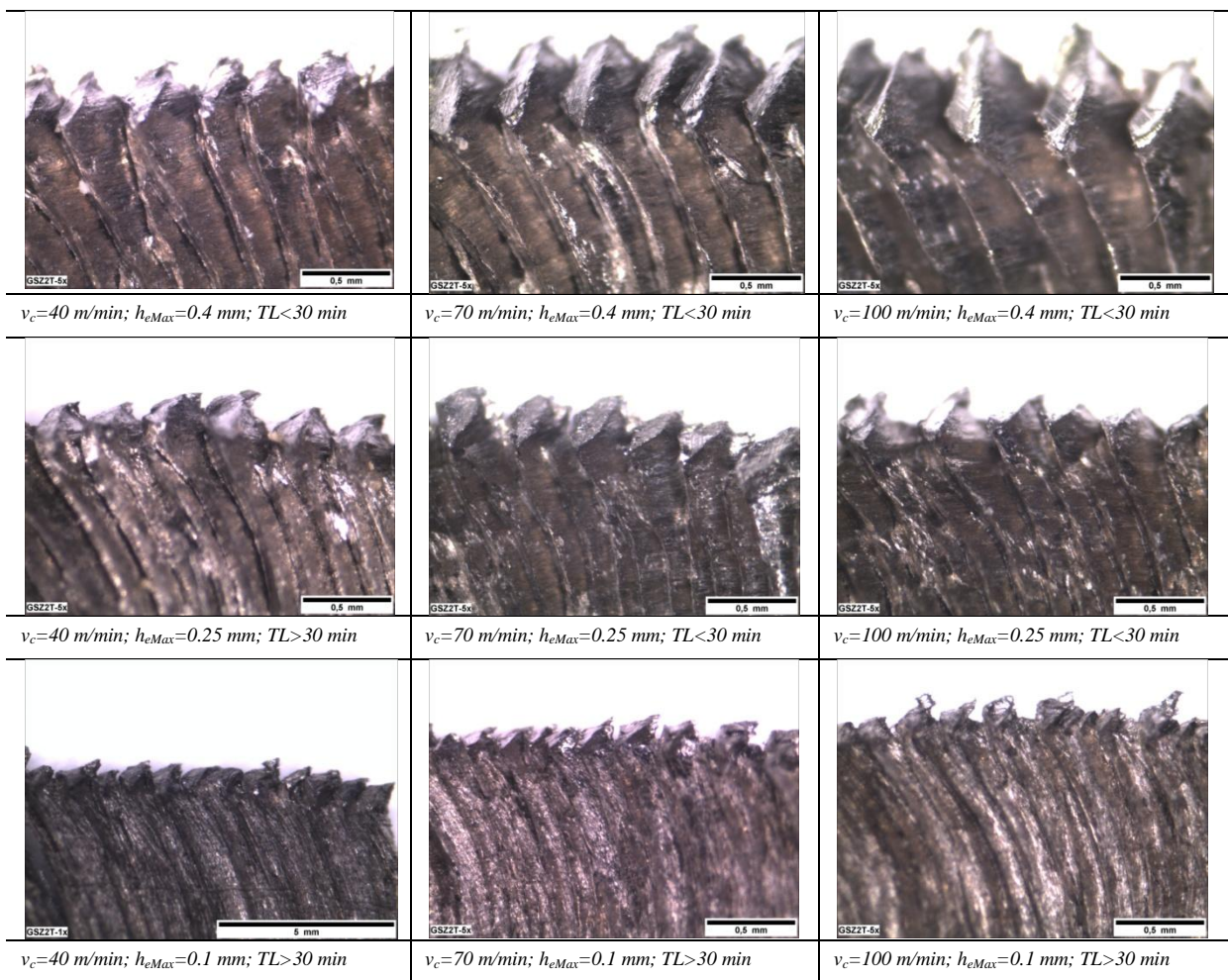
From these figures it was clear that the increase in cutting force with time was undoubtedly due to the increasing flank wear ( $V_B$ ).  $v_c$  and  $h_{eMax}$  shows no relationship with the  $NCF$  value. These results can be used in the future to determine  $V_B$  by examining the  $MF_c$  while in operation. The chips were studied around the point of  $h_{eMax}$ , which is at an engagement angle of  $90^\circ$ . The results are illustrated in Figure 5.13 and Figure 5.14 and show an increase in the thickness between the serrations with an increase in  $h_{eMax}$ .





**Figure 5.13:** Top-view of the segmented chip formation

The influence of  $v_c$  is not excessive. Figure 5.14 illustrates the difference in the thickness between the serrations with an increase in  $v_c$  and  $h_{eMax}$  from a side view of the chip.



**Figure 5.14:** Side view of the segmented chip formation

The chips were found to be segmented for all the cutting conditions. From this it is evident that the thickness of the chips increased with an increase in  $h_{eMax}$ , which can lead to higher fluctuation in the different force components and cause micro-chipping of the cutting tool.

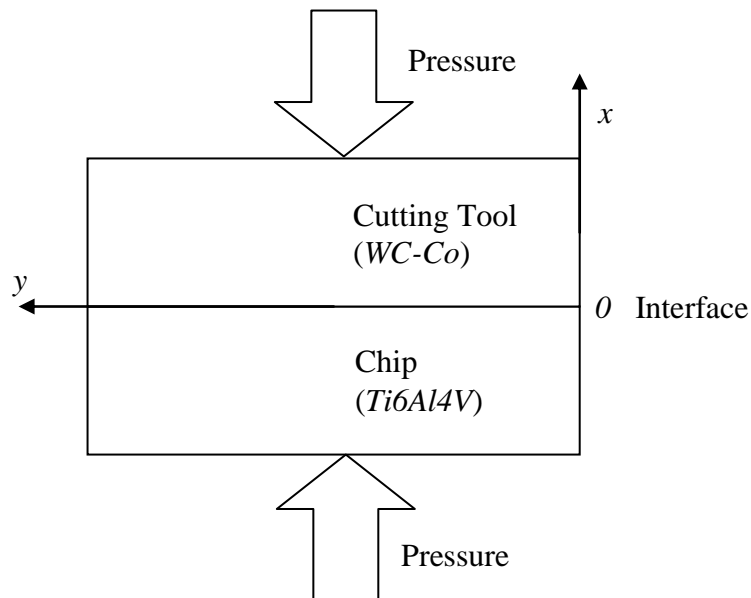
### 5.1.3 Static interaction of WC-Co/Ti6Al4V diffusion-couple

The chemical compatibility of WC-Co tool materials with Ti6Al4V has been evaluated by means of the static interaction diffusion-couples technique. Despite machining being a dynamic situation where thermodynamic equilibrium does not apply, the information provided by the interaction couple experiments reveals the potential for chemical interaction to take place at certain temperatures. A thermodynamic model for chemical wear was developed by Kramer and Judd [115] and Kramer [116].

Diffusion is controlled by the cutting temperature [117] and maximum cutting temperature between the tool and the Ti6Al4V work piece can reach 1000°C [81,60]. Therefore, the diffusion mechanism from the Ti6Al4V to WC-Co carbide tools (vice versa) at temperatures ranging from 400-1000°C was examined. In so doing, the maximum temperature at which the tool and the work piece materials are chemically compatible could be identified. The sections of the diffusion couples were studied by using a scanning electron microscopy (SEM).

#### 5.1.3.1 Experimental setup and design

The purpose is to verify at what temperature the elemental diffusion occurs if at all. Figure 5.15 shows the schematic diagram of the diffusion couple. The diffusion couples (Ti6Al4V and the WC-Co) were brought into contact and heated with different temperatures.



**Figure 5.15:** Schematic diagram of the diffusion couple.

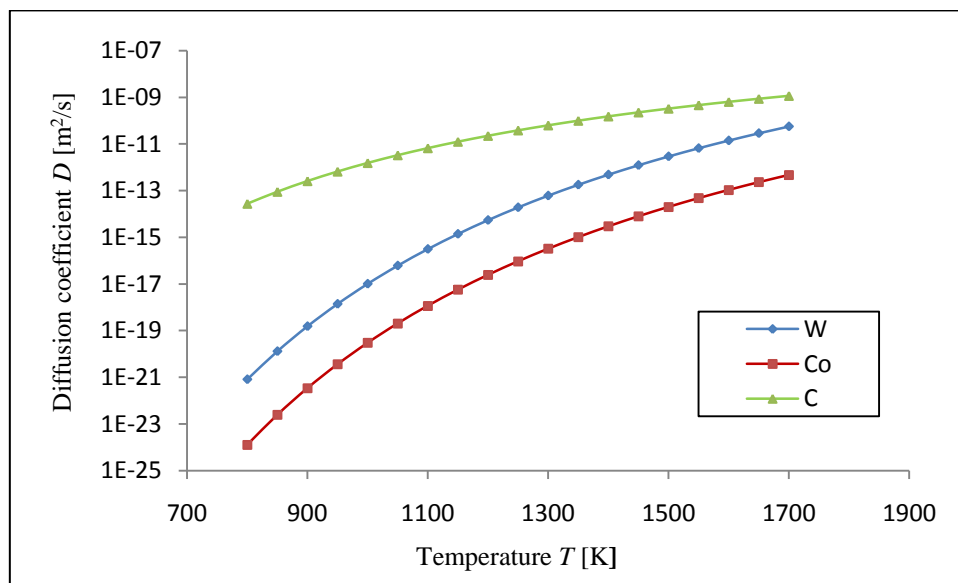
The composition, physical, and mechanical properties of the carbide tool material are listed in Table 5.6. The tool material had a hardness of  $14.5 \pm 5$  GPa, thermal conductivity of 78 W/m·K and a thermal expansion of  $5.5 \times 10^{-6}$ /K.



**Table 5.6:** Properties of the WC/Co carbide tool material

Composition	Density	Hardness	Flexural strength	Thermal conductivity	Thermal expansion
(wt. %)	[g/cm <sup>3</sup> ]	[GPa]	[MPa]	[W/m·K]	[x10 <sup>-6</sup> /K]
WC+6% Co	14.7	14.5±5	1350±30	78	5.5

The diffusion coefficients of the different elements could be calculated using eqn. (4). As illustrated in Figure 5.16 the diffusion coefficient of C is the largest, followed by the diffusion coefficient of W which is two orders of magnitude larger than that of Co at the same temperature.



**Figure 5.16:** Diffusion coefficients at different temperatures

The diffusion coefficients from the figure, illustrates that the final concentrations of W and C should be higher than that of Co at the same cross-section (e.g.  $x=15\mu\text{m}$ ) of the work piece after the same time. Considering the work piece is located in the negative direction of the  $x$ -axis (Figure 5.15). The composition and properties of Ti6Al4V are listed in Table 5.7 and Table 5.8. The Ti6Al4V experimental specimen had a hardness of 360 HV and ultimate tensile strength of 1080 MPa.

**Table 5.7:** Mechanical and physical properties of the work piece at room temperature

Test specimen	Ti6Al4V
Hardness	340 HV
Ultimate tensile strength	1080 MPa

**Table 5.8:** Chemical composition of Ti6Al4V (wt.%)

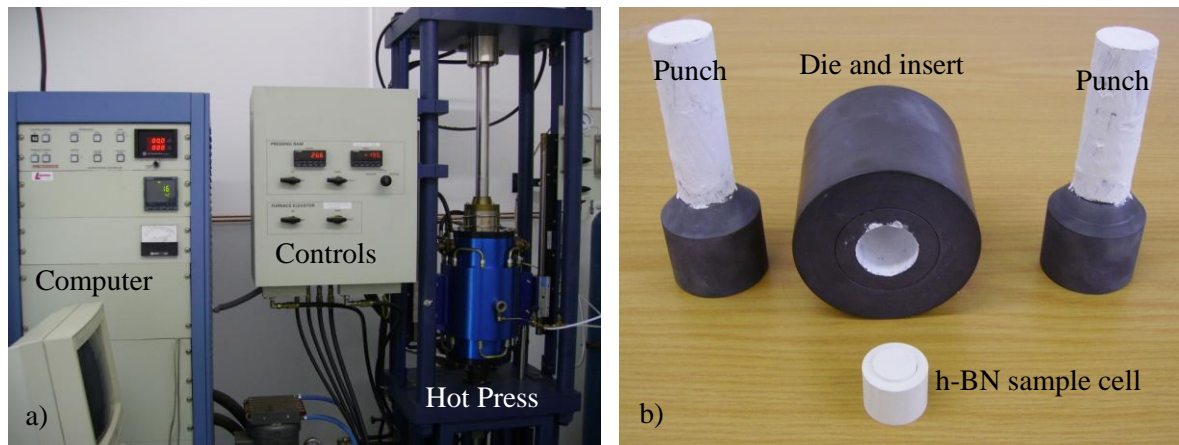
	Al	V	Fe	O	C	H	N	Ti
Min.	5.50	3.5	0.3	0.14	0.08	0.01	0.03	Balance
Max.	6.75	4.5	-	0.23	-	-	-	

The uni-axial hot press used in this work is an Astro TT HP20-3560-20. The samples were hot pressed in a flowing argon atmosphere, under an applied compressive pressure of 10 MPa at temperatures ranging from 400°C to 1000°C as illustrated in Table 5.9.

**Table 5.9:** Experimental machines, equipment and conditions used in the static interaction of WC-Co/Ti6Al4V diffusion couple experiment

Hot press	Astro TT HP20-3560-20
Scanning Electron Microscope	Jeol SEM 7500F with AnalySIS software 3.2 (Build 799)
Temperature	400 - 1000 °C
Pressure	10 MPa
Time	90 minutes
Heating rate	50 °C/min
Cooling rate	20 °C/min
Vacuum levels	10 mtorr

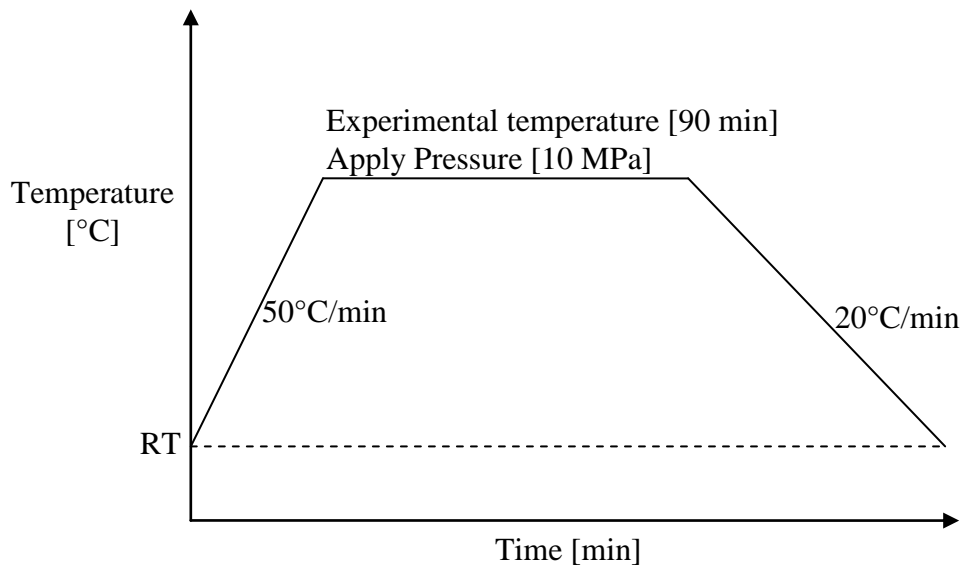
Both the surfaces of the WC/Co carbide and the Ti6Al4V alloy were polished to produce a final surface roughness  $R_a < 0.05 \mu\text{m}$ . Figure 5.17 shows the Uni-axial Hot Press and the hot zone components. A programmed computer was used to monitor the diffusion cycle during pressing at elevated temperatures.



**Figure 5.17:** The equipment for the diffusion experiment: a) The Uni-axial hot press and b) the hot-zone components

The sample cell was made from Hexagonal-BN (h-BN), while the piston was a graphite rod coated with layers of h-BN suspension. Hexagonal-BN was chosen as a crucible material, due to its high temperature stability (decomposition temperature around 3000°C), chemical inertness (stability in argon gas atmosphere up to 2200°C), high thermal shock resistance and high thermal conductivity.

The furnace was heated to the desired experimental temperature at  $50^{\circ}\text{C}/\text{min}$  intervals and held at the temperature for 90 minutes, while the load is applied. The hot press cycle is shown schematically in Figure 5.18. The system is automated to maintain constant pressure. The pressure was only removed after the furnace had cooled down and the heating elements were switched off.



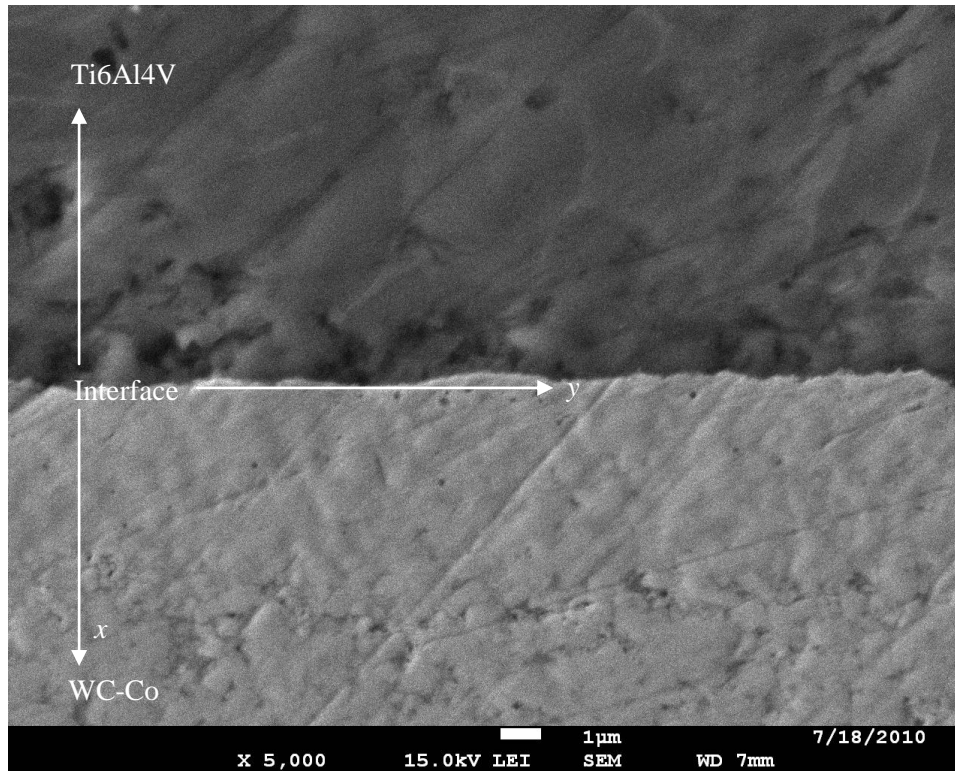
**Figure 5.18:** The temperature profile for the diffusion experiments (Not to scale, for illustrative purposes only)

The furnace was then cooled to room temperature (RT) at  $20^{\circ}\text{C}/\text{min}$ . At RT the sample cell was removed from the graphite die and insert. The scanning electron microscope used in this study was a Joel SEM 7500F equipped with AnalySIS software 3.2 (Build 799).



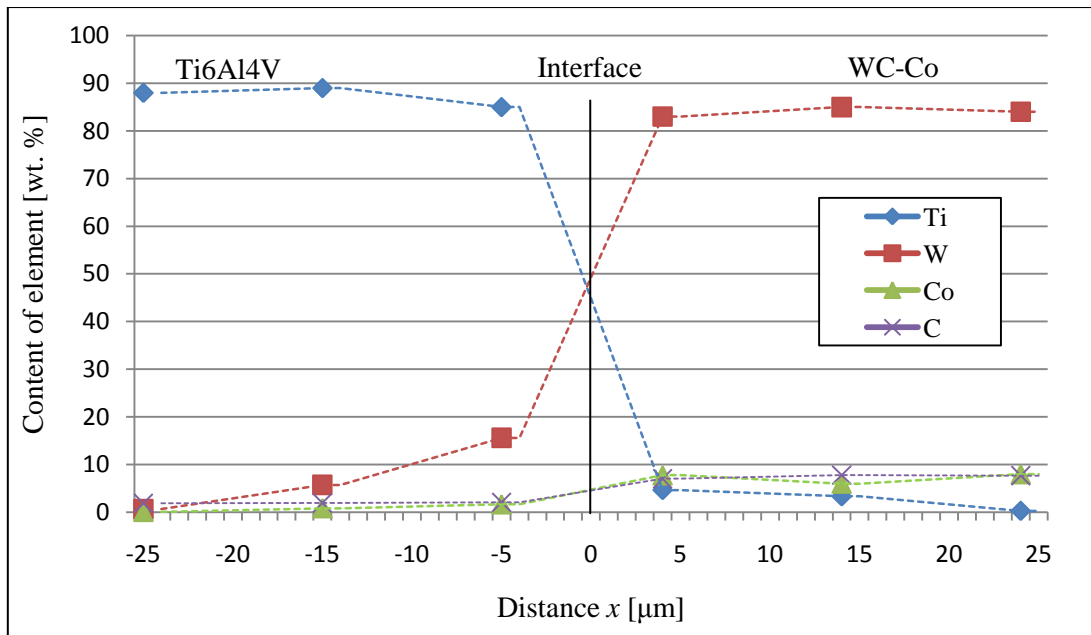
### 5.1.3.2 Experimental results

Figure 5.19 illustrates a SEM micrograph of the diffusion couple after heating for 90 minutes at 1000°C. The average accelerating voltage used was 20 keV, although much lower voltage (3 keV) was also used to image the couples.



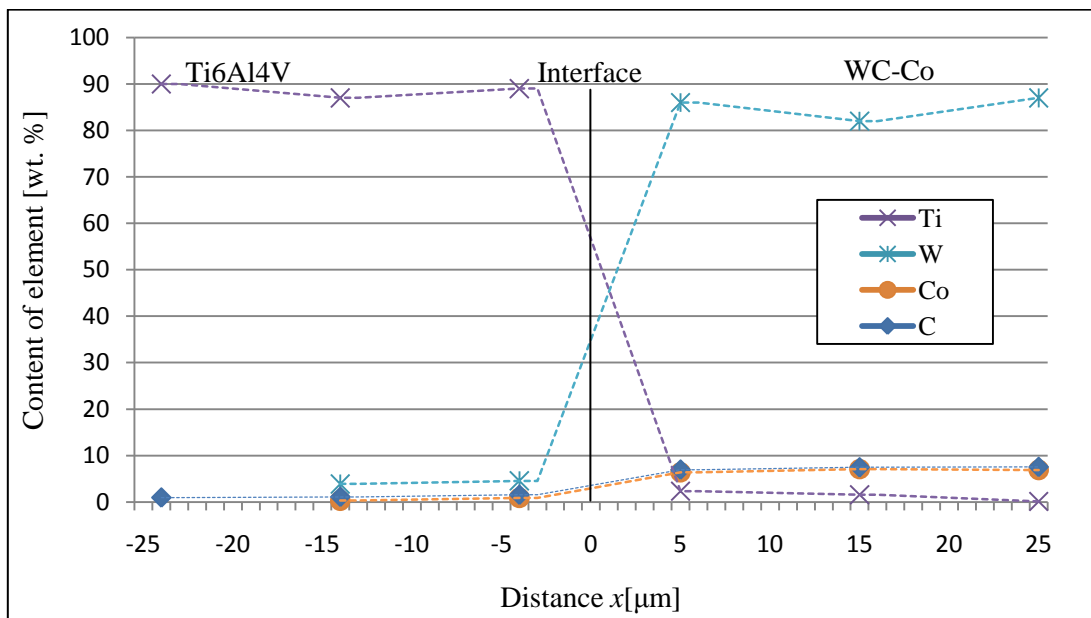
**Figure 5.19:** SEM micrograph of the diffusion couple after heating in argon for 90 minutes at 1000°C. Both secondary and backscattered electron signals were used for imaging. No chemical interaction was found at 400°C between Ti6Al4V and WC-Co. The W, C and Co elements also did not greatly penetrate into the Ti6Al4V alloy at 600°C, while at 800-1000°C, W, C and Co of the WC-Co carbide diffused into the work piece material.

This complemented results from literature [61], in which diffusion between the tool and the work piece material was found at a cutting speed of 55 m/min. According to Figure 2.11 a  $v_c=55$  m/min will generate a  $T_v \approx 600^\circ\text{C}$ . Figure 5.20 shows the Ti, W, and Co elements diffusion across the WC-Co carbide and Ti6Al4V alloy interface for 1000°C.



**Figure 5.20:** Distribution of elements along the interface of the diffusion couple after heating at 1000°C in argon for 90 minutes under a load of 10 MPa

As illustrated in the figure, the depth of W and Co penetration into the Ti6Al4V alloy is around 20μm. Figure 5.21 shows the Ti, W, and Co elements diffusion across the WC-Co carbide and Ti6Al4V alloy interface for 800°C.



**Figure 5.21:** Distribution of elements along the interface of the diffusion couple after heating at 800°C in argon for 90 minutes under a load of 10 MPa

As predicted from Figure 5.16, the final concentrations of W and were found to be higher than that of Co at the same cross-section of the work piece after the same time for both 800°C and 1000°C. These

results complemented the layout of the constructed tool wear map for the rough milling of Ti6Al4V with carbide as a chemical interaction was also found [61] 600°C onwards in cutting experiments.

## 5.2 Finish milling with PCD tool material

These experiments were designed to evaluate the constructed wear map for the finish milling of Ti6Al4V with PCD tools. Initially, different PCD (fine-, medium and coarse) materials were tested to establish which is most appropriate for the milling of Ti6Al4V. High-speed milling experiments followed to assess the finish tool wear maps. Thereafter, diffusion-couple experiments were conducted to understand the types of chemical interactions between Ti6Al4V and PCD better.

### 5.2.1 High-speed milling tests

Finish milling of Ti6Al4V with polycrystalline diamond (PCD) shows promising results at  $v_c$  ranging from 175-200 m/min [24,41] and  $h_{eMax} < 0.032$  mm [24]. Cutting speeds of 300 m/min were found to cause work piece related failure (material burn) [34,91,92]. The objective of this experiment was to compare different finish milling conditions and to evaluate the effect on tool failure mode and wear mechanisms. Cutting force and chip formation within the tool- and work piece limits were also evaluated. The goal was to validate the constructed tool wear map and to re-examine the thermal ( $v_c$ ) and mechanical ( $h_{eMax}$ ) limits. These experimental results are compared with background [114,69] work and literature [34,88,24] in terms of tool life. The safe zone for this experiment is defined by a  $TL > 30$ min.

#### 5.2.1.1 Experimental setup and design

A Ti6Al4V (ASTM B265: Grade 5) sample was used, with a hardness measured to be 360 HV and a high ultimate tensile strength (1080 MPa) as indicated in Table 5.10.

**Table 5.10** Mechanical and physical properties of the work piece at room temperature

Test specimen	Ti6Al4V
Hardness	360 HV
Ultimate tensile strength	1080 MPa

The tests were done on the Heckert HEC 500 D with PCD tool material. A Kistler 3D dynamometer (Type 9255B) was used to measure the cutting forces and Emulsion Hebro 565B (10%) coolant was used in a flood condition. The equipment used is summarized in Table 5.11.

**Table 5.11:** Experimental machines and equipment used in the high-speed milling tests

Machine tool	4-axis machining center Heckert HEC 500 D 5-axis Hermle C40U (Background experiments)
Milling tool	Custom made ( $\varnothing 25$ mm, $90^\circ$ shoulder mill), $z = 1$
Cutting insert geometry	SCMN 090308F

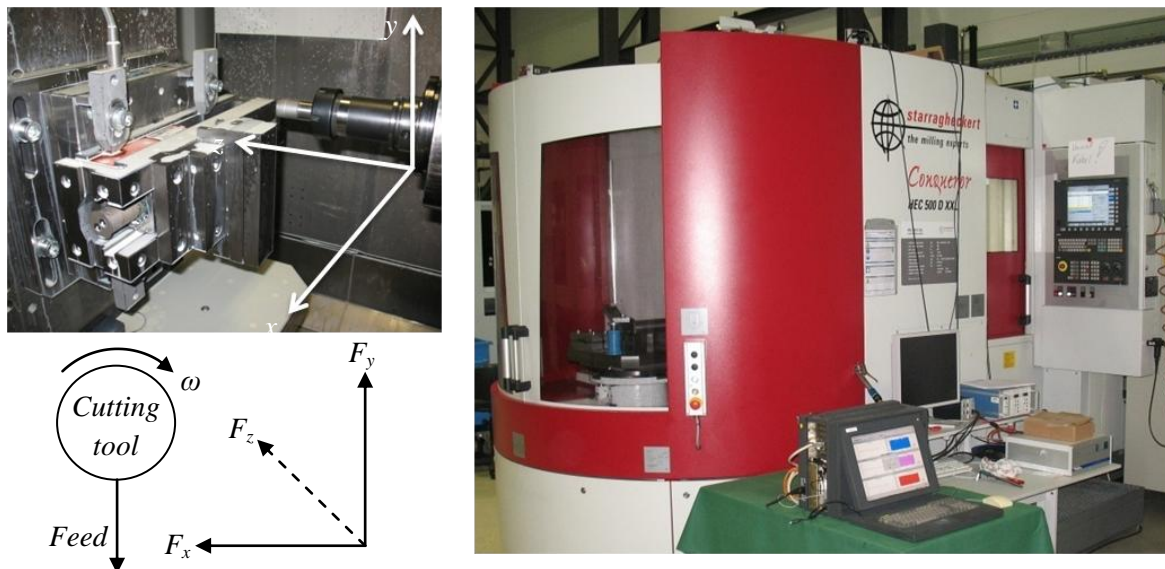
Cutting material	PCD: CMX850 (fine), CTB010 (medium), CTM302 (coarse)
Coolant	Emulsion Hebro 565B, 10%, inner coolant supply, flood
Force Measurement	Kistler 3D dynamometer type 9255B
Scanning Electron Microscope	Jeol SEM 7500F with AnalySIS software 3.2 (Build 799)
Optical Microscope	Dell Computer with Zeiss AXIOVISION4

As background work [69] different (fine-, medium and coarse grain) PCD materials were tested. The aim of the experimental design was to yield conclusive experimental results for interpolation of the effectiveness of different PCD materials. Experiments using the best performing PCD material followed in this research experiment. In this background study the  $h_{eMax}$  limit of 0.03 mm was confirmed to cause catastrophic tool failure due to a loss of the cutting edge. Therefore, due to the limited data on the milling of Ti6Al4V with PCD, together with the high experimental costs, it was decided to analyze the performance of PCD inside the tool- and work piece limits. The tool material was analysed at conditions similar to high-speed machining with  $v_c$  ranging from 100-300 m/min and  $h_{eMax}$  from 0.009-0.019 mm. The  $a_e$  was varied between 0.5-1 mm as illustrated in Table 5.12.

**Table 5.12:** Experimental conditions used for the high-speed milling tests

Cutting speed ( $v_c$ )	100-300 m/min
Feed rate ( $f_z$ )	0.025-0.05 mm/z
Radial immersion ( $a_e$ )	0.5-1 mm
Axial immersion ( $a_p$ )	2 mm

The flank wear land ( $V_B$ ) was analyzed with an optical microscope for dimensional measurements. The failure criterion due to wear on the flank [11] was set for a maximum when  $V_B=0.3$  mm. Figure 5.7 illustrates the setup and illustrates the direction of forces, the rotation angle ( $\omega$ ) and feed direction.

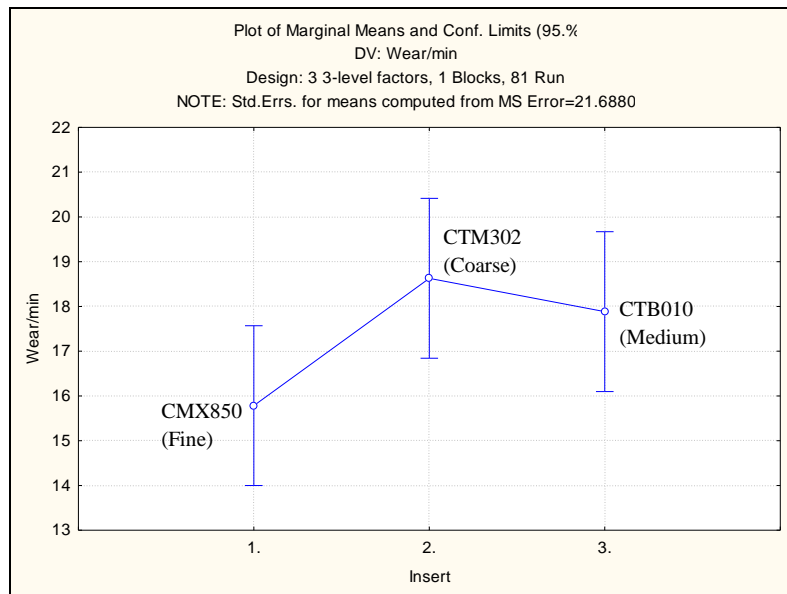


**Figure 5.22:** Experimental setup with the direction of the forces components, rotation angle and feed direction

The entry angle of the PCD tool in the down milling operation, started ( $\varphi_{st}$ ) from the negative  $y$ -axis. Once the force components in the  $x$ -,  $y$ - and  $z$ -directions were measured with a Kistler 9255B dynamometer,  $F_c$  could be expressed using eqns. (7–9). The PCD cutting tool exits the cutting segment at an angle of  $\varphi_{ex} = 90^\circ$ .

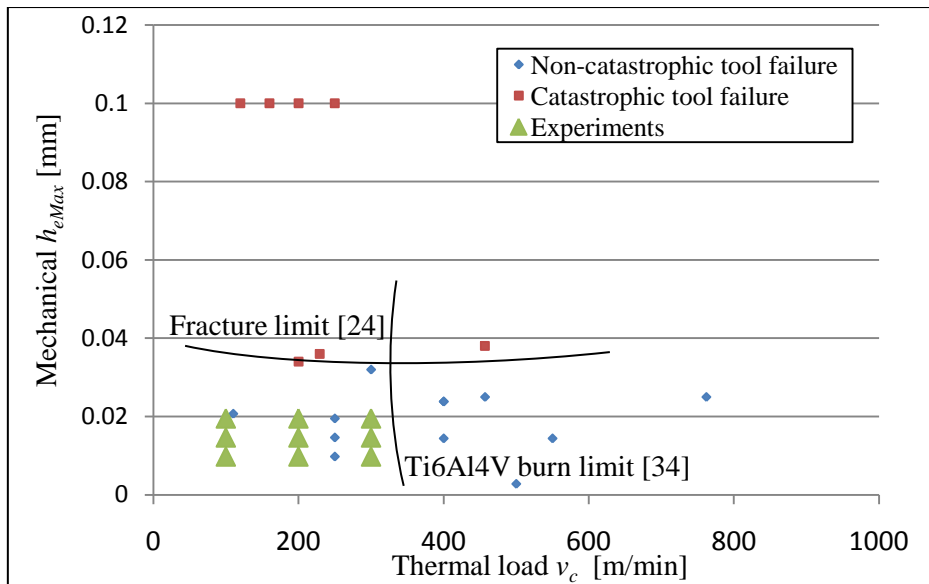
### 5.2.1.2 Experimental results

The data from the background studies [69] was analyzed using Statistica and the following graphs helped to summarize the performance for different milling conditions. Figure 5.23 illustrates the effect of the properties from different cutting materials.





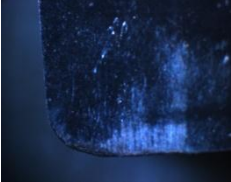
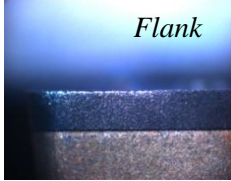
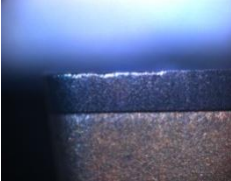
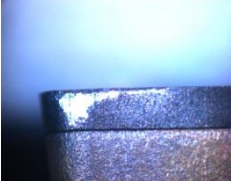

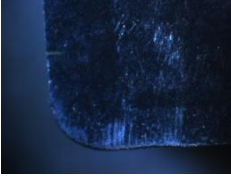
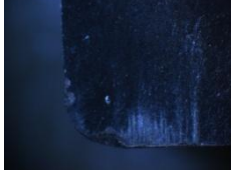
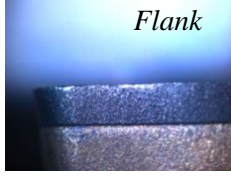
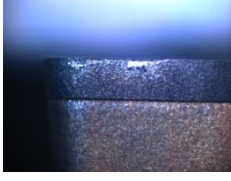
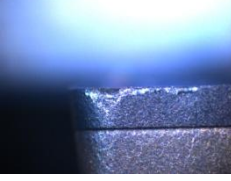
**Figure 5.23:** Performance of different PCD cutting tool material

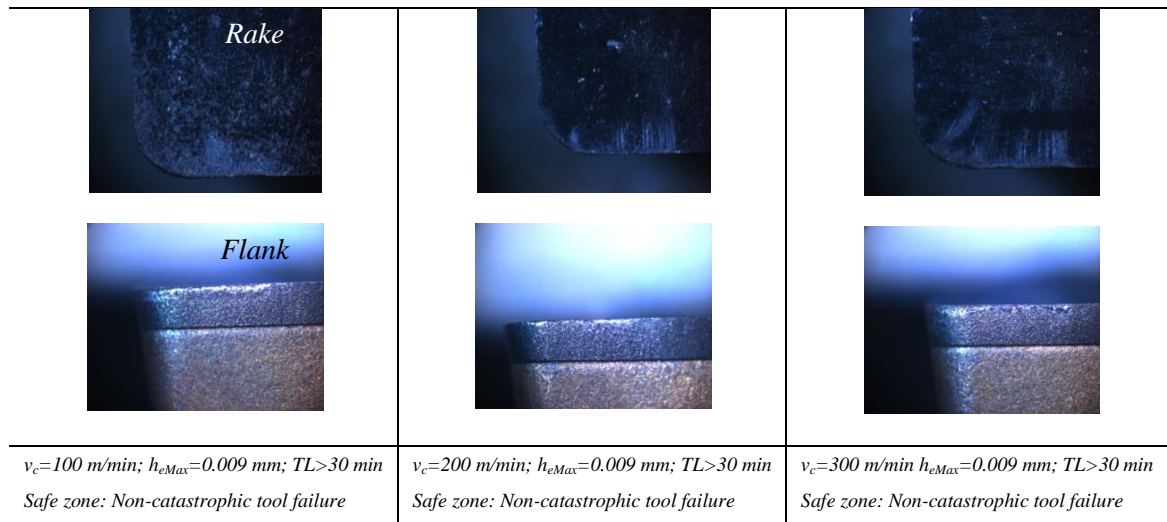
The main effects graph clearly indicates that the fine grain CMX850 (the fine grain PCD material) performed best overall, for the different cutting configurations. It is also interesting that there is a relationship between the performance and transverse rupture strength of the materials. Similar, for a decrease in grain size (increase in density) the performance improved. Figure 5.24 illustrates the mapping of trials from literature [24,87,114,43] and illustrates the experimental parameters for this study with the fine grain PCD material.



**Figure 5.24:** The constructed wear map for finish milling of Ti6Al4V with PCD tools

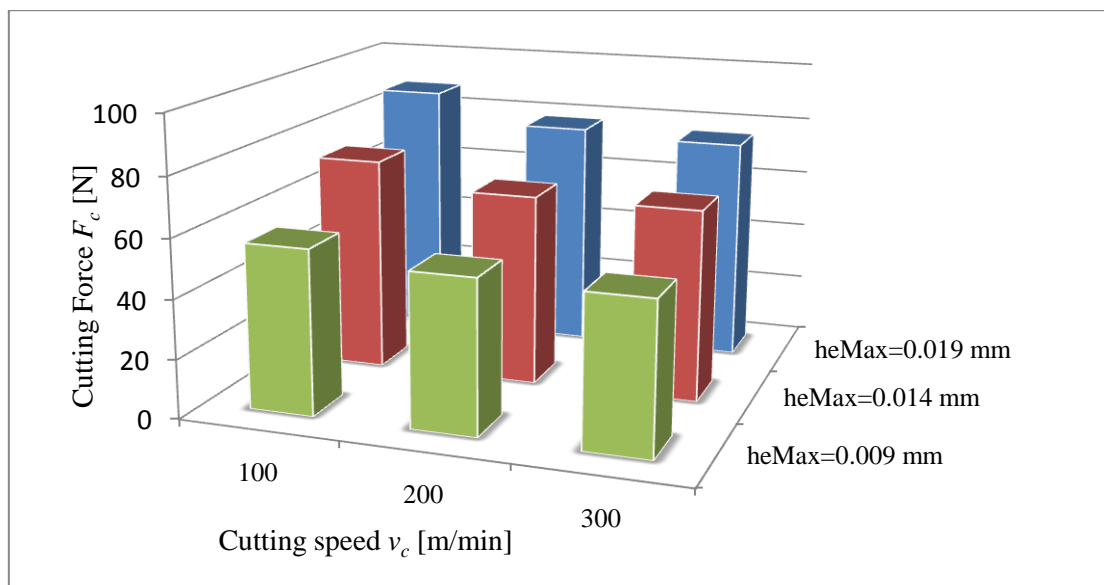
The results of the PCD cutting tools that were used for finish milling experiments are illustrated in Figure 5.25. The tools were examined and categorized into a failure region.

 <p><i>Rake</i></p>		
 <p><i>Flank</i></p>		
<p><math>v_c=100</math> m/min; <math>h_{eMax}=0.019</math> mm; <math>TL&gt;30</math> min Safe zone: Non-catastrophic tool failure</p>	<p><math>v_c=200</math> m/min; <math>h_{eMax}=0.019</math> mm; <math>TL&gt;30</math> min Safe zone: Non-catastrophic tool failure</p>	<p><math>v_c=300</math> m/min; <math>h_{eMax}=0.019</math> mm; <math>TL&gt;30</math> min Safe zone: Non-catastrophic tool failure</p>
 <p><i>Rake</i></p>		
 <p><i>Flank</i></p>		
<p><math>v_c=100</math> m/min; <math>h_{eMax}=0.014</math> mm; <math>TL&gt;30</math> min Safe zone: Non-catastrophic tool failure</p>	<p><math>v_c=200</math> m/min; <math>h_{eMax}=0.014</math> mm; <math>TL&gt;30</math> min Safe zone: Non-catastrophic tool failure</p>	<p><math>v_c=300</math> m/min; <math>h_{eMax}=0.014</math> mm; <math>TL&gt;30</math> min Safe zone: Non-catastrophic tool failure</p>



**Figure 5.25:** Failure modes for PCD tools in the finish milling of Ti6Al4V

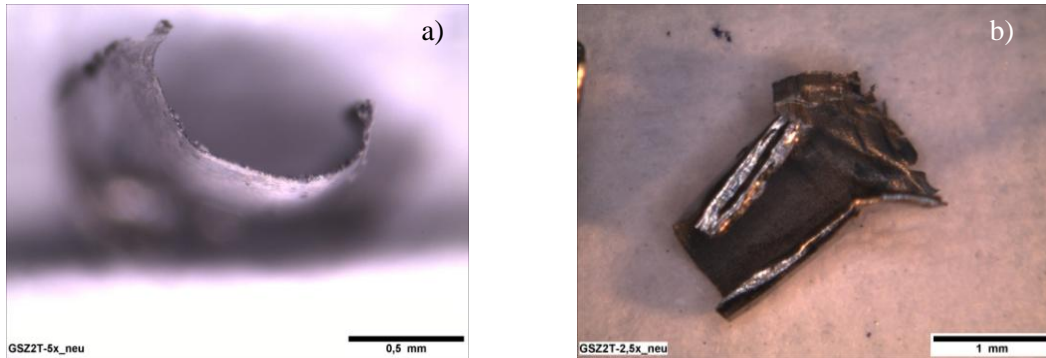
None of the PCD cutting tools failed catastrophically, but whether it is an economic viable solution still needs to be considered. This information is considered confidential. As a complementary perspective these results proved that the cutting speeds (thermal load) for PCD tools in finish milling conditions are limited to the cutting range 200-300 m/min under a low mechanical loading of  $h_{eMax}=0.019$  mm. Cutting speeds higher than 300 m/min will lead to work piece failure due to material burn. Figure 5.10 illustrates the cutting forces for the different finish milling conditions.



**Figure 5.26:** Cutting forces for PCD tools in the finish milling of Ti6Al4V

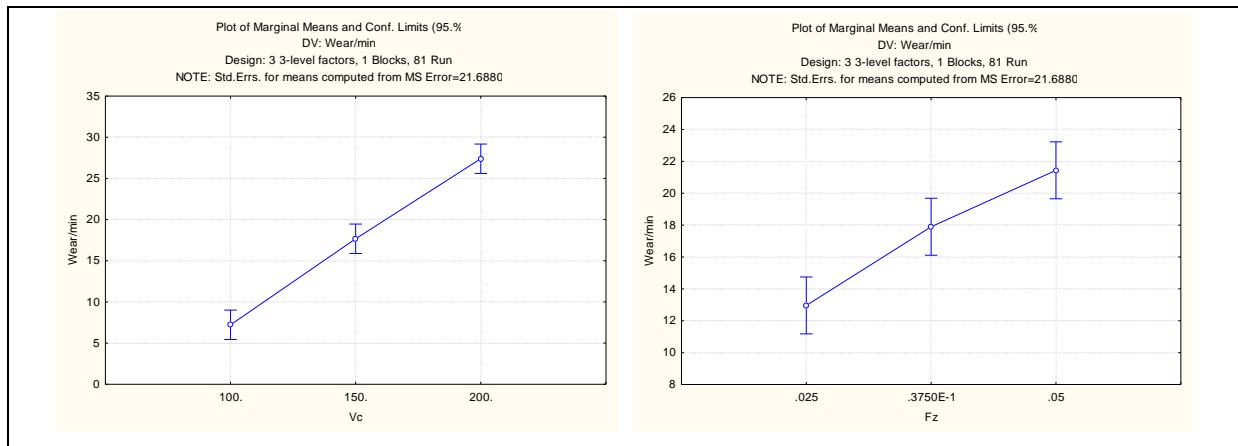
The cutting forces were generally influenced by  $h_{eMax}$ , while the  $v_c$  showed no significant influence. Cyclic variations in the force components were found. Figure 5.27 illustrates the top and front view of the produced Ti6Al4V chips.





**Figure 5.27** The a) top and b) side view of the Ti6Al4V chips ( $v_c=100$  m/min,  $h_{eMax}=0.019$  mm)

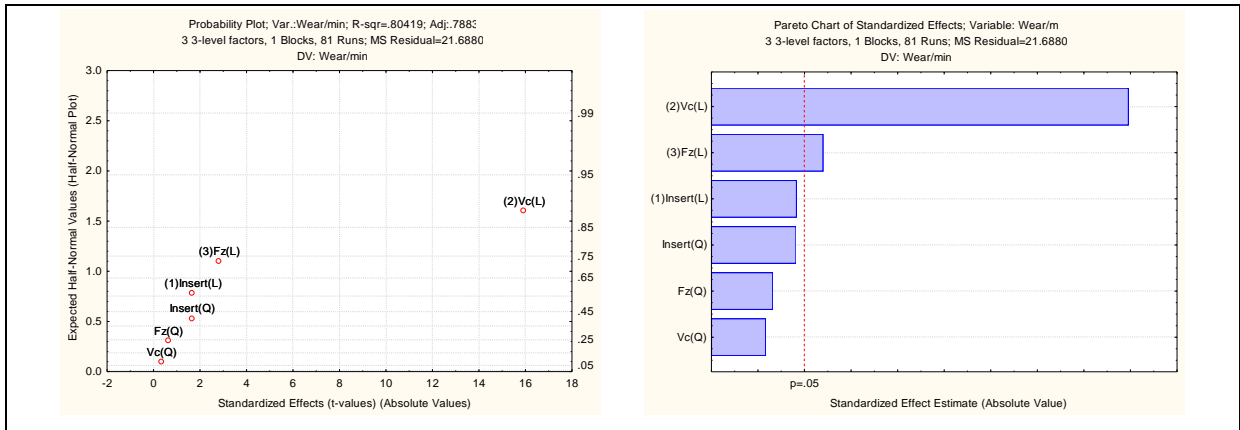
From these figures it is evident that the serrations for which Ti6Al4V are known are negligible with finishing cuts, and that the fluctuations in the cutting force while in cut, might be due to the chip curling (adhesive frictional phenomenon) away from the rake of the cutting tool. Figure 5.28 shows the effect of  $v_c$  and  $f_z$  on the performance of the tool material.



**Figure 5.28:** Influence of cutting speed ( $v_c$ ) and feed rate ( $f_z$ )

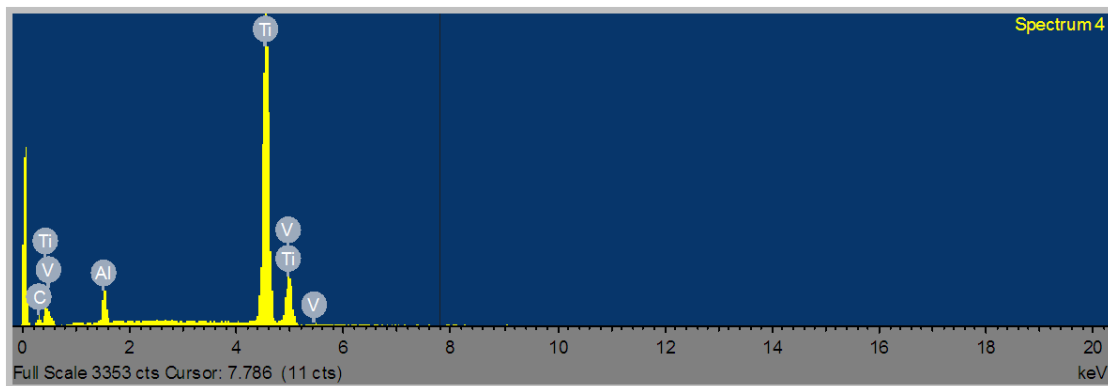
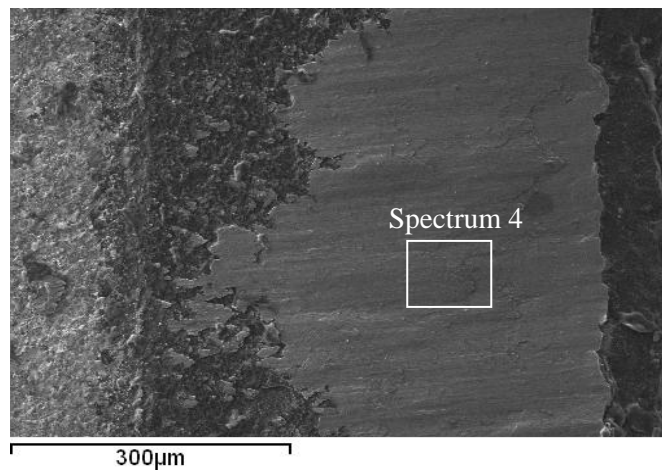
The effect of change in  $v_c$  (linear approximation by Statistica) was 20.17 compared to the 7.08 for change in  $f_z$ . This information concluded that  $v_c$  has a larger effect on tool life than  $f_z$ , similar to machining with carbide [28]. A probability plot and Pareto chart was also drawn in Statistica as shown in Figure 5.29.





**Figure 5.29:** Influence of cutting different parameters

From these figures it is also evident that  $v_c$  (linear approximation) has the largest influence followed by  $f_z$  (linear approximation). SEM analysis was also employed, using the Jeol SEM 7500F with AnalySIS software 3.2 (Build 799), in order to identify the build-up on the flank wear scar. The build-up on the PCD material was found to be Ti6Al4V. Figure 5.30 illustrates the results of this analysis. Compared with the nominal 6% wt. Aluminum, 4% wt. Vanadium in the Table 5.13, it becomes clear that the deposit is the Ti6Al4V work material.

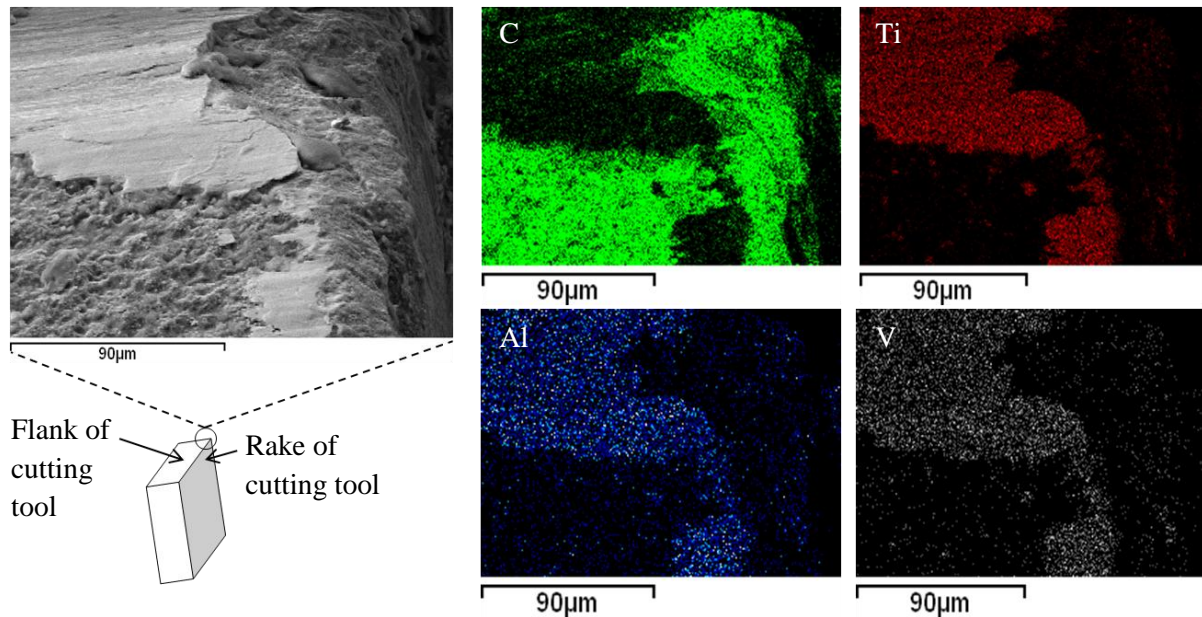


**Figure 5.30:** SEM EDAX analysis of the material build-up on the PCD tool material, as supporting evidence the build-up is Ti6Al4V

**Table 5.13:** SEM EDAX analysis of the material build-up on the PCD tool material as supporting evidence the build-up is Ti6Al4V

In stats.	C	O	Al	Ti	V	Total
weight%	3.95	-	5.34	86.9	3.81	100

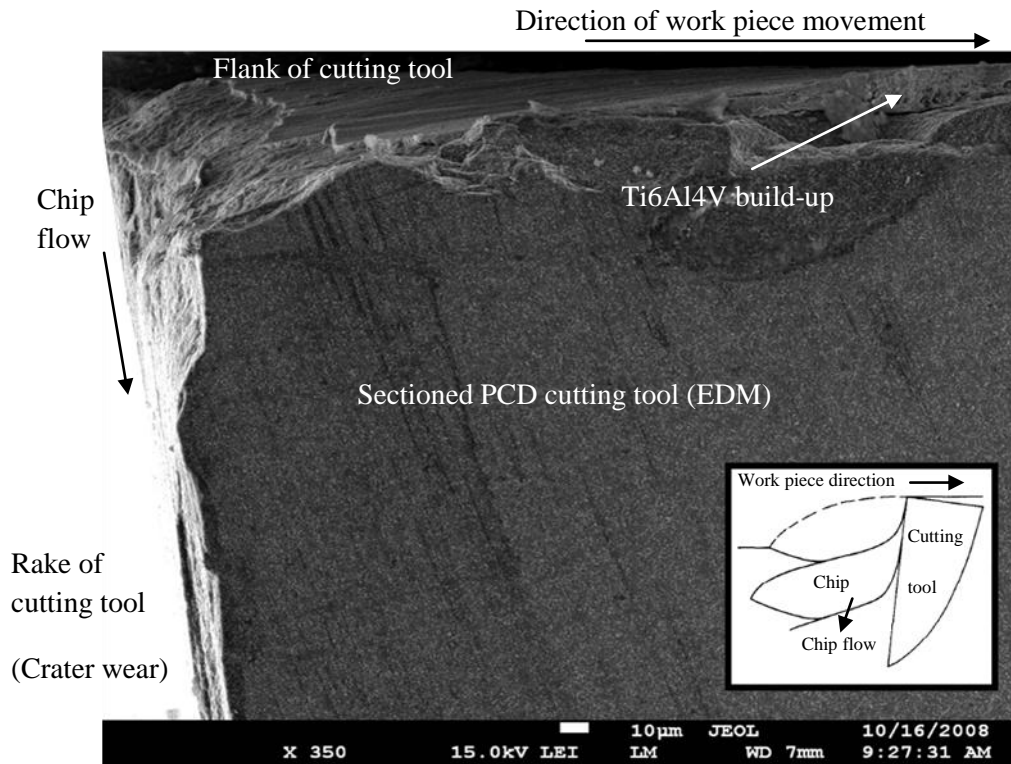
This was supported using image mapping with the SEM and its software as shown in Figure 5.31. The different color codes made it possible to establish the position of the different elements. The figure illustrates the position of the C, Ti, Al and V on the flank of the cutting tool.



**Figure 5.31:** Analysis of material build-up on the PCD using image mapping with the SEM, showing that the build-up is Ti6Al4V on the PCD tool material

Thereby, it was possible to confirm that the build-up was Ti6Al4V as the placement of the Ti, Al and V corresponded. An EDM sectioned sample gives an indication of the formed wear scar on the flank.

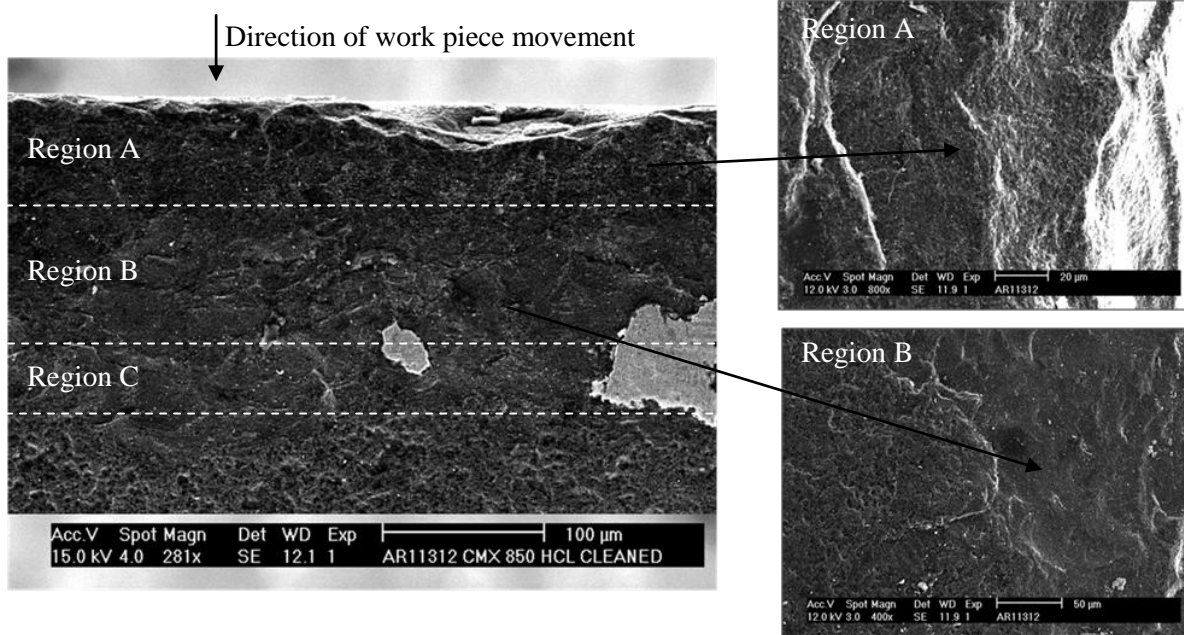
Figure 5.32 indicates where the sample was cut and the form of the wear scar. The sample was 350x enlarged under the SEM.



**Figure 5.32:** EDM sectioned wear scar of the PCD cutting tool, showing the depth of the wear on the flank and rake of the tool

As illustrated, the PCD tool was cut through the wear scar by means of electric discharge machining (EDM) and polished. The SEM on the sectioned sample yielded supportive information to establish that the depth of the wear on the flank to be around 20-25µm deep. Acid cleaning (Hydrochloric acid) enabled that the true wear scar was exposed below the deposited Ti6Al4V layer on the flank.

Post acid cleaning SEM analysis revealed that a typical flank wear scar had different wear regions as illustrated in Figure 5.33.



**Figure 5.33:** Etched PCD wear scar on the flank of the PCD cutting tool illustrating the different wear regions

These different regions from the edge inward are:

- Region A: The highest load is exerted on the edge of the insert. This zone is where the initial micro-chipping occurs, due to mechanical impact and is measured to be around 45μm deep with the SEM.
- Region B: This region is also characterized with impact related wear. The work piece material tends to stick and break away under the cutting forces. This causes small particles to be gradually dislodged out of the diamond matrix.
- Region C: This region was covered with a Ti6Al4V layer and the region is characterized by a relatively smoother (polished) surface. The removed and adhered layers caused more adhesive rubbing which is believed to increase the cutting temperature. This causes the work piece to weld onto the wear scar. The critical temperature for adhesion to occur for machining with PCD is reported [51] to be roughly 760°C, around which the high temperature strength of PCD is believed [25] to be degrading as well. Also above 800°C, the probability of chemical interaction of PCD with the work piece material [16] increases.

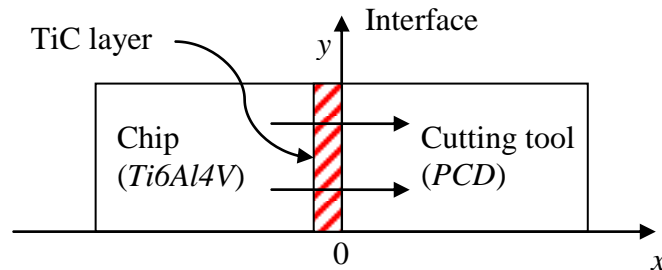
### 5.2.2 Static interaction of PCD/Ti6Al4V diffusion-couple

The chemical compatibility of PCD tool materials with Ti6Al4V has been evaluated by means of the static interaction diffusion-couples technique. The element diffusion from the Ti6Al4V to PCD tools (vice versa) at temperatures up to 1000°C was examined to establish the maximum temperature at which the tool and the work piece materials are chemical compatible. Hartung et al. [19] investigated the crater wear mechanisms by comparing the predictions from various theoretical models of tool wear with experimental results and proposed a wear mechanism for PCD. According to their results, a stable boundary layer of titanium carbide (TiC) forms at the interface so that the relative sliding motion between the chip and the cutting tool is generated internally by shear within the Ti6Al4V chip. This inert boundary layer becomes saturated with tool constituent, limiting the mass transport of tool constituents from the tool surface.

PCD is *metastable* and at ambient pressure and temperature its phase transforms very slowly (several hundred years) into graphite. However, a high temperature combined with a low pressure (less than 1 GPa) can strongly accelerate graphitization [20]. This graphitization can lead to catastrophic wear on the flank of the tool, known as notch wear. Researchers [20] observed notch at the limit of the cutting zone, because it is usually situated a few tenths of millimeters from the tool nose. In this zone, the cutting temperatures are close to those in the cutting zone (600°C-1000°C) [81,41] The distribution of pressure in the cutting zone is difficult to determine, but calculated to be very high (3 GPa for PCD [20]) according to cutting force measurements. Conversely outside of this zone the pressure is only the atmospheric one. Analyses [20] by Raman spectroscopy in PCD notch failures were carried out and carbon and boron nitride phases were discovered. This revealed the presence of graphite in the notch.

In order to simplify the diffusion analysis at the tool–chip interface, it is assumed that the concentration gradient in the *y*-direction is small with respect to the gradient in the *x*-direction. Auger electron spectroscopy [19] indicated that titanium oxy-carbides are present at the surface of the PCD tool.

As the depth below the surface of the diamond increases, the oxy-carbides decreases in quantity and a layer of relatively pure TiC exists to a depth of on the order of 100nm below the surface as illustrated in Figure 5.34.

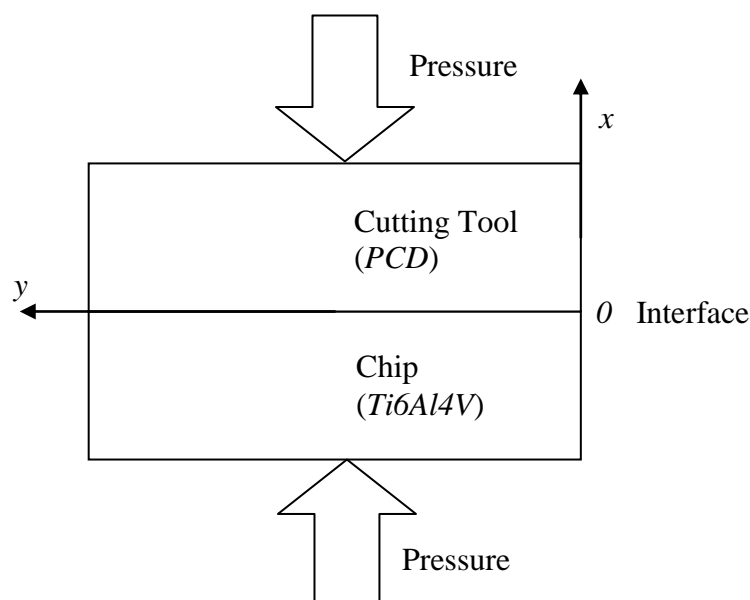


**Figure 5.34:** Coordinates in the tool–chip diffusion interface [59]

The existence of a 100nm thick layer of TiC on the surface of the diamond tool suggests that the wear rate of the tool might be calculated from the rate of diffusion of carbon through the TiC layer [19]. The work piece is located in the negative direction of the  $x$ -axis.

### 5.2.2.1 Experimental setup and design

The purpose is to verify at what temperature the element diffusion occurs and if a TiC layer forms. The aim is to find out the element diffusion occurring at the contact zone between the Ti6Al4V and the PCD tool. Figure 5.35 shows the schematic diagram of the diffusion couple. The diffusion couples (Ti6Al4V and the PCD) were brought into contact and heated with different temperatures.



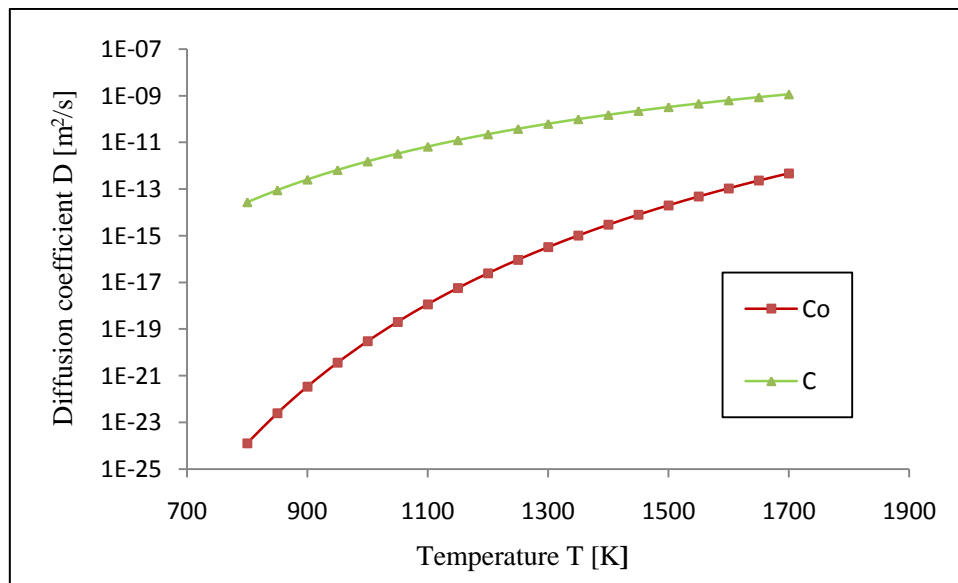
**Figure 5.35:** Schematic diagram of the diffusion couple

The composition, physical, and mechanical properties of the carbide tool material are listed in Table 5.14. The tool material had a thermal conductivity of 163 W/m·K and a thermal expansion of  $4.5 \times 10^{-6}$ /K.

**Table 5.14:** Properties of the WC/Co carbide tool material

Composition	Density	Hardness	Flexural strength	Thermal conductivity	Thermal expansion
(wt. %)	[g/m <sup>3</sup> ]	[GPa]	[MPa]	[W/m·K]	[ $\times 10^{-6}$ /K]
PCD+15% Co	4.37	-	2200	163	4.5

The diffusion coefficients of C and Co could be calculated using eqn. (4). Figure 5.36 illustrates the diffusion coefficient of C is the largest, followed by the diffusion coefficient of Co.



**Figure 5.36:** Diffusion coefficients for Co and C at different temperatures

The composition and properties of Ti6Al4V are listed in Table 5.15 and Table 5.16. The Ti6Al4V experimental specimen had a hardness of 360 HV and ultimate tensile strength of 1080 MPa.

**Table 5.15** Mechanical and physical properties of the work piece at room temperature

Test specimen	Ti6Al4V
Hardness	340 HV
Ultimate tensile strength	1080 MPa

**Table 5.16:** Chemical composition of Ti6Al4V [wt.%]

	Al	V	Fe	O	C	H	N	Ti
Min.	5.50	3.5	0.3	0.14	0.08	0.01	0.03	Balance
Max.	6.75	4.5	-	0.23	-	-	-	Balance

The uni-axial hot press used for most of this work is an Astro TT HP20-3560-20. These samples were hot pressed in a flowing argon atmosphere, under an applied compressive pressure of 10 MPa at temperatures ranging from 600°C to 800°C as illustrated in Table 5.17. In order to avoid graphitization of the PCD tool materials a higher pressure (5.5 GPa) obtained in belt type press was used for the runs at 1000°C.

**Table 5.17:** Experimental machines, equipment and conditions used for the static interaction PCD/Ti6Al4V diffusion-couple experiments

Hot press	Astro TT HP20-3560-20 Belt Type (Mk9)
Scanning Electron Microscope	Jeol SEM 7500F with AnalySIS software 3.2 (Build 799)
Temperature	1000°C (5.5 GPa) 600-800°C (10 MPa)
Pressure	10 MPa (Argon) 5.5 GPa
Time	90 minutes
Heating rate	50 °C/min
Cooling rate	20 °C/min
Vacuum levels	10 mtorr

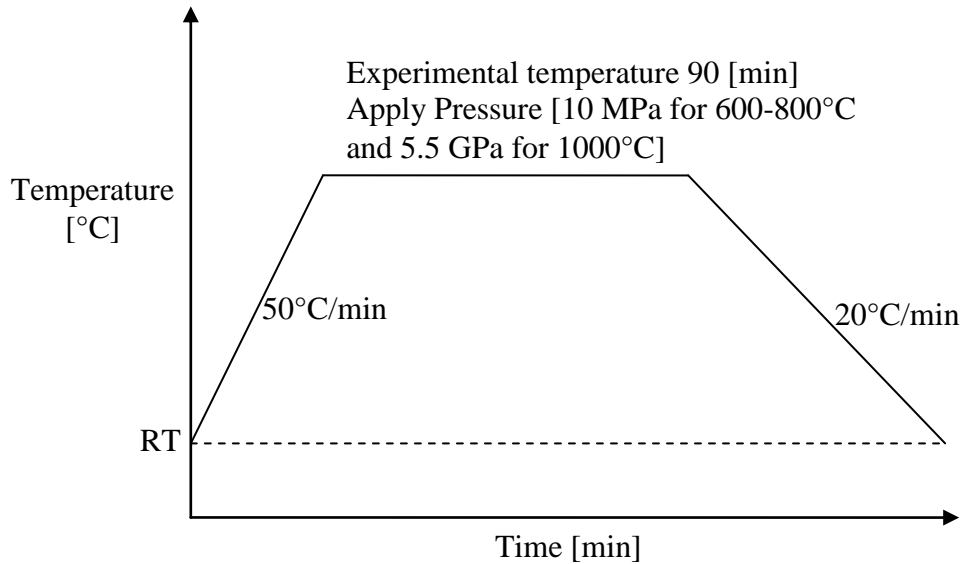
Both the surfaces of the PCD and the Ti6Al4V alloy were polished to produce a final surface roughness  $R_a < 0.05\mu\text{m}$ . Figure 5.37 shows the Uni-axial Hot Press and the hot zone components.



**Figure 5.37:** The equipment for the diffusion experiment: a) The Uni-axial hot press and b) the hot-zone components



The force is applied uni-axially through the graphite punches. A rotary vacuum pump is attached to the hot press and is capable of vacuum levels of 10 mtorr. The furnace was heated to the experimental temperature (see Table 5.17) at  $50^{\circ}\text{C}/\text{min}$  and held at this temperature for 90 minutes, to apply the load. The hot press cycle is shown schematically in Figure 5.38.

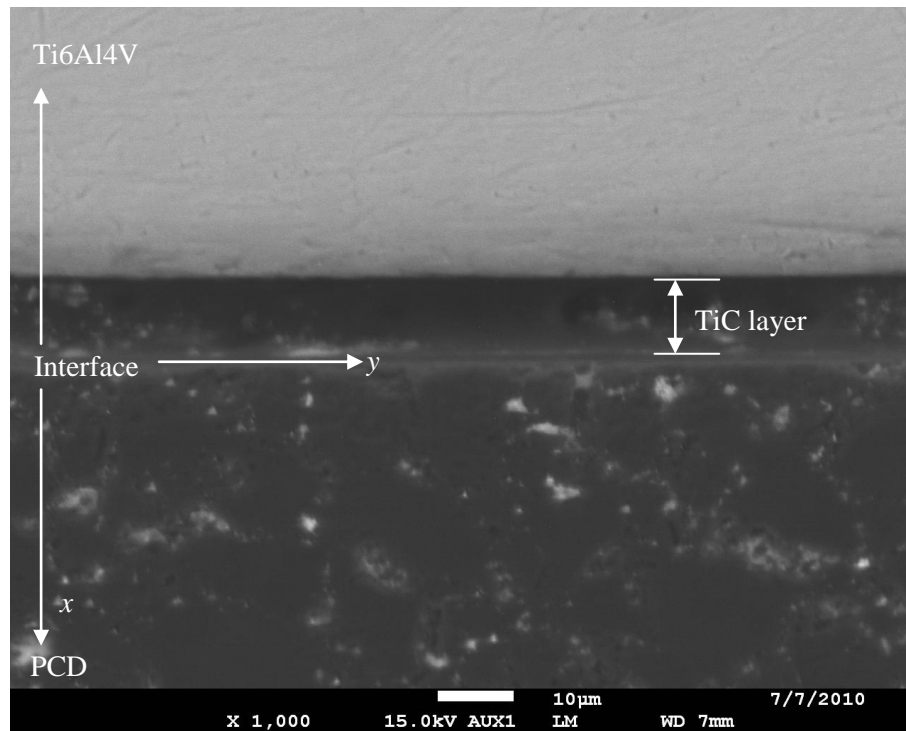


**Figure 5.38:** The temperature profile for the diffusion experiments (Not to scale, for illustrative purposes only)

The furnace was then cooled to room temperature (RT) at  $20^{\circ}\text{C}/\text{min}$ . At RT the sample cell was removed from the graphite die and insert. The system is automated to maintain constant pressure. The pressure was only removed after the furnace had cooled down and the heating elements were switched off.

### 5.2.2.2 Experimental results

The scanning electron microscope used in this study was a Joel SEM 7500F equipped with AnalySIS software 3.2 (Build 799). Figure 5.39 illustrates a SEM micrograph of the diffusion couple after heating for 90 minutes at 1000°C.

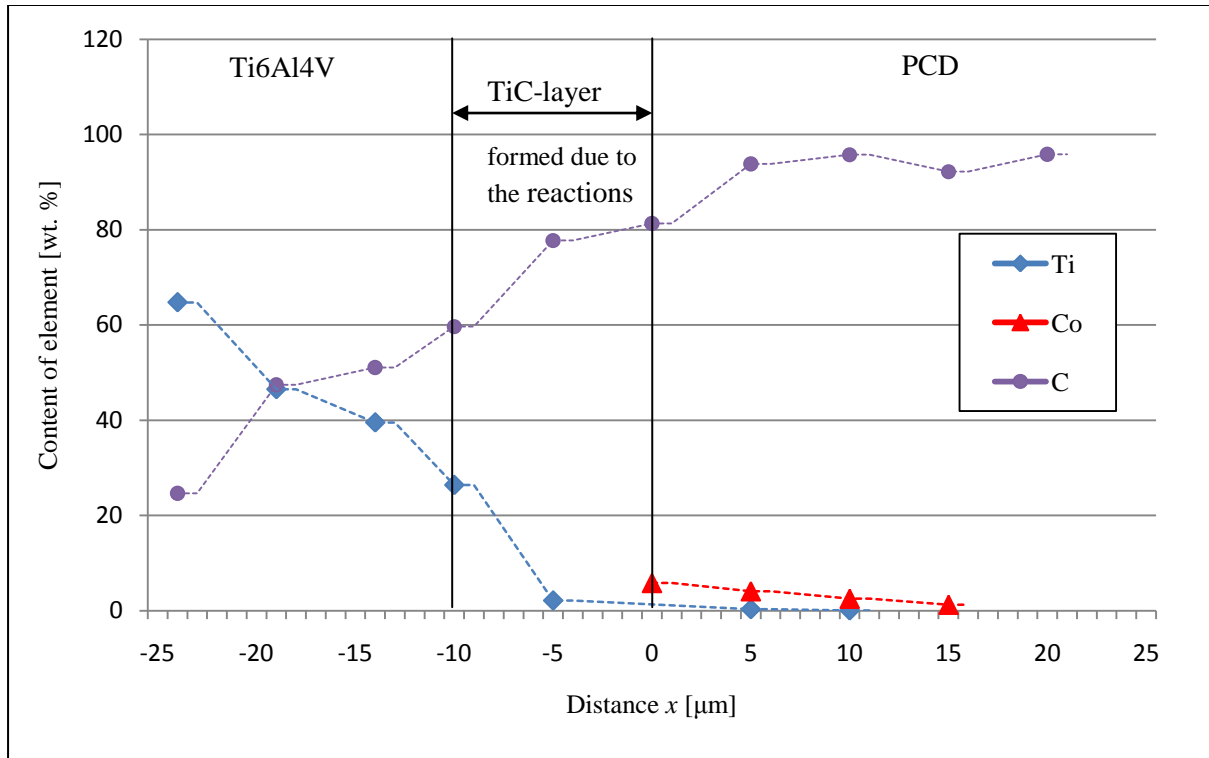


**Figure 5.39:** SEM micrograph of the diffusion couple after heating for 90 minutes at 1000°C (5.5 GPa)

Both secondary and backscattered electron signals were used for imaging. The TiC layer was found to be 10 µm thick at 1000°C, which is significantly wider than suggested during machining [19]. No chemical interaction was found at 600°C. The C elements also did not greatly penetrate into the Ti6Al4V alloy at 800°C, while at 1000°C, the C of the PCD diffused into the work piece material.

These results complemented the layout of the constructed tool wear map for the finish milling of Ti6Al4V. PCD is also known to be more chemically stable than carbide cutting tools at elevated temperatures. This was reflected by the fact that chemical interaction between the PCD and Ti6Al4V only occurred at 800°C, and not around 600°C as was found for carbide tool materials.

Figure 5.40 shows the Ti, C, and Co elements diffusion across the PCD and Ti6Al4V alloy interface for 1000°C.



**Figure 5.40:** Distribution of elements along the interface of the diffusion couple after heating at 1000°C in argon for 90 minutes under a load of 5.5 GPa

As illustrated in the figure, the depth of C penetration into the Ti6Al4V alloy is around 25μm. It was interesting to note that the TiC-layer that formed on the edge of the cutting tool material limited the diffusion of the Co into the work piece, and that the Co wt. % increased to the edge of carbide tool. This complements the findings of Hartung et al [19], that the TiC-layer forms a protective layer.

## 6. Discussion

The purpose of the experimentation was to evaluate the validity of the constructed tool wear models for rough and finish milling of Ti6Al4V. These wear characterisation maps of carbide- and PCD cutting tools contribute to understand the complex wear mechanisms found in the milling of Ti6Al4V better. The experimental results proved that the understanding and theories hold in practice.

### 6.1 Rough milling with carbide tool material

In the rough milling experiments, TiAlN (PVD) carbide tools were used to mill the Ti6Al4V work piece. In a background experiment the dynamics of chip formation is studied to understand the significance of chip serration on tool vibration. As chipping is a major, catastrophic failure mechanism of carbide tools milling titanium, a clearer perspective of force synchronisation with shear localization is pursued. Dynamic force component measurements were analyzed together with chip serration. The experimental results show that the maxima of the force components in the 2D plane ( $F_z$  and  $F_y$ ) were reached after the cutting tool has encountered the theoretical maximum effective feed ( $h_{eMax}$ ). The effect of chip serration on tool failure is found to be insignificant compared to the combined effect of the adhesive frictional phenomena between the cutting tool, chip and work piece; and the vibrations caused by the milling equipment. This is considered as a new insight in titanium machining.

In the conventional- and transition-speed milling experiments the different sets of thermal ( $v_c$ ) and mechanical ( $h_{eMax}$ ) loads were investigated and compared to the constructed wear map. As a complementary perspective the results proved that the  $v_c$  (thermal load) for carbide tools in rough milling conditions can be increased to 100 m/min under a low mechanical loading ( $h_{eMax}=0.1$  mm). The mechanical loading is limited to  $h_{eMax}=0.25$  mm at  $v_c=40$  m/min. The effect of  $V_B$  on the increase in cutting force over time was also studied and found to be directly related.

Additional static interactions of WC-Co/Ti6Al4V diffusion-couple experiments at different temperatures were conducted. The diffusion experiments clearly showed that W, C and Co elements of WC-Co penetrate into the Ti6Al4V alloy, and Ti elements of the Ti6Al4V alloy penetrate into the WC-Co at temperatures of above 600 °C. The penetration depth of the elements can reach 20.0  $\mu$ m at temperatures of 1000 °C. The diffusion of elements from the Ti6Al4V titanium alloy to a WC/Co carbide tool (and vice versa) through the tool–chip interface leads to a composition change of the tool substrate. These results complement the findings [61] that  $v_c=55$  m/min (around 600°C) are the critical thermal load for diffusion between the carbide cutting tool and work piece to occur.

These findings validated the layout of the constructed tool wear map for the rough milling of Ti6Al4V and supported the theories.

## **6.2 Finish milling with PCD tool material**

In the finish milling experiments, PCD tools were used to mill the Ti6Al4V work piece. As background work different (fine-, medium and coarse) PCD materials were tested. The fine grain performed best overall, for the different cutting configurations. It is also interesting that there is a relationship between the performance and transverse rupture strength of the materials. Similar, for a decrease in grain size (increase in density) the performance improved.

In the high-speed milling experiment different sets of thermal ( $v_c$ ) and mechanical ( $h_{eMax}$ ) loads were also investigated. The result from this experiment proved that finish milling of Ti6Al4V with PCD cutting tool materials can be done for  $v_c < 300$  m/min. The mechanical load ( $h_{eMax}$ ) ranged from 0.009-0.032 mm. Higher cutting speeds were found to cause material burn of the Ti6Al4V work piece. Observations based on the SEM analysis suggested that adhesion of the work piece took place during the milling of Ti6Al4V, after which degradation of the tool accelerated, probably due to the combined effect of the tribo-chemical wear mechanisms.

Additional static interactions of PCD/Ti6Al4V diffusion-couple experiments at different temperatures were conducted. The static diffusion-couple experiments clearly showed that C of the PCD penetrate into the Ti6Al4V alloy, and Ti elements of the Ti6Al4V alloy penetrate into the PCD at temperatures of above 800°C. The penetration depth of the elements can reach 25.0  $\mu\text{m}$  at temperatures of 1000 °C (5.5 GPa).

These results complemented the findings of other researchers [19] when a TiC-layer at 1000°C formed in the contact zone, which limited the diffusion of the Co into the Ti6Al4V. A negligible TiC-layer was found at 800°C. These results also supported the layout of the constructed tool wear map for the finish milling of Ti6Al4V.

## 7. Conclusion

Cutting tool wear maps were constructed based on experimental data obtained from literature, industry, background work. These maps were validated with experimental work. Safe operating milling zones were identified for both carbide- and PCD cutting tool materials during the milling of Ti6Al4V.

The tool wear maps have been constructed in terms of two easily controllable machining parameters,  $v_c$  and  $h_{eMax}$ . These wear maps are useful to designers and engineers when they have to make decisions where tool wear is one of the major considerations. The constructed wear maps can also play the role of a diagnostic tool during tool failure analysis. These maps combine tool failure modes and wear mechanisms observed under a certain set of milling conditions. This work provides a framework for the wear behaviour of carbide cutting tools in rough- and PCD cutting tool materials in the finish milling of Ti6Al4V. Notwithstanding this understanding, an on-going effort should be channelled into the construction of new wear maps for new innovative cutting tool materials to effectively mill other Ti-alloys as well.

Future directions for research in tool wear mapping for the milling of Ti6Al4V should include an effort to construct time-dependent wear-transition maps. These wear maps should be part of an aim to serve the end-users.

Stability diagrams to prevent chatter have been extensively used, particularly in high speed milling applications, to utilize the large stability pockets [16]. These stability diagrams for the milling of Ti6Al4V should be considered and integrated into future tool wear maps.

## References

- [1] Li X, Ng H, Lim S, A predictive mapping system for tool wear in metal cutting. *Journal of Materials Processing Technology*, 89-90: pp. 279-286, 1999.
- [2] Lim S, Recent developments in wear mechanism maps. *Tribology International*, 31(1): pp. 87–97, 1998.
- [3] Friedman T. *The World is Flat: A Brief History of the Globalized World in the 21st Century* New York: Farrar, Strauss, Giroux; 2005.
- [4] Nottbohm H. Entwicklungstendenzen im Automobilmotorenbau. In *Chemnitz Colloquium on Production Technology (CPK)*; Chemnitz; 2008.
- [5] Canton J. *The extreme future. The top trends that will reshape the world.* 1st ed. New York: Plume; 2007.
- [6] Saxton B. *Rock the boat: Why leaders need to make waves to succeed the era of globalisation:* TerraNova. Interpak Books; 2006.
- [7] Campbell K, Green Skies. *Engineering News*, 1, 2008 June.
8. Airbus. Airbus Co. [Online].; 2010 [cited 2008 February. Available from: [http://www.airbus.com/en/presscentre/pressreleases/pressreleases\\_items](http://www.airbus.com/en/presscentre/pressreleases/pressreleases_items).
- [9] Lantrip J, Co. TB, New Tools Needed. *Cutting Tool Engineering*, 60(8): pp. 72-84, 2008 August.
10. Rolls-Royce. Rolls-Royce Co. [Online].; 2010 [cited 2008 February. Available from: [http://www.rolls-royce.com/civil\\_aerospace/overview/market/outlook/default.jsp](http://www.rolls-royce.com/civil_aerospace/overview/market/outlook/default.jsp).
- [11] Watson D, Bayha T, Hofmann T, Festeau G, Technologies A, Titanium takes off. *Cutting tool engineering*, 59(3), 2007 March.
- [12] Ezugwu E, Bonney J, Yamane Y, An overview of the machinability of aeroengine alloys. *Journal of Materials Processing Technology*, 134: pp. 233-253, 2003.
- [13] Mantle A, Aspinwall D. Tool life and surface roughness when high speed machining a gamma titanium aluminide, progress of cutting and grinding. In *Fourth International Conference on Progress of Cutting and Grinding*; Urumqi and Turpan, China: International Academic Publishers; 1998. pp. 89-94.
- [14] Luther G, Williams J. *Titanium* New York: Springer-Verlag; 2003.
- [15] Kuljanic E, Fioretti M, Beltrame L, Miani F, Milling Titanium Compressor Blades with PCD cutter. *Annals of CIRP*, 47(1): pp. 61-64, 1998.

- [16] Donarchie MJ. Titanium. A Technical Guide: ASM International; 2000.
- [17] Byrne G. High Performance Cutting. An Environmental Perspective. In Proceedings of the 3rd International CIRP High Performance Cutting Conference; Spain; 2008. pp. 317-327.
- [18] Grzesik W. Advanced Machining Processes of Metallic Materials: Theory, Modeling and Applications Grzesik W, editor.: Elsevier; 2008.
- [19] Hartung PD, Kramer BM, Tool wear in Titanium machining. *Annals of the CIRP*, 31(1): pp. 75-80, 1982.
- [20] Corduan N, Himbert T, Poulachon G, Dessoly M, Lambertin M, Vigneau J, et al., Wear Mechanisms of new tool materials for Ti-6Al-4V High Performance Machining. *Annals of CIRP*, 52(1): pp. 73-76, 2003.
- [21] Dimitrov D, Hugo P, Saxer M, Treurnicht N, High performance machining of light metals with the emphasis on titanium and selected alloys. Internal Report, AMTS. Stellenbosch: Stellenbosch University, 2010.
- [22] Altintas Y, Weck M, Chatter Stability of metal cutting and grinding. *Annals of CIRP*, 53(2): pp. 619-642, 2004.
- [23] Komanduri R, Hou ZB, On thermoplastic shear instability in the machining of a titanium alloy (Ti-6Al-4V). *Metallurgical and Materials Transactions*, 33(9): pp. 2995-2301, 2002.
- [24] Barnett-Ritcey D, High-speed Milling of Titanium and Gamma-Titanium Aluminide: An Experimental Investigation. McMaster, Canada: 2004.
- [25] Ezugwu E, Wang Z, Titanium alloys and their machinability-a review. *J. Mater. Process. Technol*, 68: pp. 262-274, 1997.
- [26] Kennedy B, Light-Heavyweight Machining. *Cutting Tool Engineering*, 59(12), 2007 December.
- [27] Byrne G, Dornfeld D, Denkena B, Advancing cutting technology. Keynote papers STC "C". *Annals of CIRP*, 52(2): pp. 483-508, 2003.
- [28] Sandvik , Titanium Machining Guide. Sweden: 2007.
- [29] Budak E, Improving productivity and Part Quality in Milling of Titanium Based Impellers by Chatter Suppression and Force Control. *Annals of CIRP*, 49(1), 2000.
- [30] Kendall L. Machining, *Metals Handbook*. 9th ed. Davies JR, editor.: ASM International; 1989.
- [31] Hauschild M, Jesweit J, Alting I, From Life Cycle to Sustainable Production: Status and perspectives. *Annals of the CIRP*. CIRP Keynote Paper, 2005.
- [32] Weinert K, Dry or near Dry Cutting. *Annals of the CIRP*. CIRP keynote paper STC C, 2004.



- [33] Henry S, Reidenbach F, Davidson G, Boring R, O'Loughlin AM, Scott WJ. ASM Speciality Handbook. Tool materials Davis J, editor. United States of America: ASM international. The materials Information Society; 1995.
- [34] Ten Haaf P, Mielnik K, Lauwers B. Development of HSC strategies and tool geometries for the efficient machining of Ti6Al4V. In Proceedings of the 3rd International CIRP High Performance Cutting Conference; University College Dublin (UCD) Belfield Campus; 2008. pp. 753-761.
- [35] Quinto D, Technology Perspective on CVD and PVD Coated Metal-Cutting Tools. International Journal of Refractory Metals & Hard Materials, 14: pp. 7-20, 1996.
- [36] Kendall L. ASM Metals Handbook. 9th ed.; 1989.
- [37] Trent E, Metal cutting and the tribology of seizure: part I seizure in metal cutting. Wear, 128: pp. 29-45, 1988.
- [38] Trent E. Metal cutting. 3rd ed. London: Butterworth-Heinemann; 1991.
- [39] Trent E, Three wear processes with control performance of cemented carbide cutting tools. SME.; pp. 1-15, 1971.
- [40] Barry J, Akdogan G, Smyth P, McAvinue F, O'Halloran P, Application areas for PCBN materials. Industrial Diamond Review, 66(3): pp. 46-53, 2006.
- [41] Narutaki N, Murakoshi A, Study on Machining of Titanium alloys. Annals of CIRP, 32(1): pp. 65-69, 1983.
- [42] Machado A, Wallbank J, Machining of titanium and it's alloys. Journal of Engineering Manufacture, 204(1): pp. 53-60, 1990.
- [43] Nurul Amin A, Ismail A, Nor Khairusshima M, Effectiveness of uncoated WC-Co and PCD inserts end milling of titanium alloy-Ti6Al-4V. Journal of Materials Processing Technology, 192-193: pp. 147-158, 2007.
- [44] Wang Z, Sahay C, Rajurkar K, Tool temperatures and crack development in milling cutters. International Journal of Machine Tool and Manufacture, 36(1): pp. 129-140, 1996.
- [45] Nabhani F, Machining of Aerospace titanium alloys. Robotics and computer-Intergrated Manufacturing, 17: pp. 99-106, 2001.
- [46] Jianxin D, Yousheng L, Wenlong S, Diffusion wear in dry cutting of Ti-6Al-4V with WC/Co carbide tools. Wear, 265: pp. 1776-1783, 2008.
- [47] Komanduri R, Reed J, Evaluation of carbide grades and a new cutting geomtry for machining titanium alloys. Wear, 92: pp. 113-123, 1983.
- [48] Abdel-Aal H, Nouari M, El Mansori M, Tribo-energetic correlation of tool thermal properties to

wear of WC-Co inserts in high speed dry machining of aeronautical grade titanium alloys. *Wear*, 266: pp. 432-443, 2009.

- [49] Dearnley P, AN G, Evaluation of principal wear mechanisms of cemented carbides and ceramics used for machining Titanium alloy IMI318. *Materials Science and Technology*, 2(1): pp. 47-58, 1986.
- [50] Bhaumik S, Divakar C, Singh A, Machining Ti-6Al-4V alloy with a wBN-cBN composite tool. *Materials and Design*, 16(4): pp. 221-226,.
- [51] Nabhani F, Wear mechanisms of Ultra-hard cutting tools materials. *Journal of Processing Technology*, 115: pp. 402-412, 2001.
- [52] Mishnaevsky LJ. Computational mesomechanics of composites Mishnaevsky LJ, editor.: Wiley-Interscience; 2007.
- [53] Konig W, Fritsch R, Kammermeier D, Physically vapor deposited coatings on tools: performance and wear phenomena. *Surface coating technology*, 49: pp. 316-324, 1991.
- [54] Che-Haron C, Jawaid A, Sharif S. Evaluation of wear mechanisms of carbide tools in machining of titanium alloy. In *Proceedings of the Fourth International Conference AMPT; Kuala Lumpur, Malaysia; 1998.*
- [55] Loladze T, On the theory of diffusion wear. *Annals of the CIRP*, 30(1): pp. 71-76, 1981.
- [56] Maerheim Y, Trent E, Diffusion wear of Cemented carbide tools when cutting steel at high speed. *Met Technol*, 4(12): pp. 548-555, 1977.
- [57] Jawaid A, Che-haron C, Abdullah A, Tool wear characteristics in turning of titanium alloy Ti-6246. *Journal of Materials Process. Technolog*, 92-93: pp. 329-334, 1999.
- [58] Su Y, He N, Li L, Li X, An experimental investigation of effects of Cooling/Lubrication Conditions on Tool Wear in High-Speed End Milling of Ti-6Al-4V. *Wear*, 261(7-8): pp. 760-766, 2006.
- [59] Zhang S, Li J, Deng J, Li Y, Investigation of diffusion wear during high-speed machining Ti-6Al-4V alloy with straight tungsten carbide tools. *International Journal of Advanced Manufacturing Technology*, 44: pp. 17-25, 2009.
- [60] Zoya Z, Krishnamurthy R, The Performance of CBN tools in the machining of titanium alloys. *Journal of Materials Processing Technology*, 100: pp. 80-86, 2000.
- [61] Jawaid A, Sharif S, Koksai , Evaluation of wear mechanisms of coated carbide tools when face milling titanium alloy. *Materials Processing Technology*, 99: pp. 266-274, 2000.
- [62] Jiang H, Shivpuri R, A cobalt diffusion based model for predicting crater wear of carbide tools in machining titanium alloys. *J Eng Mater Technol*, 127(1): pp. 136-144, 2005.

- [63] Nouari M MA, Experimental verification of a diffusion tool wear model using a 42CrMo4 steel with an uncoated cemented tungsten carbide at various cutting speeds. *Wear*, 259: pp. 1151–1159, 2005.
- [64] Naerheim Y, Trent E, Diffusion wear of cemented carbide tools when cutting steel at high speed. *Met Technol*, 4(12): pp. 548-555, 1977.
- [65] Shewmon P. *Diffusion in solids* New York: McGraw-Hill; 1963.
- [66] Committee AIH. *ASM Handbook. Friction, Lubrication, and wear Technology*. 4th ed. Henry S, editor. United States of America: ASM International; 1992.
- [67] Mai YW, Thermal shock resistance and fracture-strength behaviour of two tool carbides. *Journal of the american ceramic society*, 59: pp. 11-12, 1976.
- [68] Koen D, Herselman E, Oosthuizen G, Treurnicht N. Investigating novel cooling methods for titanium machining. In *International Conference on Competitive Manufacturing*; Stellenbosch; 2010. pp. 243-248.
- [69] Oosthuizen G, Innovative cutting materials for finish shoulder milling Ti-6Al-4V Aero-engine alloy. MScEng Thesis Stellenbosch University. Stellenbosch: 2009.
- [70] Komanduri R, Some clarifications on the mechanisms of chip formation when machining titanium alloy. *Wear*, 1(76): pp. 15-34, 1982.
- [71] Bayoumi A, Xie J, Some metallurgical aspects of chip formation in cutting Ti–6wt.%Al–4wt.%V alloy. *Mater. Sci. Eng, A*(190): pp. 173-180, 1995.
- [72] Barry J, Byrne G, Lennon D, Observations on chip formation and acoustic emission in machining Ti-6Al-4V alloy. *International Journal of Machine Tools and Manufacture*, 41: pp. 1055-1070, 2001.
- [73] Vyas A, Shaw M, Mechanics of saw tooth chip formation in metal cutting. *Trans. ASME J. Manufac. Sci. Engng*, 121: pp. 163–172, 1999.
- [74] Obikawa T, Usui E, Computational machining of titanium alloy—finite element modelling and a few results. *Journal of Manufacturing Science and Engineering-Transactions of the ASME*, 1(118): pp. 208-215, 1996.
- [75] Shivpuri R, Hua J, Mittal P, Srivastava A, Microstructure-Mechanics Interactions in Modeling Chip segmentation during Titanium machining. *Annals of the CIRP*, 51(1): pp. 71-74, 2002.
- [76] Hua J, Shivpuri R, Prediction of chip morphology and segmentation during the machining of titanium alloys. *Journal of Materials Processing Technology*, 150: pp. 124–133, 2004.
- [77] Subramanian S, Gekonde H, Zhu G, Zhang X, Role of microstructural softening events in metal cutting. *Machining science and technology*, 6(3): pp. 353–364, 2002.

- [78] Merchant M, Basic mechanics of the metal cutting process, parts 1 and 2. *J. Appl. Mech.*, A(11): pp. 168–175, 1944.
- [79] Oxley P, Development and application of a predictive machining theory. *Mach. Sci. Technol.*, 2(1): pp. 65-189, 1998.
- [80] Komanduri R, Turkovich B, New observations on the mechanism of chip formation when machining titanium alloys. *Wear*, 69: pp. 179-188, 1981.
- [81] Kitagawa T, Kubo A, Maekawa K, Temperature and Wear of cutting tools in High-speed Machining of Inconel 718 and Ti-6Al-6V-2Sn. *Wear*, 202(2): pp. 142-148, 1997.
- [82] Li H, Zeng H, Chen X, An experimental study of tool wear and cutting force variation in the end milling of Inconel 718 with coated carbide inserts. *J Mater Proc Tech*, 180(1): pp. 296–304,.
- [83] Rotberg J, Shoal S, Ber A, Fast Evaluation of Cutting Forces in Milling, Applying no Approximate Models. *Int. J. Adv. Manuf Technol*, 13: pp. 17-26, 1997.
- [84] Eckstein M, Lebküchner G, Blum D, Schaftfräsen von Titanlegierungen mit hohen Schnittgeschwindigkeiten - Teil 2. Schichten, *VDI-Z*, 134(6): pp. 61-67, 1992.
- [85] Hoffmeister HW. Hochgeschwindigkeitszerspanung von Titan- und Nickelbasis-legierungen. In *Hochgeschwindigkeitsspanen metallischer Werkstoffe Begleitband zum Kolloquium*; 2006. pp. 29-40.
- [86] Sortina M, Application of statistical filtering for optical detection of tool wear. *International Journal of Machine Tools and Manufacture*, 43(5): pp. 493-497, 2003.
- [87] Kuljanic E, Study of wear in single-tooth and multi-tooth milling, Doctor of Philosophy Dissertation. Cincinnati, Ohio, USA: 1972.
- [88] Kuljanic E, Sortina M, TWEM, a method based on cutting forces-monitoring tool wear in face milling. *International Journal of Machine Tool and manufacture*, 45: pp. 29-34, 2005.
- [89] Italo Sette Antonialli A, Eduardo Diniz A, Pederiva R, Vibration analysis of cutting force in titanium alloy milling. *International Journal of Machine Tools and Manufacture*, 50(1): pp. 65-74, 2010.
- [90] McEvily A, Failures in inspection procedures: case studies. *Engineering Failure Analysis*, 11(1): pp. 167–176, 2004.
- [91] Van Trotsenburg S, Laubscher R. The effect of high speed machining on the surface integrity of certain titanium alloys. In *COMA'10 International Conference on Competitive Manufacturing; Stellenbosch*; 2010. pp. 186-190.
- [92] Van Trotsenburg S, The effect of high speed machining on the surface integrity of certain titanium alloys. *Magistrae Ingenieriae*. Johannesburg: University of Johannesburg, 2008.

- [93] Kuriakose S, Shunmugam M, Characteristics of Wire Electro-discharge Machined Ti6Al4V Surface. *Materials Letters*, 58: pp. 2231-2237, 2004.
- [94] Welsch G, Wolfgang B, Defirmation models of the alpha-phase of Ti-6Al-4V as a function of oxygen concentration and ageing temperature. *Metallurgical Transactions A*, 13A(5): pp. 889-899, 1982.
- [95] Ezugwu E, Bonney J, Da Silva Rosemar B, Cakir O, Surface integrity of finished turned Ti-6Al-4V alloy with PCD tools using conventional and high pressure coolant supplies. *International Journal of Machine Tools and Manufacture*, 47: pp. 884-891, 2007.
- [96] Schulz H, Moriwaki T, High-Speed Machining. *Annals of the CIRP*, 41(2): pp. 637-643, 1992.
- [97] Rahman M, Wang Z, Wong Y, A review on High-speed machining of titanium alloys. *JSME International journal Series C*, 49(1): pp. 11-20, 2006.
- [98] Armendia M, Garay A, Villar A, Davies M, Arrazola P, High bandwidth temperature measurement in interrupted cutting of difficult to machine materials. *Annals of the CIRP*, 2010.
- [99] Ashby M. *Materials selection in Mechanical Design*: Pergamon Press; 1999.
- [100] Kingery W. *Introduction to Ceramics* NY: John Wiley & Sons; 1976.
- [101] Hasselman D, *Thermal Stress Resistance Parameters for Brittle Refractory Ceramics: A Compendium*. *Ceramic Bulletin*, 49(12): pp. 1033-1037, 1970.
- [102] Corporation MM. *Mitsubishi Tooling Technology Metric Version Level 2*. 1st ed.: Mitsubishi Materials Corporation; 2006.
- [103] Italo Sette Antonialli A, Eduardo Diniz A, Pederiva R, Vibration analysis of cutting force in titanium alloy milling. *Machine Tools and Manufacture*, 50: pp. 65-74, 2010.
- [104] Koenigsberger F, Tlustý J. *Machine Tool Structures-Vol 1: Stability against chatter*: Pergamon Press; 1967.
- [105] Budak E, Altintas Y, *Analytical Prediction of Chatter Stability in Milling-Part 1: General Formulation; Part II: Application to common Milling Systems*. *Journal of Dynamic systems*, 120: pp. 22-36, 1998.
- [106] Altintas Y, Budak E, *Analytical Prediction of Stability Lobes in milling*. *Annals of CIRP*, 44(1): pp. 357-362, 1995.
- [107] Hong S, Markus I, Jeong W, *New cooling approach and tool life improvement in cryogenic machining of titanium alloy Ti-6Al-4V*. *Int. J. Mach. Tools Manuf.*, 41: pp. 2226-2245, 2001.
- [108] Zhen-Bin H, Komanduri R, *On a thermomechanical model of shear instability in machining*. *Annals of CIRP*, 44(1): pp. 69-73, 1995.

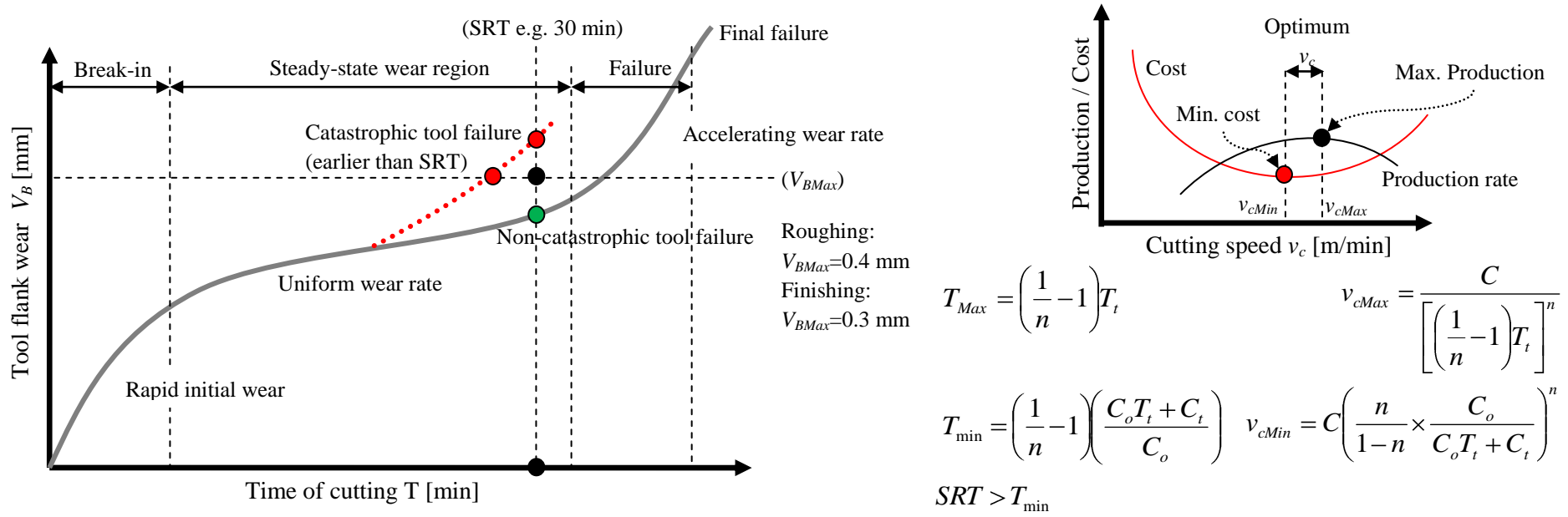
- [109] Abele E, Dietz S, Schiffler A, Analysis of cutting force during milling with regards to the dependency on the penetration angle. *Prod. Eng. Res. Develop.*, 3: pp. 483-487, 2009.
- [110] Bouzakis KD, Klocke F, Michailidis N, Witty M. Characterization-Qualification of PVD coatings for machining Ti6Al4V. In *International Conference on Competitive Manufacturing; Stellenbosch; 2010.*
- [111] Sun S, Brandt M, Dargusch M, Characteristics of cutting forces and chip formation in machining of titanium alloys. *International Journal of Machine Tools and Manufacture*, 49: pp. 561-568, 2009.
- [112] Lo'pez de Lacalle L, Lamikiz A, Sa'nchez J, Fern'andez de Bustos I, Recording of real cutting forces along the milling of complex parts. *Mechatronics*, 16(1): pp. 21–32, 2006.
- [113] Lopez de Lacalle L, Perez J, Llorente J, Sanchez J, Advanced cutting conditions for milling aeronautical alloys. *Journal of Mater. Process. Technology*, 100: pp. 1-11, 2000.
- [114] Oosthuizen G, Joubert H, Treurnicht N, Akdogan G. High-speed milling of Ti6Al4V. In *International Conference on competitive manufacturing; Stellenbosch; 2010.*
- [115] Kramer B, Judd P, J. *Vac. Sci. Technol.*, A3(6), 1985.
- [116] Kramer B, J. *Vac. Sci. Technol.*, A4(6), 1996.
- [117] Nouari Molinari M, Modeling of tool wear by diffusion in metal cutting. *Wear*, 252: pp. 135-149, 2002.

A

*Appendix A: Factors to consider when calculating the SRT value*

Expected tool wear makes it possible to schedule tool replacements and to find the optimum cutting parameters, relative to the rate- and cost of production as illustrated in Figure A.1. The different factors which are considered to calculate the scheduled replacement time for different components are also shown in the figure. According to our research, literature and tool suppliers the TL for the milling of Ti6Al4V should currently be at least 30 minutes (SRT) to ensure an economically viable solution.

Therefore, if a cutting tool material withstands the cutting demands for longer, the cutting conditions define a safe operating zone. Premature, catastrophic tool failure is the least desirable failure mode, because it is the most unpredictable, can be damaging to the work piece and cause costly downtime. This type of failure can be minimized through an understanding of the physical demands on the cutting tool and the effect of changing the operating conditions.



where:  $n, C$ =Taylor tool life parameters  $C_o$ =cost rate for operator and machine  $T_t$ =tool change time  $C_t$ =cost/TL

**Figure A.1:** The different factors that influence the calculation of the Scheduled Replacement Time (SRT) value

**Table A.1:** Different characteristics for various wear regions

Characteristics	Break-in Wear	Steady State wear	Rapid, Failure
Visual indications	<ul style="list-style-type: none"> <li>Repetitive radius of curvature chip with smooth reflective underside</li> <li>Part's surface finish smooth</li> <li>No collar formation</li> <li>Slight flank wear</li> </ul>	<ul style="list-style-type: none"> <li>Chips begin to show changing curvature and duller underside</li> <li>Surface finish and part poorer</li> <li>Collar begins to form</li> <li>More flank wear</li> </ul>	<ul style="list-style-type: none"> <li>Chips irregular and broken with uneven serrations and dull underside</li> <li>Dull surface finish</li> <li>Large collar</li> <li>Heavy flank wear</li> </ul>
Aural indications	<ul style="list-style-type: none"> <li>"Clean hiss" of serrations and constant "trickle" of regular chip sections</li> <li>No unusual spikes</li> </ul>	<ul style="list-style-type: none"> <li>Less regular chip sections interrupt even "trickle"</li> <li>Some "spikes" heard</li> </ul>	<ul style="list-style-type: none"> <li>Chips uneven</li> <li>Spikes intense with squealing possible</li> </ul>
Tactile indications	<ul style="list-style-type: none"> <li>Part surface feels smooth</li> </ul>	<ul style="list-style-type: none"> <li>Some "ears" on part surface</li> </ul>	<ul style="list-style-type: none"> <li>Rough "ears" on part</li> </ul>
Machinist's thoughts	<ul style="list-style-type: none"> <li>Tool basically "new" and working smoothly</li> </ul>	<ul style="list-style-type: none"> <li>Expected deterioration occurring</li> </ul>	<ul style="list-style-type: none"> <li>Must stop before damage occurs</li> </ul>



## ***Appendix B: Tool failures mode limits and remedial actions***

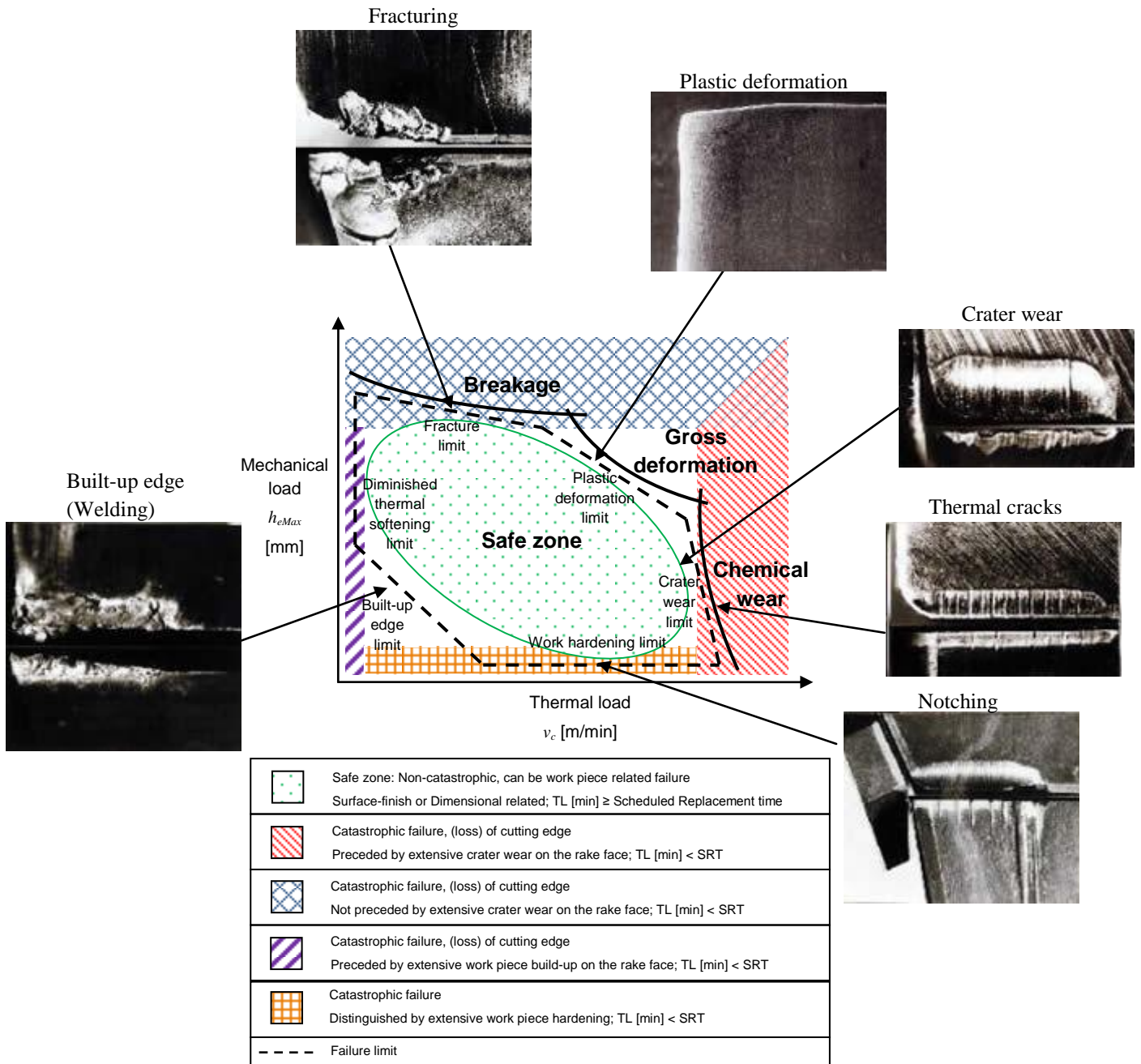
The tool wear map serves the purpose of clarifying the complex interaction between the machining parameters to process designers. Thereby a knowledge based iterative process improvement is facilitated, simultaneously enhancing machining knowledge needed in South Africa.

Prior to this work, a map for the milling of Ti6Al4V were neither created nor remedial actions to optimize the production process, integrated. As illustrated in Figure B.1 this framework has been used to discuss the observed effects and remedial actions that are developed by tool suppliers.

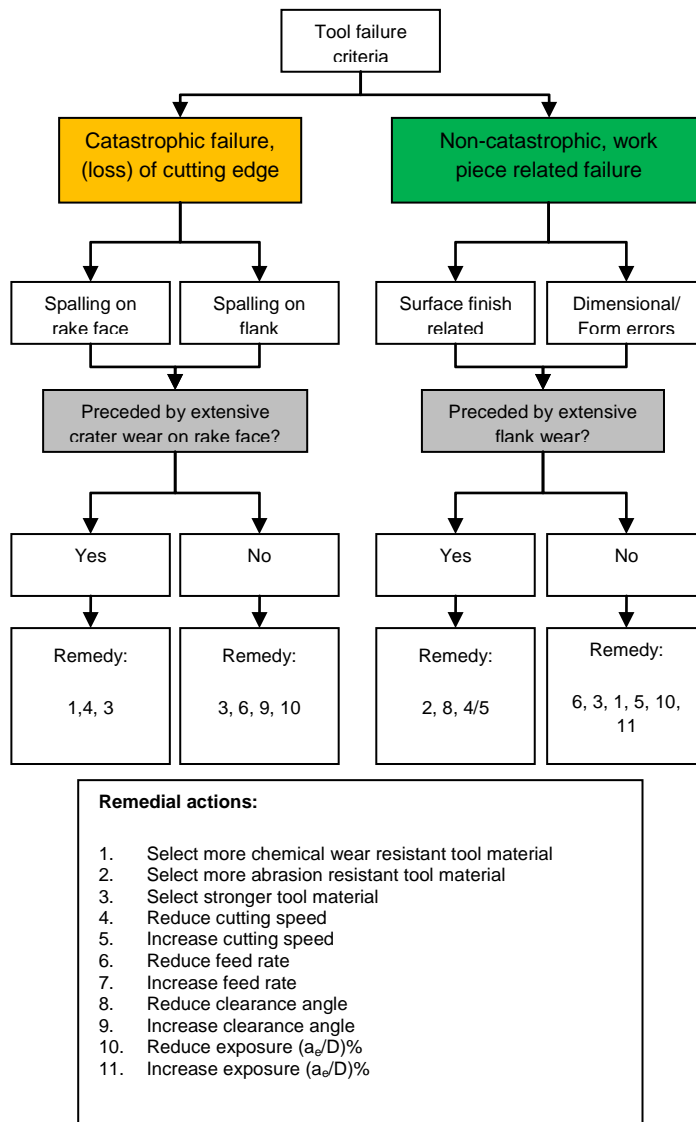
The decision flow chart illustrated in Figure B.2 was developed from this study, in order to take remedial action.

The remedial actions that are developed by tool suppliers are shown in Figure B.3.








Table B.1 illustrates a basic troubleshooting checklist to identify solutions for various milling problems



**Figure B.1:** Categorizing the characterized tool failure modes into tool wear map failure regions. Thereby, it is possible to consider remedial actions.



**Figure B.2:** Common failure modes for the milling of Ti6Al4V and possible remedial actions

<i>Tool Failure</i>		<i>Causes</i>	<i>Remedial action</i>
Flank wear		<ul style="list-style-type: none"> <li>- Tool grade is too soft.</li> <li>- <math>v_c</math> is too high.</li> <li>- Flank angle is too small.</li> <li>- <math>f_z</math> is extremely low.</li> </ul>	<ul style="list-style-type: none"> <li>- Tool grade with high wear resistance.</li> <li>- Lower <math>v_c</math>.</li> <li>- Increase flank angle.</li> <li>- Increase <math>f_z</math>.</li> </ul>
Crater wear		<ul style="list-style-type: none"> <li>- Tool grade is too soft.</li> <li>- <math>v_c</math> is too high.</li> <li>- Feed rate is too high.</li> </ul>	<ul style="list-style-type: none"> <li>- Tool grade with high wear resistance.</li> <li>- Lower <math>v_c</math>.</li> <li>- Lower <math>f_z</math>.</li> </ul>
Fracturing		<ul style="list-style-type: none"> <li>- Tool grade is too hard.</li> <li>- <math>f_z</math> is too high.</li> <li>- Lack of cutting edge strength.</li> <li>- Lack of shank or holder rigidity.</li> </ul>	<ul style="list-style-type: none"> <li>- Tool grade with high toughness.</li> <li>- Lower <math>f_z</math>.</li> <li>- Increase honing. (Round honing is to be changed to chamfer honing.)</li> <li>- Use large shank size.</li> </ul>
Plastic Deformation		<ul style="list-style-type: none"> <li>- Tool grade is too soft.</li> <li>- <math>v_c</math> is too high.</li> <li>- <math>f_z</math> and <math>a_e</math> are too large.</li> </ul>	<ul style="list-style-type: none"> <li>- Lower <math>v_c</math>.</li> <li>- Decrease <math>a_e</math> and <math>f_z</math>.</li> <li>- Tool grade with high thermal conductivity.</li> </ul>
Adhesion (Welding)		<ul style="list-style-type: none"> <li>- <math>v_c</math> is low.</li> <li>- Poor sharpness.</li> </ul>	<ul style="list-style-type: none"> <li>- Increase <math>v_c</math>.</li> <li>- Increase rake angle.</li> <li>- Tool grade with low affinity.</li> </ul>
Thermal cracks		<ul style="list-style-type: none"> <li>- Expansion or shrinkage due to cutting heat.</li> <li>- Tool grade is too hard.</li> </ul>	<ul style="list-style-type: none"> <li>- Dry cutting. (For wet cutting, flood work piece with cutting fluid)</li> <li>- Tool grade with high toughness.</li> </ul>
Notching		<ul style="list-style-type: none"> <li>- Hard surfaces such as uncut surface, chilled parts and machining hardened layer.</li> <li>- Friction caused by jagged shape chips. (Caused by small vibration)</li> </ul>	<ul style="list-style-type: none"> <li>- Tool grade with high wear resistance.</li> <li>- Increase rake angle to improve sharpness.</li> <li>Increase <math>a_e</math> and <math>f_z</math></li> </ul>

**Figure B.3:** The possible causes to different tool failure modes and the various remedial actions developed by the various tool suppliers

Source: Corporation MM. Mitsubishi Tooling Technology Metric Version Level 2. 1st ed.: Mitsubishi Materials Corporation; 2006.

Sandvik , Titanium Machining Guide. Sweden: 2007.

			Remedial actions (Counter measures)																			
			Cutting tool grade choice				Cutting conditions				Cutting tool geometry							Machine/clamping				
Problem	Causes (Factors)		Harder grade / Higher hot hardness	Tougher grade (Toughness and TRS)	Higher thermal shock resistance	High weld-resistant grade	Cutting speed $v_c$ [m/min]	Feed rate $f_z$ [mm/z]	Radial depth of cut $a_e$ [mm]	Lubrication strategy	Rake angle	Corner angle	Cutting edge strength / Honing	Number of teeth	Chip pockets	Wiper geometry	Run-out accuracy	Tool rigidity	Work piece/Tool clamping	Tool overhang	Power/Machine backlash	
			Catastrophic tool failure characterized by	Crater wear	Improper cutting conditions					x		x	x									
	Improper tool cutting edge geometry	x										x	x	x								
Edge chipping or fracture	Improper cutting conditions							x	x													
	Improper tool cutting edge geometry			x								x	x			x	x	x	x	x	x	x
Cracks due to thermal shock	Improper cutting conditions						x		x	x												
	Improper tool cutting edge geometry				x						x		x									
Plastic deformation	Improper cutting conditions						x	x	x													
	Improper tool cutting edge geometry	x																				
Notch wear	Improper cutting conditions							x	x	x												
	Improper tool cutting edge geometry			x								x										
Built-up (Adhesion)	Improper cutting conditions					x	x		x													
	Improper tool cutting edge geometry				x					x		x										
Work piece failure	Poor surface finish	Tool wear / Cutting tool run-out	x			x	x	x	x	x			x			x	x					
	Burr formation	Improper cutting conditions					x	x	x													
		Improper tool cutting edge geometry									x	x	x			x						
	Work piece chipping	Improper cutting conditions						x	x													
		Improper tool cutting edge geometry									x	x	x	x		x		x				
	Poor flatness and parallelism	Tool / Work piece clearance						x	x		x	x		x		x	x	x	x	x	x	x

Source: Corporation MM. Mitsubishi Tooling Technology Metric Version Level 2. 1st ed.: Mitsubishi Materials Corporation; 2006

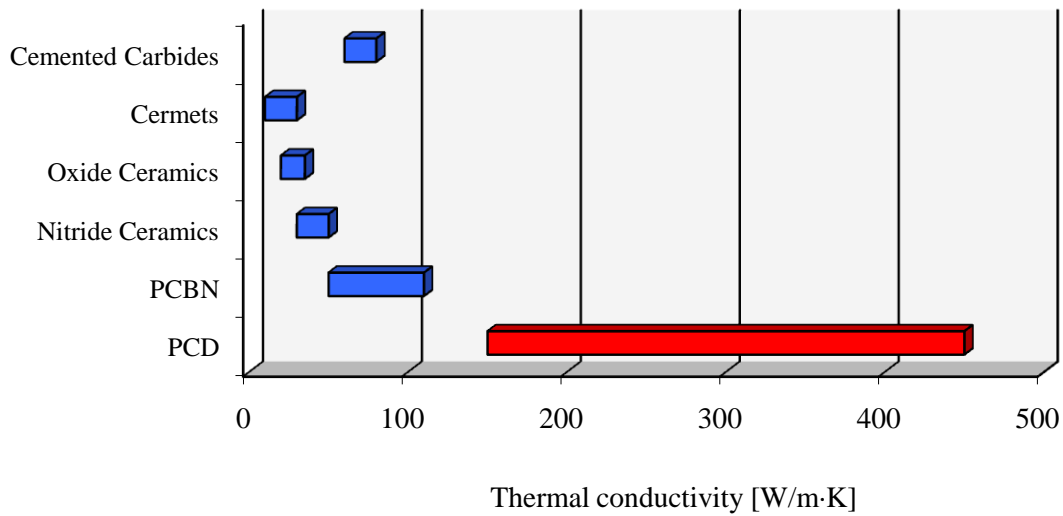
**Table B.1:** Basic troubleshooting checklist to identify solutions for various milling problems

## *Appendix C: Critical cutting tool material properties*

Different properties enable materials to have their respective suitable applications and work piece materials. It was discovered through this machining research on titanium alloys, that the cutting inserts require the following properties in order to mill Ti6Al4V competitively:

- a. High Transverse rupture strength
- b. Reduced tendency to react with titanium
- c. High hardness at elevated temperatures
- d. Toughness and fatigue resistance to withstand the chip segmentation process
- e. High thermal conductivity to minimize thermal shock on the tool

The following figures (Figures C.1-5) compare different critical properties of various tool materials



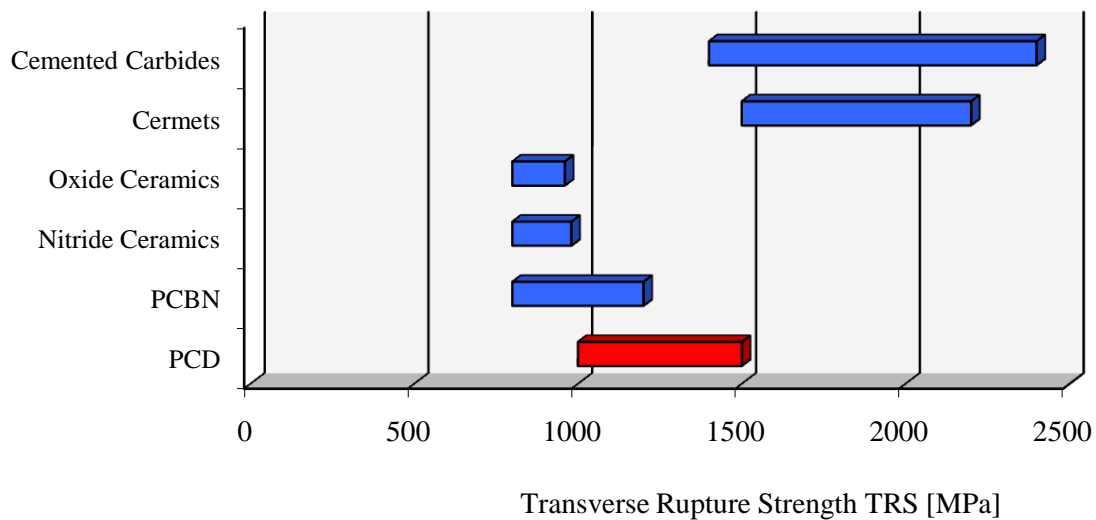
**Figure C.1:** Thermal conductivity of different cutting tool material

Thermal conductivity is a property characterizing the ability of both the machined-, and cutting material to conduct heat. The figure illustrates PCD's advanced thermal conductivity properties. Thermal conductivity plays a critical role for efficient machining of titanium.



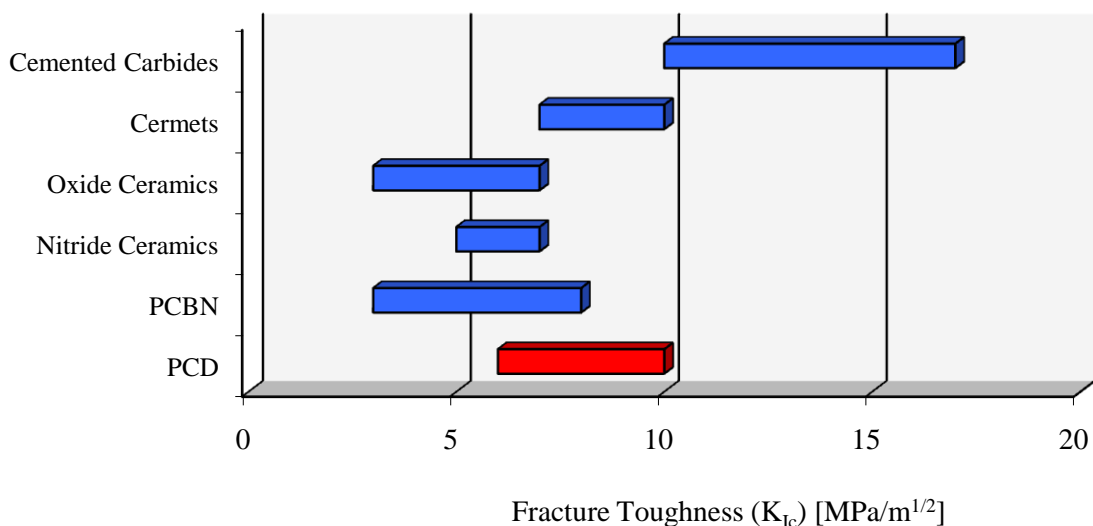
**Figure C.2:** Hardness of different cutting tool material

Hardness is the measure of a material's resistance to deformation by surface indentation or by abrasion. Harder cutting material causes less the wear and results in a longer tool life. This comparison clearly indicates the superior hardness of PCD, followed by PCBN.



**Figure C.3:** Transverse Rupture Strength of different cutting tool material

The transverse rupture strength (TRS) can be defined as the resistance to crack initiation. To avoid rake face chipping from mechanical overload, this property of the tool material should be greater than the applied load. TRS is the ability to withstand brittle fracture (chipping). Chipping is a dominant wear mechanism in superhard cutting materials. Therefore it is an important performance characteristic. The figure clearly shows that carbide has much higher transverse rupture strength than PCD.

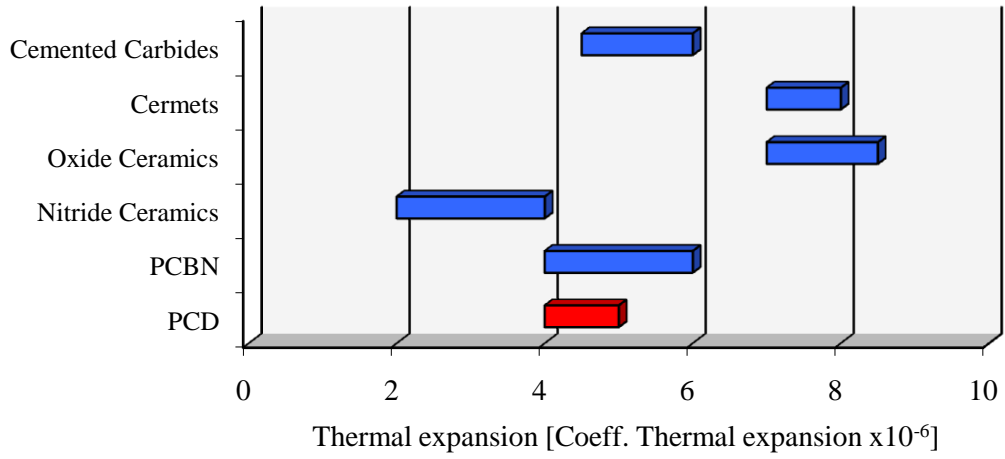


**Figure C.4:** Fracture Toughness of different cutting tool material

Fracture toughness is the property of a material to withstand rapid crack propagation. Various subscripts are used to denote different loading conditions or fracture toughness. Fracture toughness of polycrystalline diamond (PCD) increased with increasing diamond particle size. This may be attributed to increasing tensile components of the internal stresses occurred in PCD with decreasing particle size due to thermal mismatch between sintered



diamond and Co



**Figure C.5:** Thermal expansion of different cutting tool material

Thermal expansion is the change in volume as a function of temperature. PCD has a relative low thermal expansion coefficient compared to that of carbides.

D

## *Appendix D: Altered Material Zones (AMZ's)*

Surface Alterations occur during both conventional and non-conventional machining. These Altered Material Zones (AMZ's) are caused by plastic deformation, high temperatures and temperature gradients, chemical reactions between the tools and work pieces, excessive electrical currents and excessive energy densities during processing.

The level of material alteration needs to be accounted for when selecting manufacturing processes. A certain level of imperfection should be allowed for to make selected machining process feasible and economical. Altered material zones are grouped into five categories according to what type of energy causes them.

The five categories are mechanical, chemical, metallurgical, electrical and thermal.

AMZ due to mechanical energy mode:

- Tears, laps and crevice-like defects associated with built-up edge may be produced in milling
- Plastic deformation caused by hot or cold working
- Hardness of surface layer may change
- Micro- and macro-cracking may occur
- An undesirable distribution of residual stress in the surface layer may occur
- Process inclusions may be introduced
- Plastically deformed debris may result from grinding
- Voids, pits, burrs, or foreign material inclusion may be introduced to the surface

AMZ due to metallurgical energy mode:

- Phase transformation may occur
- Grain size and distribution may be altered
- Precipitate size and size may be altered
- Foreign inclusions in the material may be introduced
- Twinning may occur
- Re-crystallization may occur
- Un-tempered martensite or over-tempered martensite may form
- Re-solutioning or austenite reversion may occur

AMZ due to chemical energy mode:

- Inter-granular attack and preferential solution of micro-constituents may occur
- Inter-granular corrosion may occur
- Inter-granular oxidation may occur
- Contamination may occur
- Embrittlement may occur through the chemical absorption of elements such as hydrogen and halogen
- Pits or selective etch may occur
- Corrosion and stress corrosion may occur

AMZ due to thermal energy mode:

- Heat-affected zones may form
- Re-cast or re-deposited material may be present
- Re-solidified material may be present

- Coatings of re-melted metal deposited on the surface during electrical discharge, electron beam or laser machining may spatter

AMZ due to electrical energy mode:

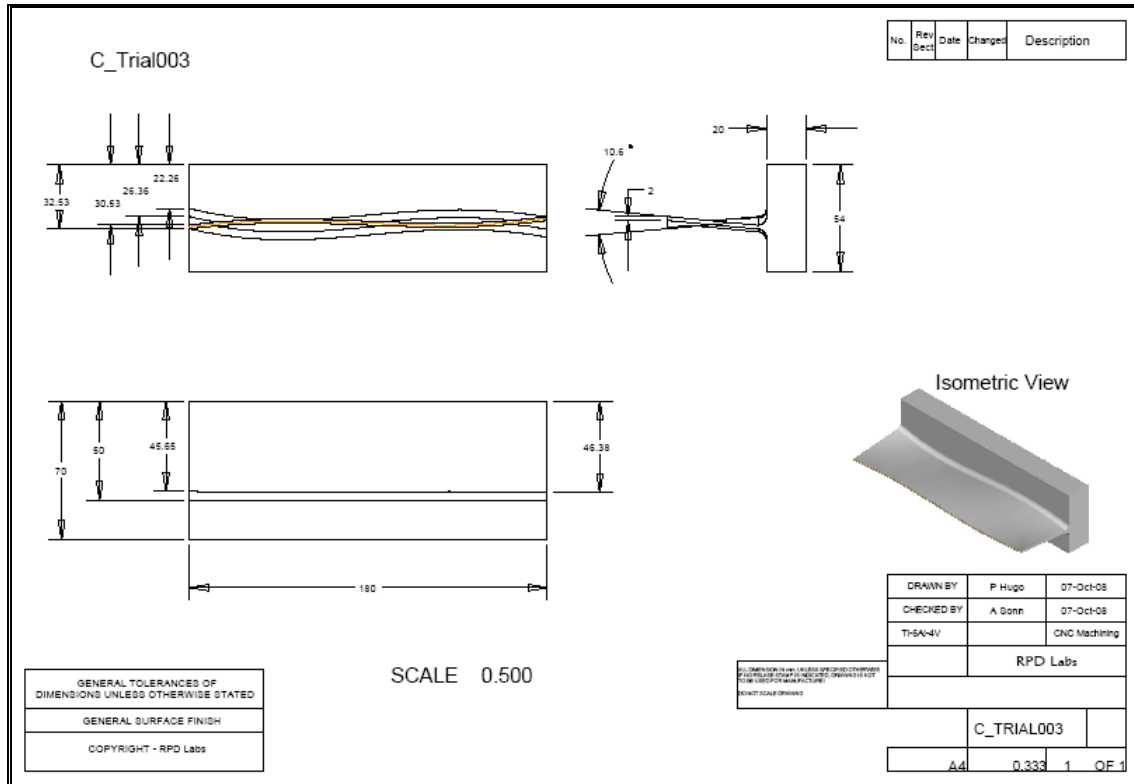
- Change in conductivity may occur
- Change in magnetic properties may occur
- Resistive heating or overheating may occur

**Source:** Machinability Data Center (1980) Machining Data Handbook, 3<sup>rd</sup> Edition, Metcut Research Associates Inc., USA.

## *Appendix E: Benchmark component*

Titanium alloys are used for high value components, not only components used in an aircraft's frame and engine, but also in the biomedical field. Workshops able of sustained growth will migrate toward higher-end work, meaning that a growing percentage of machining shops will encounter titanium alloys. Therefore attention to milling titanium is worth attention in order to achieve higher productivity, when raising the cutting speed is not an option. In a collaborative research study between the academia and aerospace industry a benchmark part was used to understand the tool demands from the Ti6Al4V work piece and to improve the milling strategies used currently in industry. This benchmark part is illustrated in Figure E.1.

Using the wear characterization map developed from this research study, improved parameters and milling strategies were realised for the cutting of the corner fillet of the component. The used tools were examined with an optical microscope and scanning electron microscope (SEM) imaging and were characterized so as to categorize them into a failure region. Thus, remedial actions could be considered to improve the process. Both the roughing and the semi-finishing for this benchmark component can now be completed in less than 20 minutes.



**Figure E.1:** Drawing of benchmark component used for collaborative study between academia and industry.

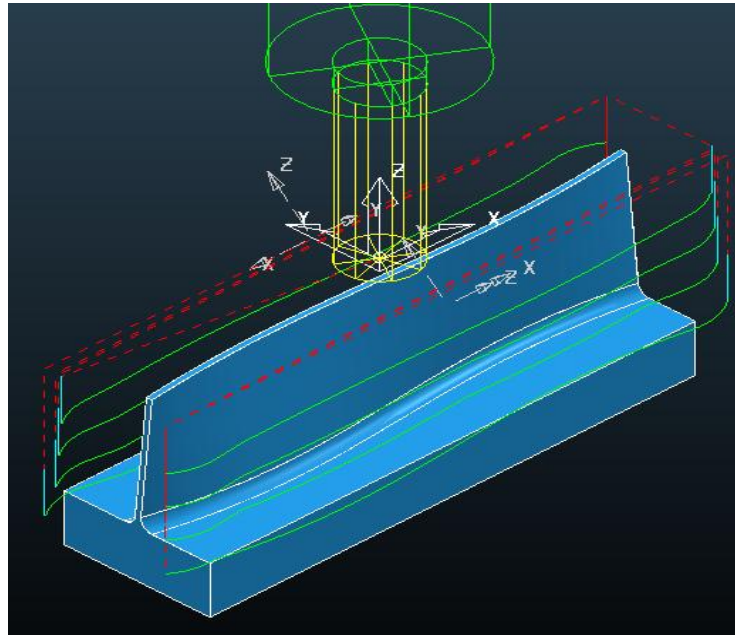
Table E.1 illustrates the different operations to machine this component. Test 1 and test 2 are the result of various simulations and background experimental studies. Cutting tool materials and cutting parameters were varied to improve the machining time.

**Table E.1:** Summary of the operational for two experimental tests in order to reduce the total machining time of a benchmark component

	<b>Operation</b>	<b>Test 1 (min)</b>	<b>Test 2 (min)</b>	<b>MR (cm<sup>3</sup>)</b>	<b>MR (%)</b>
1	First Rough	7.09	7.09	283.898	61.01
2	Semi Finishing	12.25	12.25	141.858	30.49
3	Flat Area Finishing	2.32	2.32	1.665	0.357
4	Side Wall Finishing	12.16	12.16	33.957	7.30
5	Corner Fillet Roughing	49.02	0.3	3.608	0.775
6	Corner Fillet Finishing	30.96	4.1	0.348	0.074
7	Blade Final Finish	2.56	2.56	0	0
	<b>Machining Time</b>	<b>116.36</b>	<b>40.78</b>	<b>465.334</b>	<b>100</b>

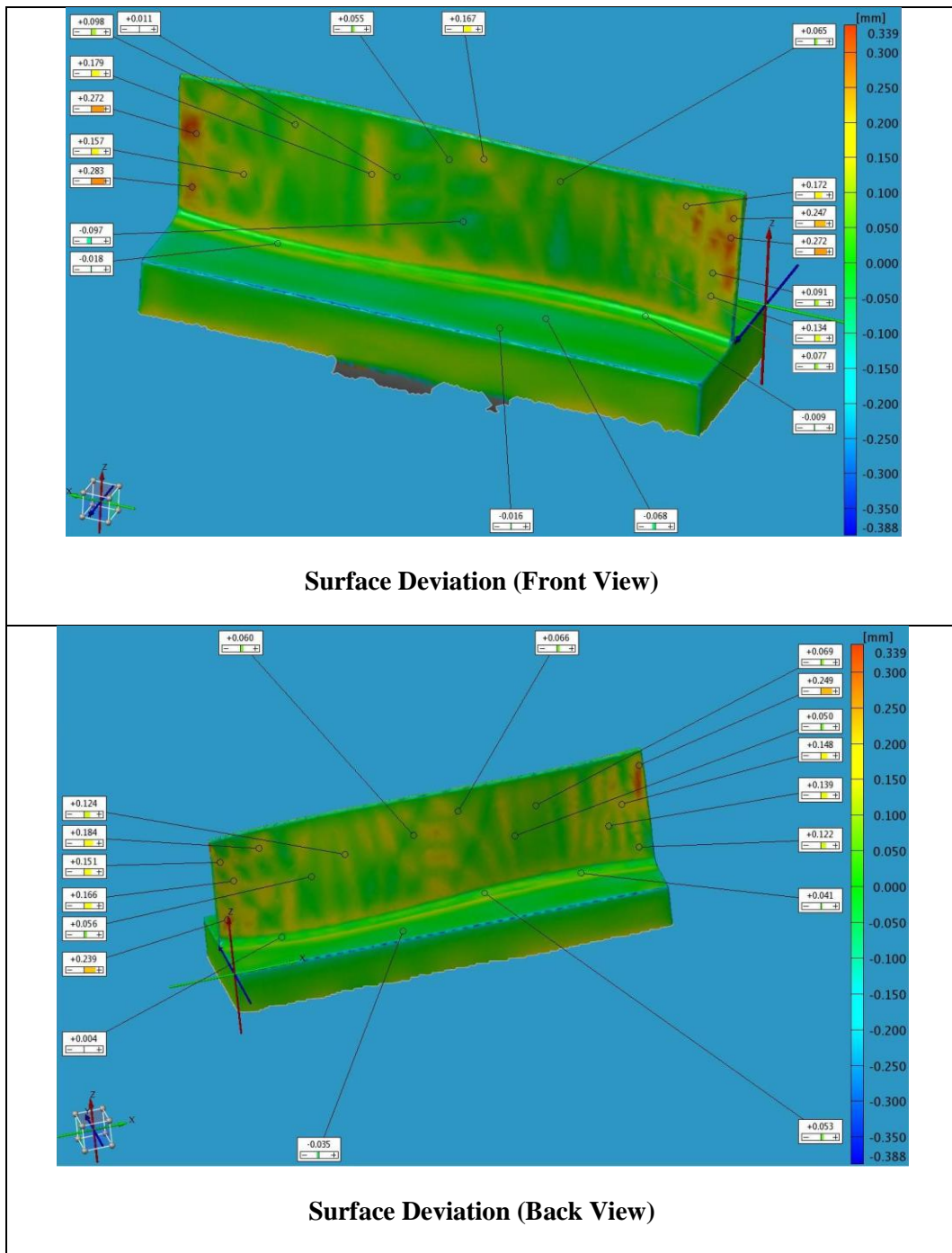
The revision of the machining strategies with new generation cutting tools showed a significant reduction from 116 minutes to 41 minutes in the total machining time. An Aluminium version of the

same benchmark component required nominally 14 minutes to machine. Compared to the 41 minutes to machine a Ti6Al4V part, it is evident why titanium machining needs further experimentation. Figure E.2 illustrates the first roughing operation of this component.



**Figure E.2:** Illustration of the simulated run for the first rough operation

Similarly it is calculated that the tool life in the aerospace industry should exceed 30 minutes to ensure an economical viable solution as most scheduled tool replacement times (SRT) are less than this time. A Geometrical Optical Measurement system (Atos1) machine was also used to do a surface deviation inspection, comparing the scanned data with the actual CAD data as can be seen in Figure E.3. Once again the inspection indicates deviation towards the edges of the ‘S’ profile surface for the titanium part. The ‘S’ profile surface also has a few deviations at certain points (yellow marks). The poor surface finish marks at the ends of the ‘S’ surface is due to the semi-finish cycle, where the rotary table moves at a faster feed rate than the cutting feed rate, causing the ‘S’ blade to deflect on the tool, thus causing the marks.



**Figure E.3:** Surface deviation of Titanium Test Piece to CAD (GOM)

Mitutoyo SurfTest 211 was used to take surface measurements.  $R_a$  is selected as the roughness parameter to be measured and a cut-off-length of 0.8mm used.

**Table E.2:** Surface roughness after machining benchmark component according to safe zone parameters

<i>Direction</i>	<i><math>R_a</math> (<math>\mu m</math>)</i>
x	1.03
x	1.16



x	0.79
x	0.81
x	0.59
<b>x (avg.)</b>	<b>0.876</b>
y	1.1
y	0.51
y	2.31
y	0.57
y	0.95
<b>y (avg.)</b>	<b>1.088</b>
z	1.14
z	0.83
z	0.91
z	1.28
z	1.21
<b>z (avg.)</b>	<b>1.074</b>
<b>Pattern (avg.)</b>	<b>1.0127</b>

The titanium part had a good surface roughness value ( $R_a=1.0127\mu m$ ) and the component's accuracy was acceptable. These results helped with the construction of the tool wear maps for both rough- and finish milling of Ti6Al4V.

## *Appendix F: Publications*

The construction of wear maps for the rough- and finish milling of Ti6Al4V formed part of the outputs. The wear characterisation of carbide cutting tools in the rough milling of Ti6Al4V and PCD tools in the finish milling of Ti6Al4V contribute to the understanding of these complex wear mechanisms. Scanning electron microscopy, energy dispersive X-ray analysis and optical microscopy were employed to assist in the identification of the various dominant wear mechanisms operating under these milling conditions. The different forms of chip formation and measured cutting forces will also enable to improve simulation models of the milling of titanium alloys.

The acceptance of publications and articles in peer reviewed conferences will be a measure of the success of this research work. This study is based on the following publications shown in Table C.1, which also formed part of the outputs.

**Table C.1:** Publications from research study

#	<i>Publication</i>	<i>Chapter (s)</i>
1	Treurnicht, NF; Oosthuizen, GA. 2008. <i>High performance machining of titanium: Charting the challenge</i> . 2nd SAIAS Symposium, 14-16 September 2008, Stellenbosch, South Africa.	1
2	Oosthuizen, GA; Joubert, HJ; Treurnicht, NF. 2009. <i>Using palletised work holding to emulate 5-axis machining of aerospace components in the developing world</i> . South African Journal of Industrial Engineering. Vol. 20 (2). November 2009.	1
3	Oosthuizen, GA; Treurnicht, NF; Akdogan, G. 2009. An Evaluation of the wear characterisation in milling Ti-6Al-4V. <i>SA Inst. of Industrial Engineering Annual Conference</i> , 28-30 October 2009, Pretoria, South Africa.	3, 5
4	Treurnicht, NF; Joubert, HJ; Oosthuizen, GA; Akdogan, G. 2010. <i>Investigating of Eco-energy efficient lubrication strategies for the drilling of light metal alloys</i> South African Journal of Industrial Engineering – <i>Accepted for publication</i> .	2, 3
5	Oosthuizen, GA; Joubert, HJ; Treurnicht, NF; Akdogan, G. 2010. <i>High-speed milling of Ti6Al4V</i> . COMA'10 International Conference, 3-5 February 2010, Stellenbosch, South Africa.	5
6	Koen, D; Herselman, EJ; Oosthuizen, GA; Treurnicht, NF. 2010. <i>Investigating novel cooling methods for titanium machining</i> . COMA'10 International Conference, 3-5 February 2010, Stellenbosch, South Africa.	3
7	Oosthuizen, GA; Akdogan, G; Treurnicht, NF. 2010. <i>The Performance of PCD Tools in High-speed Milling of Ti6Al4V</i> . International Journal of Advanced Manufacturing Technology - <i>Accepted for publication</i> .	5
8	Oosthuizen, GA; Akdogan, G; Treurnicht, NF. 2010. <i>Towards understanding the tool demands for HSM of Ti6Al4V</i> . Materials Science & Technology Conference & Exhibition (MS&T), 17-21 October 2010. Houston, Texas, United States.	3, 5
9	Dimitrov, D; Neugebauer, R; Oosthuizen, G; Schmidt, G; Treurnicht, N.; Blaine, D. 2010. <i>High Performance Machining of Selected Titanium Alloys for Aerospace Applications</i> . International. Chemnitz Manufacturing Colloquium (ICMC), 29-30 September 2010. Chemnitz, Germany.	5
10	Oosthuizen, GA; Akdogan, G; Dimitrov, D; Treurnicht, NF. 2010. <i>Titanium alloys and their machinability</i> . Journal of The South African Institution of Mechanical Engineering (SAIMechE) - <i>Accepted for publication</i> .	2, 3 & 5

#	<i>Publication</i>	<i>Chapter (s)</i>
11	Oosthuizen, GA; Akdogan, G; Dimitrov, D; Schmidt, G. 2010. <i>Investigating the effect of chip serration on forced vibration in the milling of Ti6Al4V</i> . International Journal of Advanced Machine Tool and Manufacture - Submitted for publication.	5
12	Oosthuizen, GA; Akdogan, G; Treurnicht, NF. 2010. <i>Performance enhancement in the milling of Ti6Al4V</i> . SA Inst. of Industrial Engineering Annual Conference, 6-8 October 2009, Muldersdrift, South Africa.	5
13	Treurnicht, NF; Oosthuizen, GA. 2010. <i>An overview of recent machining improvements in titanium</i> . SA Inst. of Industrial Engineering Annual Conference, 6-8 October 2009, Muldersdrift, South Africa.	2, 3